EXCITATION ENERGY TRANSFER IN INTACT PHYCOBILISOMES FROM CYANOBACTERIA

By

Sourav Sil

A DISSERTATION

Submitted to
Michigan State University
in partial fulfillment of the requirements
for the degree of

Chemistry – Doctor of Philosophy

2024

ABSTRACT

The phycobilisome is the primary light-harvesting protein complex in cyanobacteria and red algae. Phycobilisomes absorb mid-visible solar energy and transfer that energy to PS II and PS I with very high quantum efficiency (> 90%). The mechanisms of this excitation energy transfer process are controlled by the structure of phycobilisomes. Phycobilisomes contain disk-shaped $(\alpha\beta)_6$ hexameric phycobiliproteins (PBPs) that prepare cylindrical core and rod-like structures. The rods incorporate blue-shifted PBPs phycoerythrin (PE, λ_{max} = 570 nm) and phycocyanin (CPC, λ_{max} = 620 nm) whereas the core contains allophycocyanin (APC_{660}, λ_{max} = 650 nm). In this way phycobilisomes create a funnel-shaped energy structure where a green photon absorbed by a bilin chromophore (linear tetrapyrrole molecule) in PE at the end of the rod can transfer energy down the rod to CPC to APC_{660} in the core efficiently. Then excitation moves to terminal emitter (TE) or APC_{680}, a special segment in the core containing red-shifted APC, that transfers energy to PS II or PS I. Broadband two-dimensional electronic spectroscopy (2DES) with 7-fs laser pulses was employed to determine the excitation energy transfer processes in intact phycobilisomes isolated from *Fremyella diplosiphon* grown under illumination of white light. Excitation transfer can be followed from PE at the end of the rod to the TE through CPC and APC_{660} by observing the development of below the diagonal cross-peaks in the 2DES spectra at longer waiting time. In the short time the rapidly damped cross-peaks in 2DES spectra strongly suggest the presence of coherences. The global and target model for the 550-580 nm of the excitation strip shows the excitation moves down the rods very fast within 1 ps and reaches to the core in ~10 ps. The evolution-associated difference spectra (EADS) and coherence analysis using FT spectra and oscillation maps indicates that the

chromophores in intact phycobilisomes share a common ground state and delocalized excitons present in the rods. Furthermore, coherent wavepackets dominated by the Hydrogen out-of-plane (HOOP) vibration mode of the bilin chromophores, mediate the excitation energy in the rods. Then excitation slows down in the core due to the localization and uses a Förster style mechanism to transfer to the TE. The localization of excitation in the core is accelerated by the intramolecular charge transfer (ICT) character in the lowest energy chromophore (β84) in APC originating from the ring-flipping in the excited state. As a part of the complementary chromatic adaptation (CCA) response, red-light grown *Fremyella diplosiphon* produce phycobilisomes with shorter rod lengths due to the absence of PE disks at the end of the rods. The effect of shorter rod length can be observed from the kinetic model for the 560-580 nm excitation strip of the 2DES spectrum obtained from the red-light grown phycobilisomes. The model shows a faster energy transfer rate from rod to the core as compared to that of the white-light grown samples. The excited-state lifetimes for TE in phycobilisomes are significantly shorter (~400 ps) than literature reported value (1.5 ns). Time-correlated single photon counting (TCSPC) experiments were performed to understand this phenomenon. Although both white and red light grown samples show ~1.5 ns fluorescence lifetime in TCSPC experiments. Further studies and analysis are required to understand the picture in more detail.

To my parents and Saro

ACKNOWLEDGEMENTS

My academic journey started from a small town ‘Rajbalhat’ in West Bengal, India. After completing my high school, I moved to the nearest big city Kolkata to study my undergraduate degree in Chemistry from University of Calcutta. Then I went to Indian Institute of Technology (IIT) Kharagpur for my master’s degree in chemistry. Next, I got the opportunity to pursue the doctoral degree at Michigan State University (MSU). Now I am about to finish up my PhD and I am looking forward to starting my next chapter in the industrial sector. During this journey not only, I gained knowledge in science but also, I learned important life lessons and grew as a person. There are so many people who have supported and helped me in my academic and personal life to make it successful and enjoyable. It is not possible to write all of their names here, but I want to acknowledge a few of them who have contributed the most.

I would like to thank my advisor Professor Warren F. Beck for giving me the opportunity to work in his laboratory. Your passion for science and our conversation always motivated me. Throughout my PhD journey you guided me and helped me to stay in focus. The biggest thing that I learned from you is how to focus on the big picture of a project and think critically about the results of a project. You taught me that before starting an experiment one should learn about the topic enough to build a hypothesis about the problem, design an experiment and know what to expect as an outcome from it. These steps became a protocol for me to approach an unknown problem. In that way I feel ready to take any challenge that I might face in future. I would like to thank my committee members (Professor Marcos Dantus, Professor James McCusker and Professor Kathrine Hunt) for helping me understand my projects better by asking impactful questions.

I was fortunate enough to work with smart and talented labmates. In the initial days my senior labmates Ryan (Dr. Ryan Tilluck) and Jason (Dr. J K Gurchiek) helped me to settle down in the laboratory and get things started. I want to thank Ryan for teaching me how to operate the 2DES spectrophotometer, perform data analysis and global modeling. Also, I would like to thank Jason for helping me with the fluorescence instrument, MATLAB and LabVIEW coding. Later, Nila (Dr. Nila Mohan T M) and Justin (Justin B Rose) helped me with the 2DES and fluorescence experiments. I want to thank Nila for always there for me in each and every step of my PhD journey. You were my go-to person in the lab. Most importantly I got a good friend in you. I want to thank Justin for all his help with the fluorescence experiments and data analysis. You also helped me to have a better understanding about American culture. Moreover, you became one my dear friends. I would like to thank my junior labmates Chase for his help with the oscillation analysis, Kunwei, Shanu and Megha for all the support and friendship. I wish you all the best for the rest of your journey.

I want to thank our collaborator Prof. Cheryl A. Kerfeld and Prof. Beronda Montgomery for allowing me to use their laboratory for the isolation of phycobilisomes. Their group members always made me feel welcome. Special thanks to Dr. Sigal Lechno-Yossef, Damien Sheppard, Dr. Maria A. Domínguez-Martín, Dr. Wenjing Lou, Dr. Han Bao, Dr. Roberto Espinoza, Carrie Hiser, Alicia Layer for teaching me the phycobilisomes isolation process and helping me with the all the instruments in that laboratory.

Apart from my academic life I would like to thank some people who constantly supported mentally and financially in my personal life during this journey. I want to start that by thanking my parents ('*ma*' and '*baba*') for their unconditional love. You believed in me, gave me self-confidence and allowed me to follow my passion. Most importantly, you

taught me to become a good human being. I would also like to thank my brother Rahul, sister Rakhi, grandparents ('*dadu*', '*thakuma*'), uncles (*'boro picimosai*', '*choto picimosai*', '*jethu*'), aunts (*'boro picima'*, '*chotot picima*', '*jethima*') and cousins (Maman didi, Sonai didi, Baban dada, Tutai da, Bipasa di) for their support and guidance for my academic journey. I want to thank my wife, Saro for being there with me in each and every moment of my life and helping me to get through the ups and downs. You always motivate me to become a better person and push boundaries in achieving goals.

I was lucky enough to have many great friends throughout my journey. I want to thank my friends from school (Sandip, Taimur, Minakshi, Ayan, Mainak, Riya), and college (Debankur, Pavel, Pritam, Antarip, Avijit, Chinmoy, Dhrub, Roni, Sharajit, Anupom, Nahid) for their help and creating good memories. A special thanks to my schoolteachers specifically Amrit Bhattacharjee, Vivekanada Patra and SK Jahir Abbas for their guidance and motivating me to choose science as my career. Here at MSU, I got many good friends (Arnab, Atanu, Soumik, Shreya, Estak, Dipti, Soham, Prakash, Susanta, Tathagata, Manoj, Kiyoto, Deborshi). Eventually they became my extended family and helped me enjoy the PhD journey. Also, they guided me to understand the new culture at USA and adapt in the new social environment. I am thankful to them.

This dissertation work was supported by the U.S. Department of Energy, Office of Basic Energy Sciences, Photosynthetic Systems Program under Award Number DE- SC0010847.

TABLE OF CONTENTS

LIST OF ABBREVIATIONS

2DES	two-dimensional electronic spectroscopy
APC	allophycocyanin
ATP	adenosine triphosphate
CCA	complementary chromatic adaptation
CCD	charge-coupled device
CFD	constant fraction discriminator
CI	conical intersection
CPC	cyanobacterial phycocyanin
CT	charge transfer
CTD	C-terminal Domain
CYS	cysteine
CW	continuous wave
DNA	deoxyribonucleic acid
EADS	evolution associated difference spectra
EAS	evolution associated spectra
EDTA	ethylenediaminetetraacetic acid
EET	excitation energy transfer
ESA	excited state absorption
FFT	fast Fourier transform
FMO	Fenna-Mathew-Olson
FROG	frequency resolved optical gating
FT	Fourier transform

FWHM	full width at half maximum
GSB	ground state bleaching
HOOP	hydrogen-Out-of-Plane
HPLC	high performance liquid chromatography
ICT	intramolecular charge transfer
IR	infrared
LED	light emitting diode
LH	light harvesting
LO	local oscillator
LPSVD	linear prediction singular value decomposition
MCA	multichannel analyzer
MIIPS	multiphoton intrapulse interference scan
NADPH	nicotinamide adenine dinucleotide phosphate
ND	neutral-density filter
NOPA	noncollinear optical parametric amplifier
NPQ	nonphotochemical quenching
NTD	N-terminal domain
OAP	off-axis parabolic mirrors
OCP	orange carotenoid protein
OCP^O	orange carotenoid protein-orange state
OCP^R	orange carotenoid protein-red state
OD	optical density
PBP	phycobiliprotein

PBS	phycobilisome
PCC	Pasteur culture collection
PCB	phycocyanobilin
PCP	peridinin-chlorophyll *a* protein
PDB	protein data bank
PE	phycoerythrin
PEB	phycoerythrobilin
PMSF	phenylmethylsulfonyl fluoride
PMT	photomultiplier tube
PS	photosystem
RC	reaction center
SE	stimulated emission
SEM	scanning electron microscopy
SHG	second harmonic generation
SLM	spatial light modulation
TA	transient absorption
TAC	time-to-amplitude converter
TCSPC	time-correlated single photon counting
TE	terminal emitter
TEM	transmission electron microscopy
THG	third harmonic generation
UTEX	university of Texas culture collection
UV	ultraviolet

WMEL	wave-mixing energy level diagram
WT	wild type

OVERVIEW OF THE DISSERTATION

The main objective of the work presented in this dissertation is to determine the excitation energy transfer mechanisms in intact phycobilisome, principal light-harvesting chromoprotein complex in cyanobacteria and red algae. Intact phycobilisomes were isolated from *Fremyella diplosiphon* grown under white and red-light illumination. Two-dimensional electronic spectroscopy (2DES) experiments were performed using broadband laser spectrum and 7-fs short pulses to study the excitation energy transfer processes in intact phycobilisomes. The broadband of the laser spectrum (520-700 nm) enables us to cover the absorption region of the highest energy chromophores to the emission region of the lowest energy chromophore in the energy transfer chain. The short excitation laser pulses allow us to observe the quantum coherences present in the system. The 2DES spectra show the evolution of the excitation transfer from donor to acceptor as crosspeaks at different delay times. The non-oscillatory signal was used to perform global and kinetic models to obtain an average time for excitation transfer steps. The oscillatory part of the signals was used to generate FT amplitude spectra and oscillation maps that permits us to identify the major oscillation frequencies originating from quantum coherences that are involved in the excitation transfer processes. Additionally, picosecond time-correlated single photon counting (TCSPC) experiments were performed to determine the energy transfer processes at longer time (> 500 ps).

Using all these tools mentioned above we address the following questions:

1. What is the mechanism for the fast excitation energy transfer observed in the rod segments of the intact phycobilisome?
2. How does the excitation transfer slowdown in the core of the intact phycobilisomes?

3. What are the effects in the kinetics of the excitation energy transfer process due to structural change (like shortening of the rods) of the intact phycobilisomes?

The dissertation is organized as follows:

Chapter 1 provides a brief introduction to the function and structure of the photosynthetic light harvesting proteins along with the excitation energy transfer mechanisms. This chapter includes detailed structural information of phycobilisomes and summarizes the excitation energy transfer study of phycobilisomes reported in the literature. The final section of this chapter provides a brief introduction about the 2DES, the third-order nonlinear signals and 2DES data processing and analysis steps. This chapter provides the background that one might need to understand the results presented in the following chapters.

Chapter 2 shows the results of the 2DES study of the excitation energy transfer processes in intact phycobilisomes isolated from *Fremyella diplosiphon* grown under white light. We reported 2DES spectra, global and kinetic models and frequency analysis from this study. The results show that the delocalized exciton present in the rods of the phycobilisomes and vibronic coherent wavepackets dominated by Hydrogen out-of-plane (HOOP) mode mediate the fast excitation transfer in the rods. But the excitation slows down in the core of phycobilisomes due to the intramolecular charge transfer (ICT) character of the lowest energy chromophores in allophycocyanin and energy transfer occurs via a traditional Förster pathway. These results answer the first two questions from above.

Chapter 3 presents the results of the 2DES and TCSPC study from the red-light grown intact phycobilisomes from *F. diplosiphon*. A summary of the structural information from

previous complementary chromatic adaptation (CCA) studies was included in this chapter. Also, we reported the 2DES spectra, global and target models from 2DES and TCSPC studies. The results indicate that excitation reaches to the core of the phycobilisomes from the rods faster for red-light grown samples than that of the white-light grown samples due to the shorter rod lengths for the red-light grown phycobilisomes. TCSPC studies reveal that fluorescence lifetime of the bilins in phycobilisomes is ~1.5 ns, which is significantly higher than the excited state lifetime (~400 ps) of the last compartment of the model from 2DES data. Probably further experiments need to be performed to understand this picture.

Chapter 4 provides a brief discussion about the non-photochemical quenching process in phycobilisomes by orange carotenoid protein as a future work. Currently this project is going on in the Beck laboratory. This chapter presents enough background of this process to identify the main problem with the current picture and provides a probable solution.

Chapter 1: Introduction to Photosynthetic Light Harvesting by Phycobilisomes

1.1 Photosynthetic Light Harvesting Proteins

Photosynthesis is the most important process for the survival of life on earth. Through that process plants, bacteria and algae convert solar photons to biochemical energy. Structure of photosynthetic apparatus in organisms varies depending on their habitat. Although, they have a similar basic structure that includes light harvesting protein systems attached to a reaction center. Light harvesting proteins are the highly ordered array of chromophores inside protein residues. The protein residues help to protect and tune the photophysical property of the chromophores by holding them at a constant position and environment. On the other hand, the chromophores absorb solar energy and then transfer that energy to the reaction center through excitation energy transfer (EET) processes involving several chromophores. The excitation energy initiates an electron transfer process in the reaction center. The electron is first transferred to a lower energy acceptor; then it is followed by a cascade of downhill electron transfer reactions to separate charges across the membrane. Finally, the separated charges stabilized in photosynthesis by forming new molecules like adenosine triphosphate (ATP) and nicotinamide adenine dinucleotide phosphate ($NADPH^+$). Along with that carbon dioxide is reduced to form sugars that will be used in different cellular processes.[1]

The success of photosynthesis depends on the efficient and fast transfer of excitation energy to the reaction center from the light harvesting proteins. The quantum efficiency of the light-to-charge separation is higher than 90%.[2,3] These excitation energy transfer processes are controlled by the structure of light-harvesting proteins. To understand the

mechanisms of the energy transfer process first we need to learn about the structure of the light harvesting protein in detail.

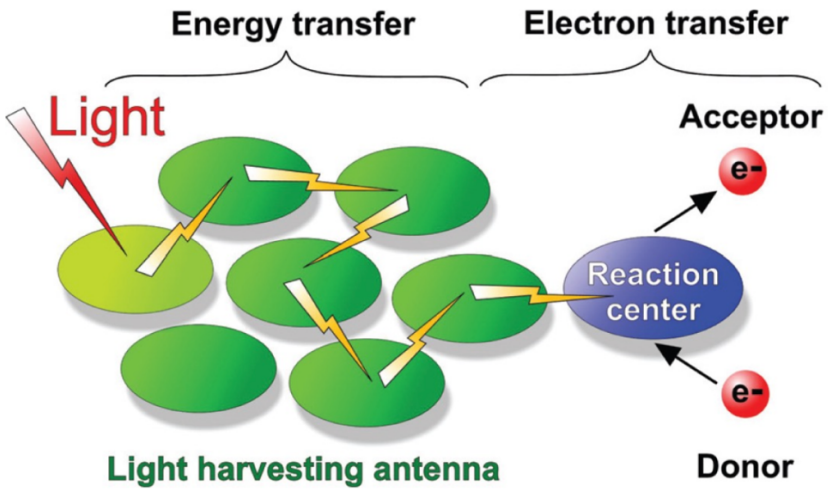

Figure 1.1. Schematic description of a light harvesting and energy transfer to reaction center in photosynthetic organism. From reference 1. Copyright (2021) John Wiley & Sons, Ltd, used with permission.

1.2 Structure of Light Harvesting Proteins

Over the years researchers have obtained high resolution X-ray crystal structures of the different light harvesting proteins. Information from crystal structure and ultrafast spectroscopy can be used to study excitation energy transfer mechanisms. Examples of commonly studied light harvesting protein complexes are Fenna-Matthews-Olson complex (FMO),[4-7] the light harvesting complex II (LH2),[8-11] and phycobilisomes.[12-15]

1.2.1 Fenna-Mathews-Olson (FMO) Complex

The Fenna-Mathews-Olson (FMO) complex was the first chlorophyll-containing protein complex to have X-ray crystal structure from green sulfur bacteria *Prosthecochloris aestuarii* (3EOJ.pdb) and *Chlorobaculum trpidum* (3ENI.pdb).[16] The function of FMO complex is to transfer energy from peripheral light harvesting complex chlorosomes to the membrane-bound reaction centers. The structure of the FMO complex exists as a trimer

[Figure 1.2]. In each cluster there are seven bacteriochlorophyll *a*. The metal center of the chlorophylls is attached through ligation with the amino acids of the protein residue. Seven chromophores in a small protein pocket creates strong electronic coupling among chromophores leading to the formation of exciton states. Therefore, it would be a good model system to study interchromophore coupling and exciton relaxation processes.

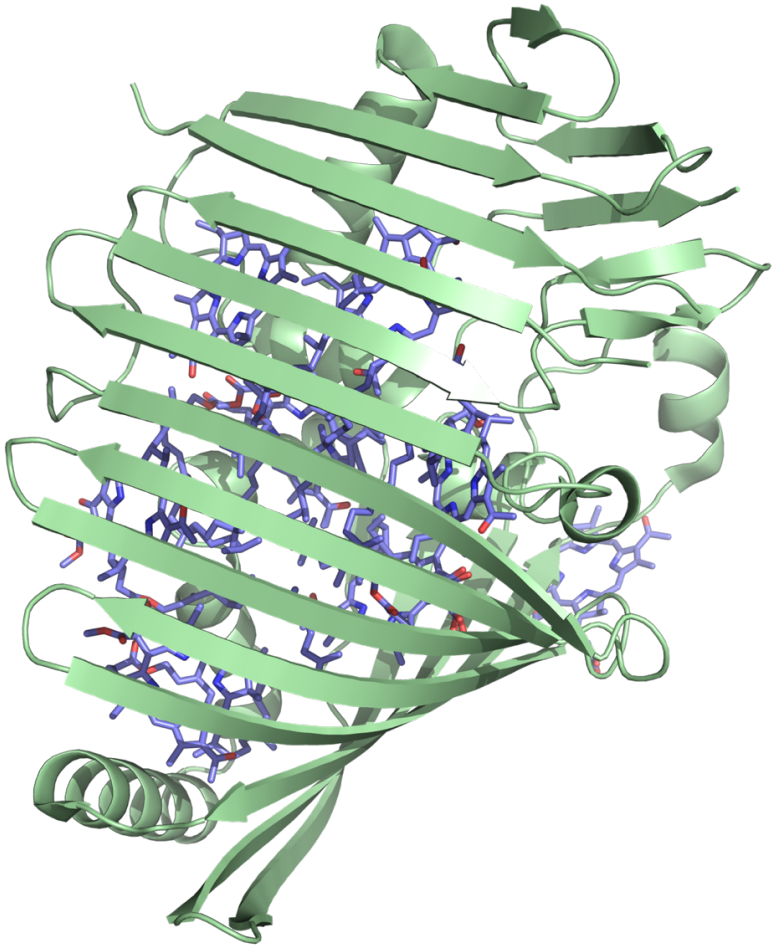

Figure 1.2. X-ray crystal structure of the Fenna-Mathews-Olson Protein from *Chlorobaculum teoidum* (3ENI.pdb).[16] This is a picture of one monomer out of trimer. The blue sticks are chlorophyll molecules in a β-sheet represented in green ribbons.

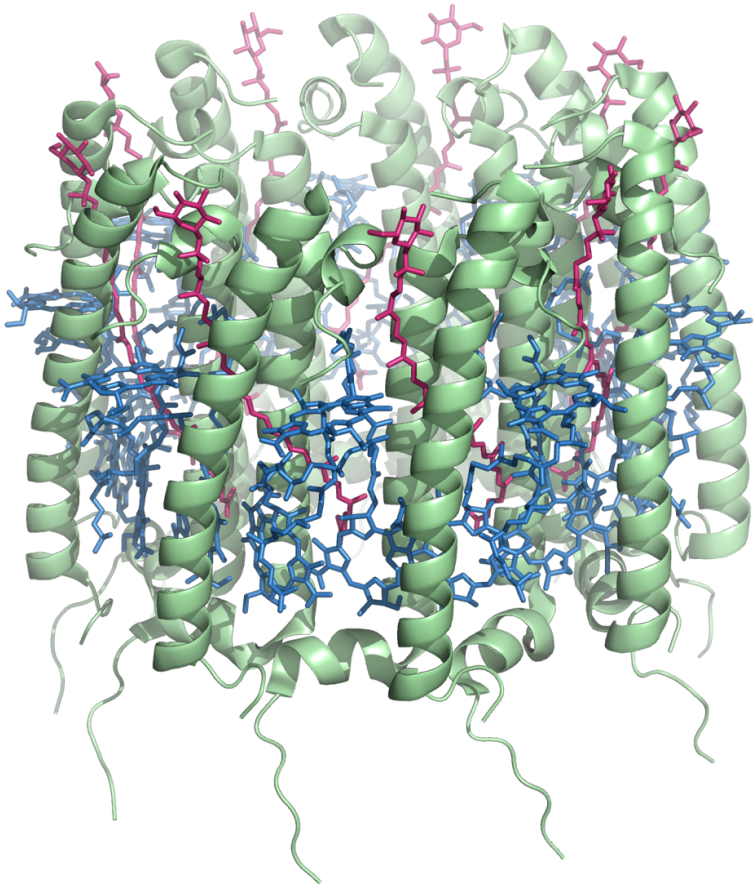

Figure 1.3. X-ray crystal structure of the LH2 complex from *Rhodopseudomonas acidophila* (1NKZ.pdb).[18] This is a side view where the bacteriochlorophylls of the B800 bands are at the top and those of the B850 bands are at the bottom. Bacteriochlorophylls are in blue stick structure whereas the carotenoids are in red.

1.2.2 Light Harvesting Complex II

The X-ray crystal structure of the Light-Harvesting 2 (LH2) complex was obtained from *Rhodopseudomonas acidophila* (1NKZ.pdb).[17,18] The structure of LH2 has nine subunits that form a ring-like structure. Each subunit contains three bacteriochlorophylls and a single carotenoid. Bacteriochlorophylls form two concentric rings - B800 and B850 (based on the position of the Q_y band). In the B800 ring there are nine bacteriochlorophylls 21 Å apart from each other, whereas in the B850 ring there are 18 bacteriochlorophylls 9 Å apart from each other. Therefore, the bacteriochlorophylls in the B850 ring would have strong

electronic coupling among themselves and form delocalized exciton states whereas the bacteriochlorophylls in the B800 ring would interact weakly. The carotenoids are ~ 3.5 Å apart from the pigments of B800 and B850 rings. Here the carotenoids act as additional pigments that harvest blue-green light and transfer excitation energy initially to B800, and finally relaxes to the lowest energy chromophore, B850.[10,19] In this an energy funnel is created to operate the excitation energy transfer process smoothly. Although it is more likely that carotenoids would behave as a photoprotection agent since they are outnumbered by bacteriochlorophylls.

1.2.3 Phycobilisomes

The phycobilisomes (PBSs) are the primary light harvesting complex in cyanobacteria and red algae.[20-22] They are placed in between thylakoid membranes attached to the membrane bound PS I and PS II. The function of the phycobilisome is to absorb mid-visible solar light and transfer that energy to the nearest chlorophyll in PS I and PS II. The structure of the intact phycobilisome from various cyanobacteria and red algae was determined by different methods like TEM, SEM[23,24] and recently with cryo-EM.[25-27] Four morphological types of PBS are known - hemidiscoidal, hemielipsoidal, block-type and bundle-type.[27] We will mostly focus into hemidiscoidal structures that have two main parts - core region (2-5 inner cylinders) and rods (6-8 cylinders around core).[20,24,28] The rods are the cylindrical stack of disk-shaped phycobiliproteins phycocyanin, phycoerythrin, and phycoerythrocyanin attached to the core region. The core is the cylindrical structure made of disk shaped phycobiliproteins allophycocyanin. The bilin molecules (open chain tetrapyrrole) covalently bind to the phycobiliprotein as chromophores via a specific thio-ether bond. There are a second class of proteins that are called Linker Proteins (LPs) which

are mostly non-chromophorylated.[29] The function of LPs is to structurally link adjacent phycobiliprotein disks to form cylindrical structure. Recent studies suggested that LPs might be assisting energy propagation through the complex by tuning the spectra of the phycobiliproteins.[28,30]

The smallest structural unit in a phycobilisome is the (αβ) monomer that is a heterodimer made of one α-subunit and one β-subunit of phycobiliproteins. Three monomers self-assemble in a circular trimer $(\alpha\beta)_3$ and then two trimers attach face-to-face to form hexamer $(\alpha\beta)_6$. This hexamer represents a 'disk' in the structure of phycobilisomes. Each disk has a diameter of ~12 nm and ~6 nm of thickness. Also, disks are subdivided into two equal halves with ~3 nm thick.[24] Usually the rods contain 2-4 hexameric $(\alpha\beta)_6$ disks of phycocyanin (PC). The phycocyanin (PC) binds with three phycocyanobilin chromophores at specific sites; α84, β84 and β155. In a trimer α84 and β84 phycocyanobilin form a pair and center-to-center distance between two chromophores is ~20 Å. In adjacent hexamers the chromophores are located in even closer proximity that facilitate disk to disk energy transfer.[27] The phycocyanobilin absorbs a broad range (500-680 nm) of solar light (λ_{max} = 620 nm). AN Glazer[20,31] reported that linker proteins in the rods tune the spectroscopic properties of each disk in the rods in a way that the core-distal disks have slightly blue-shifted absorption maxima than the core-proximal disks. This arrangement creates a funnel shaped energy structure. This funnel structure enhances for some phycobilisomes when they incorporate phycoerythrin (PE) or phycoerythrocyanin (PEC) at the end of the rods. The phycoerythrin (αβ) monomer contains six phycoerythrobilin chromophores which have even more blue-shifted absorption maxima at ~570 nm. In the core four $(\alpha\beta)_3$ trimeric allophycocyanin (APC) form a cylinder. Each (αβ) monomer APC contains two

phycocyanobilin chromophores at the α84 and β84 position which have red-shifted absorption maximum than chromophores in CPC at 652 nm. The APC trimers closer to the photosystem (PS) II and I contain a special type of APC (terminal emitter) that absorbs light with even longer wavelengths (λ_{max} = 672 nm). In that way terminal emitters can exhibit better spectral overlap with chlorophyll a. So, intact phycobilisomes have constructed a nice funnel shaped energy landscape so that excitation energy can transfer from the rods to PS II through the core unidirectionally. A linker protein connects the terminal emitter to the membrane bound PS II.

Some cyanobacteria can participate in complementary chromatic adaptation (CCA) which is a response to the change in ambient light color and intensity.[32] Cyanobacteria capable of CCA have some photoreceptor that can sense the wavelength of the illuminating light and send a signal to synthesize more of the relevant phycobiliproteins and linker polypeptides to capture sufficient amounts of photons.[33] During CCA mostly the amount of the CPC and PE in the rods changes. In red light condition CPC accumulates in the rods and in presence of green light PE has higher number disks in the rods. Under red light illumination PBSs tend to have a lower number of average disks in the rods than that of the white light grown PBS.[23] In low light conditions like in the depth of the sea, cyanobacteria produce phycobilisomes with longer rods or higher number of phycobilisomes per cell so that they can capture maximum photons. More detailed information regarding CCA has been written in section 3.1.

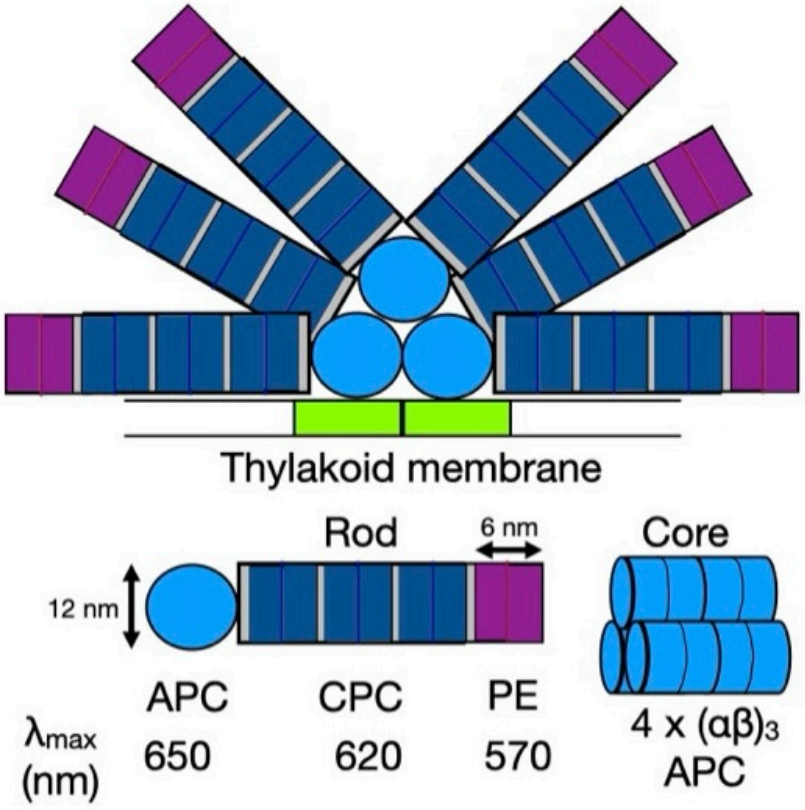

Figure 1.4. Schematic representation of a model intact phycobilisomes that has six rods and a tricylindrical core isolated from *Fremyella diplosiphon* grown under white light.[23] The green rectangles are photosystem II. Each cylinder in the core contains four $(\alpha\beta)_3$ trimeric allophycocyanin (APC, light blue color). The rods have three phycocyanin (CPC, dark blue color) and one phycoerythrin (PE, pink color) disk. The diameter of each disk is 12 nm and thickness is 6 nm. Absorption maximum for each phycobiliprotein is provided.

1.3 Energy Transfer Mechanisms

The electronic excitation energy transfer mechanism involving coupling of the electric dipole-dipole interaction of the chromophores depends on the relative orientation of the chromophores and distance between them. There are mainly two types of energy transfer mechanisms: incoherent and coherent energy transfer mechanisms. The relative coupling between the chromophores and with the surroundings (system-bath coupling) dictates which mechanism to follow for transferring excitation energy.

1.3.1 Incoherent Mechanism

Excitation energy moves via an incoherent mechanism if the interchromophore coupling is weak compared to the system-bath coupling. In this scenario there is no mixing of the energy states of the chromophores and excitation energy is localized on the donor before the transition. Therefore, energy transfer occurs by hopping from donor (D) to acceptor (A). The energy transfer rate for a donor-acceptor pair can be calculated from the expression of the Förster theory[34,35]

$$k = \frac{2\pi}{\hbar} |V|^2 \int_0^\infty d\varepsilon \, I(\varepsilon_D, \varepsilon_A, \varepsilon) \qquad (1.1)$$

where k is the excitation energy transfer rate, V is the electronic coupling between chromophores, and $I(\varepsilon_D, \varepsilon_A, \varepsilon)$ is the spectral overlap. Usually, it takes several picoseconds to transfer energy from donor to acceptor via this incoherent mechanism.

1.3.2 Coherent Mechanism

In the case of the strong electronic coupling between chromophores compared to system-bath coupling, energy transfer occurs via a coherent mechanism. In this scenario excited energy states of the chromophores are mixed to create exciton states and they share a common ground state. Excitation energy is delocalized over the chromophores.

Here a simplified quantum picture for the formation of the exciton states from two identical monomers has been shown following Cantor and Schimmel.[36] Assume there are two chromophores, A & B, which have two electronic states; ground state, 0 and excited state, 1. In the first case, there is no interaction between two chromophores. So, the ground state of the dimer would be when both monomers are in the ground state. The first excited state would be one monomer in the excited state and the other one in the ground state. It does not matter which one is in the excited state since they both have the same energy. The

dimer's Hamiltonian would be the addition of the monomer Hamiltonians (equation 1.2) and wavefunction of the dimer would be the multiplication of the monomer wavefunctions.

$$\hat{H} = \hat{H}_A + \hat{H}_B \quad (1.2)$$
$$\Psi_{A0,B0} = \Phi_{A0}\Phi_{B0} \quad (1.3)$$
$$\Psi_{A1,B0} = \Phi_{A1}\Phi_{B0} \quad (1.4)$$
$$\Psi_{A0,B1} = \Phi_{A0}\Phi_{B1} \quad (1.5)$$

Equation 1.3 represents the ground state of the dimer. Equations 1.4 and 1.5 are the excited states of the dimer. In Equation 1.4 the monomer A is in the excited state and the monomer B is in the ground state. In Equation 1.5 monomer A is in the ground state and monomer B is in the excited state.

In the second case we would assume that two monomers are electronically interacting, but the electrons are localized on each monomer (weak coupling). In this scenario the Hamiltonian would have a new term (V_{AB}) due to the dipole-dipole interaction (Equation 1.6). Since the new interaction is only a perturbation, the same noninteracting monomer wavefunctions can be used. The ground state wavefunction would not have any effect in the new interacting system. But the perturbation would create exciton states that can be expressed as the linear combination of the excited state wavefunction of the noninteracting dimers (Equation 1.7 and 1.8).

$$\hat{H} = \hat{H}_A + \hat{H}_B + V_{AB} \quad (1.6)$$
$$\Psi_{1+} = 1/\sqrt{2}\,(\Psi_{A1,B0} + \Psi_{A0,B1}) \quad (1.7)$$
$$\Psi_{1-} = 1/\sqrt{2}\,(\Psi_{A1,B0} - \Psi_{A0,B1}) \quad (1.8)$$

The energy of the exciton states can be calculated using the Schrödinger equation. The energy of the two states is no longer the same which is the case for the noninteraction dimer case. Here two exciton states are separated by $2V_{12}$. The electronic coupling has splitted the excited state of the dimer which is also called exciton splitting.[36]

1.4 Energy Transfer in Intact Phycobilisomes

The intact phycobilisome would be a great model system to study excitation energy transfer mechanisms due to its unique properties like water solubility, abundant in each corner of the world, funnel-shaped energy structure and major light-harvesting complex in single cellular prokaryotes. Also, phycobilisomes have high quantum efficiency (<90%).[37] If we can understand the excitation energy transfer mechanisms then we can design better artificial light-harvesting materials that would extract more energy from solar panels, store more energy in batteries and speed up information transport and processing.

Over the years researchers studied excitation energy transfer processes in intact phycobilisomes and phycobiliproteins in vivo and in vitro employing different instrumental techniques. In late 1950s and 1960s, Rabinowitch and co-authors measured the fluorescence lifetimes of Chlorophyll a and phycobiliproteins in *Porphyridium cruentum* using a nanosecond flashlamp technique which entailed deconvolution of the fluorescence decay from the flashlamp profile.[38–40] They reported that B-phycoerythrin transfers energy to R-phycocyanin in 300 ± 200 ps timescale and then energy moves to chlorophyll a through allophycocyanin in 500 ± 200 ps time.[39]

In the 1970s and 1980s researchers studied several photophysical properties of the isolated phycobiliproteins like the excitation energy transfer and coupling between chromophores, fluorescence lifetimes and quantum yield.[41–49] Fluorescence lifetime of an individual bilin chromophore in isolated phycobiliproteins was reported 2-4 ns.[41,43] Kobayashi et al. reported from their picosecond studies on CPC that energy transfer occurs faster between chromophores in larger aggregates (hexamer, trimer) than monomers.[42] Similar results were obtained by Holzwarth et al.[45] and Sauer et al.[48] This result indicates

that chromophores are better positioned in $(\alpha\beta)_6$ hexameric form in phycobiliproteins to perform an efficient energy transfer process. This might be the driving force to form hexameric disks in intact phycobilisomes. The entire phycobilisome assemble that has even higher ordered packing, would accelerate this process.

The first picosecond laser spectroscopy study of excitation energy transfer in intact phycobilisomes inside the *Porphyridium cruentum* cells and isolated condition was reported by Searle et al.[50,51] They showed that energy moves from B-phycoerythrin to R-phycocyanin in 70 ps and to allophycocyanin in 120 ps in isolated phycobilisomes. A much slower kinetics was suggested by Grabowski and Gantt for energy transfer from phycoerythrin to phycocyanin in 280 ps that would take about 28 energy jumps to reach energy to the final point. Several picosecond fluorescence spectroscopy studies produced similar time constants to Searle et al.[52–58] All these kinetic models suggested hoping style Förster mechanism for excitation energy transfer between chromophores in rods and core of phycobilisomes. This is no surprise given that the chromophores are ~2 nm apart in the protein residue and expected to have weak interaction between them with respect to the surroundings. It takes about 10 ps to transfer energy between two chromophores 2 nm apart. Therefore the results suggest that excitation transfer from the rod to the core of the phycobilisomes try to minimize the 'random walk' of the excitation quantum and be as direct as possible.[20] T Katoh and coworkers observed specific few energy transfer pathways in intact phycobilisomes at -196 ^{0}C.[59]

In apparent conflict with this picture, several femtosecond and picosecond spectroscopy studies indicated that there is delocalized exciton state present in isolated allophycocyanin due to intermediate to strong electronic coupling between α84 and β84 chromophores.[60–65]

Beck and co-authors measured a ~30 fs anisotropy component originated from interexciton state relaxation using two-color femtosecond pump-probe anisotropy experiment on allophycocyanin trimers.[61] This delocalized exciton picture was supported by single-molecule fluorescence experiments from Ying and Xie.[66] Their experiments showed the formation of exciton traps within the three quasi-independent pairs of strong interacting α84 and β84 chromophores in APC and photobleaching of individual chromophores. The work of Womick and Moran further supported the delocalized picture.[67] They performed transient grating and photon echo spectroscopies in dimer of allophycocyanin and applied a vibronic exciton picture where the electronic coupling is enhanced by matching the exciton state energy gap with the ~800 cm^{-1} Hydrogen out-of-plane (HOOP) mode of the bilin chromophores in APC trimer.[67,68] They also studied the excited state relaxation mechanisms R-phycoerythrin and C-phycocyanin using their transient grating and two-dimensional photon echo spectroscopy instrument.[69,70] The α84-β84 pairs in CPC have stronger system-bath interaction and showed three times slower electronic relaxation than that of the APC. In R-PE delocalized states are present between six pairs of phycoerythrobilin chromophores and sub-100 fs exciton relaxation processes occur. Wang and Moerner performed single-molecular experiments on monomers and trimers of allophycocyanin. They reported that after trimer formation α-chromophore shows red-shifted spectral properties and β-chromophore quenches the excited state of the α-site.[71] Here they assumed the chromophores in weak-coupling regime and failed to explain the narrow lineshape and fast energy transfer.

In recent times van Amerongen and coworkers performed picosecond time-resolved fluorescence measurements using the streak-camera instrument which has ~9 ps

instrument response in whole cells[72] and in isolated intact phycobilisomes from *Synechocystis* 6803.[12] They reported transfer of excitation in whole cells from CPC to down the rods in 6-9 ps. Then it takes 40 ps to move energy from CPC to APC_{660}. Finally, excitation transfers to APC_{680} in 120 ps. Another study from van Stokkum et al. showed more complicated global and target model with more compartments from time-resolved difference absorption spectroscopy measurements on intact phycobilisomes isolated from *Synechocystis* 6803.[13] In these models energy transfer pathways were considered as reversible. Akhtar et al. reported longer time constants for transfer of excitation in intact phycobilisomes isolated from *Anabaena variabilis* (PCC 7120) where they employed TCSPC experiments with 50 ps IRF. In this study they found an additional time constant 500-700 ps which might have originated from an energy transfer process in the core of the phycobilisome or an intrinsic quenching mechanism.[73] All these picosecond energy transfer steps were modeled using the Förster picture.

A femtosecond pump-probe spectroscopy (IRF 120m fs) work by Nganou et al.[14] in intact phycobilisomes isolated from *Thermosynechococcus vulcanus* detected sub-ps (900 fs) time constants that were assigned to excitation transfer down the rods via a coherent energy transfer mechanism. To flow energy in sub-ps time scale chromophores in rods need to form delocalized exciton states and that requires a structure where the chromophores in adjacent hexamers are in fairly short distances. Single-particle EM and cryo-EM structures of the intact phycobilisome from cyanobacteria[30] and red algae[27] respectively suggest that the chromophores are closer to each other in adjacent hexamer compared to that of the trimer. This information indicates that there is possibility to have intermediate to strong electronic couplings down the rods.

From the previous discussion, it is evident that there are two excitation energy transfer mechanisms (incoherent and coherent) present in the literature for intact phycobilisomes. Presence of delocalized exciton states were detected for other light-harvesting complexes like FMO, phytochromes, peridinin-chlorophyll *a* protein (PCP) using multidimensional femto-second ultrafast spectroscopy.[4,74–76] Therefore, it is strongly suggested that multidimensional spectroscopy with ultrashort pulses will be used to study excitation energy transfer mechanisms in intact phycobilisomes isolated from cyanobacteria. This study can answer whether or not there is delocalized exciton state present in the rods of the phycobilisomes. Also, it can be investigated how excitation slows down in the core of phycobilisomes to operate photoprotection mechanisms smoothly.

1.5 Two-dimensional Electronic Spectroscopy (2DES)

Two-dimensional electronic spectroscopy (2DES)[77–81] is a powerful tool to investigate the excitation energy transfer mechanisms in natural[4,74,75,82–84] and artificial[85–90] light-harvesting systems. 2DES is a correlation spectroscopy that measures the pump induced change in the emission signal from the sample. 2DES have several advantages over the conventional femtosecond pump-probe and transient absorption spectroscopy. 2DES provides high resolution in the spectral and temporal space simultaneously. The broadband laser spectrum (Figure 1.14) used in 2DES can cover several excited states at the same time. Also, the short laser pulses can identify the electronic and vibrational coherences in the ground and excited states and their involvement in the excitation energy transfer process. More importantly 2DES can detect the evolution of the excitation energy from donor to acceptor over time.

1.5.1 Excitation Pulse Sequence in 2DES

2DES is a nonlinear spectroscopic technique that uses three short (<10 fs) laser pulses scanned over two different time delays (Figure 1.5). The time delay between the first two pulses is coherence time τ and the delay between second and third pulse is population time T. In this setup the first two pulses are pump pulses that excite the sample, and the third one is the probe pulse that detects the excited state dynamics of the sample. The first pulse ($\boldsymbol{k_1}$) interacts with the sample and creates a coherence. Coherence is a linear superposition of ground and excited states. The coherence then evolves over the coherence time τ and undergoes free-induction decay. When the second pulse ($\boldsymbol{k_2}$) interacts with the sample, it drives the coherence into a population localized in either ground or excited state. The population then evolves along the population time T when the third pulse ($\boldsymbol{k_3}$) interacts with the sample. The interaction with the third pulse creates another coherence that in turn emits an electric field. The emitted signal ($\boldsymbol{k_s}$) travels along a specific direction ($\boldsymbol{-k_1+ k_2+ k_3}$). For the boxcar setup a low intensity laser beam passes through the sample named local oscillator (LO) used for heterodyne detection along the direction of the signal. For the pump-probe geometry the pump pulses propagate along the same direction ($\boldsymbol{k_1 = k_2}$) and the signal emits along the direction of the probe ($\boldsymbol{k_3}$) and therefore, the probe beam acts as a LO. The emitted signal is detected as a pump-induced change in the probe transmission.

1.5.2 Third-Order Nonlinear Optical Responses

There are three types of signals that can be detected using 2DES. They are ground-state bleaching (GSB), stimulated emission (SE), and excited-state absorption (ESA). Jonas group[77,91,92] and Fleming group[78,80] developed the fundamental theoretical formulation for the two-dimensional electronic correlations. The phenomenological interpretation of the

third order signals presented in this section are adopted from the work of Mukamel,[93] Hamm, and Zanni.[94] The above mentioned signals will be explained with the Albrecht wave mixing energy level diagram (WMEL).[95] WMEL representation is similar to the double-sided Feynman diagram (not shown here). Only three energy level systems are shown here to keep it simple. The horizontal lines in the WMEL represent energy levels in the system. The energy levels are labeled as '*g*' for ground state, '*e*' for the first excited state, and '*f*' for the second excited state at a higher energy level. The vertical arrows in the WMEL represent the interaction of each laser pulse with the sample. The solid arrows act on the 'bra' side and the dotted arrows acts on the 'ket' side. The only dotted lines represent the third order signal from the sample. Time progresses from left to right in WMEL.

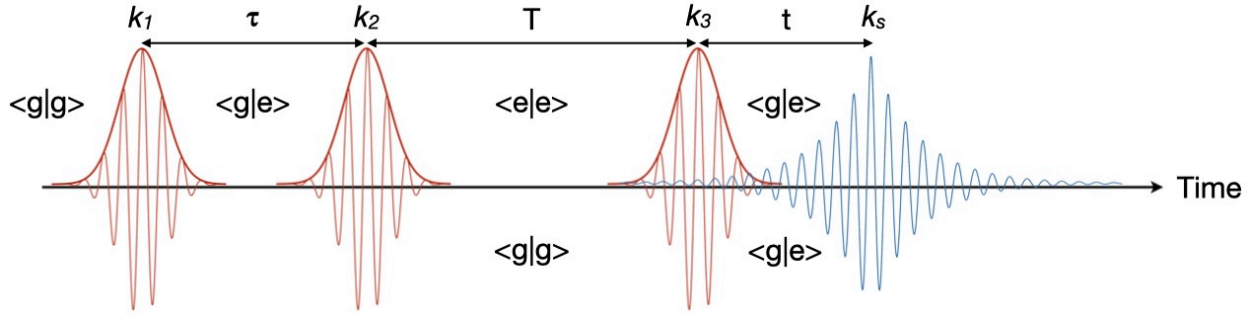

Figure 1.5. Broadband pulse sequences in the 2DES experiment. The red Gaussian pulse envelopes depict the excitation pulses in the pulse sequence. The blue signals represent the coherences emitted from the sample after the interaction of the pulses. The first pulse creates coherence that evolves over time, followed by the interaction of the second pulse to create a population. The third pulse interacts with the system to create another coherence and an evolving electric field (blue) is emitted from the sample. The bra-ket notation shows a probable nonlinear third order pathway where '*g*' refers to ground state and '*e*' stands for excited state. Adapted from work by the Jonas group.[77]

Ground-state bleaching (GSB) is the signal emitted by the system after the first two pump pulse interactions prepares the population in the ground state. The ground state in the system is represented as <g|g> (Figure 1.6). After the interaction of the first pump pulse the system evolves to <g|e> or <e|g> state which is a coherence state between ground and

first excited state. The <g|e> state of the system is created by the action on the ket side and the <e|g> state is created after the action on the bra side. After coherence time τ second pulse interact with the sample and generates population in the ground state (<g|g>). The third pulse interaction produces another coherence <g|e> or <e|g> in the system which emits a signal. There are two types of pathways: rephasing and non-rephasing, depending on the phase of the two coherences created in the system. When the phase of the coherences originating from the first and third pulse action are same, the pathway is termed as 'non-rephasing'. In contrast, for the 'rephasing pathway' the first and third pulse action generate opposite phases.

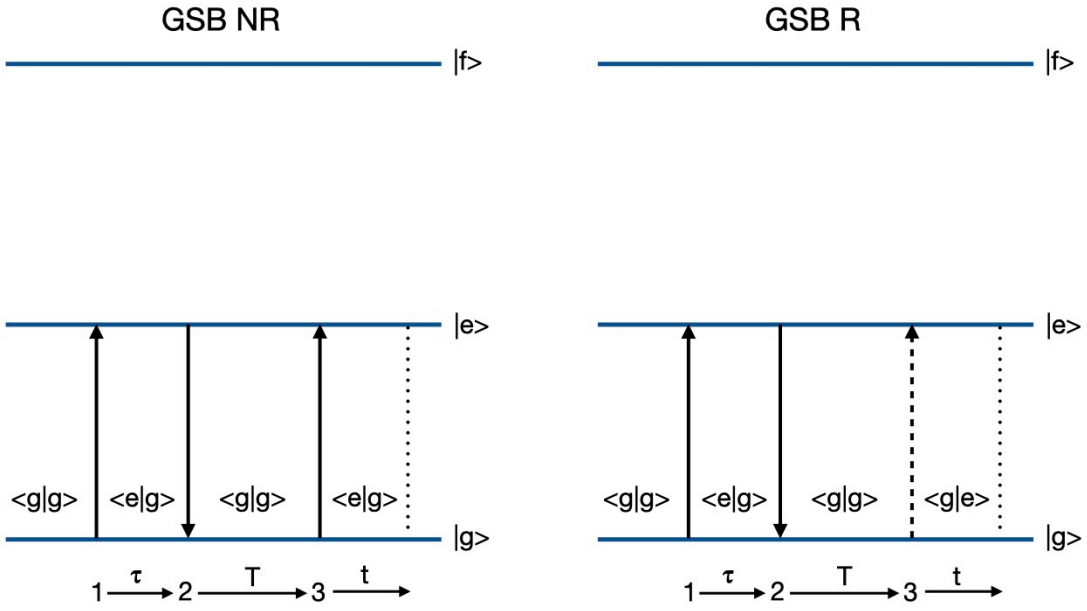

Figure 1.6. WMEL diagram of ground-state bleaching signal. The figure on the left correspond to the non-rephasing pathway, whereas the one on the right correspond to the rephasing pathway. In the WMEL diagram, time evolves towards the right, and the field matter interactions are numbered as 1, 2, and 3 with marked time delays. The solid arrows represent the field-matter interaction on the *bra* side, whereas the dashed arrows represent the interaction on the *ket* side. The dotted line in the WMEL and dashed arrows represent the emitted signal after a series of field-matter interactions.

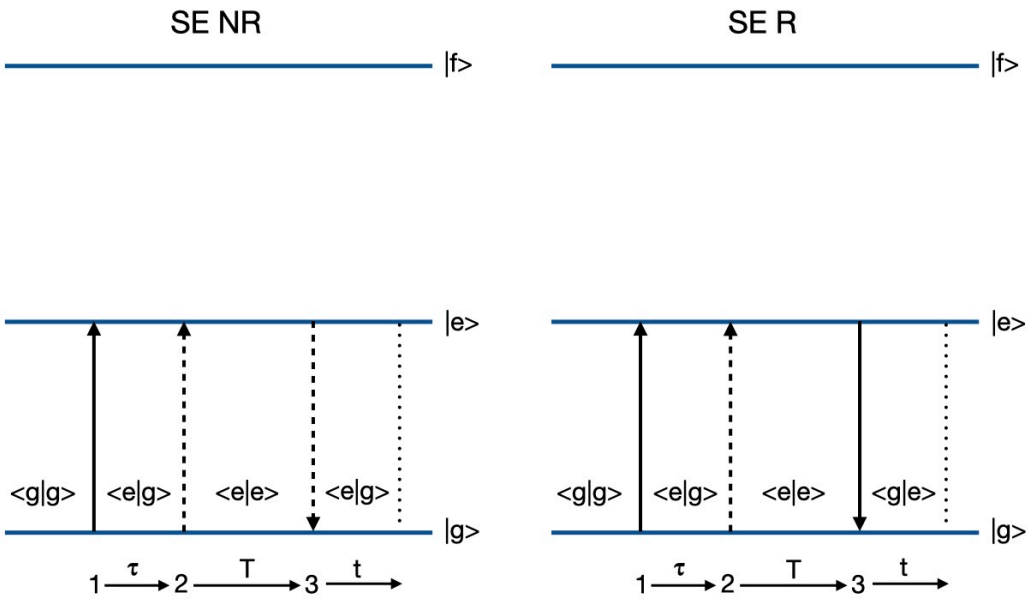

Figure 1.7. WMEL diagram of stimulated emission signals. The figure on the right correspond to the rephasing pathway, whereas the one on the left correspond to the non-rephasing pathway.

Stimulated emission (SE) is the signal emitted by the system after the first two pulses constructed the population in the first excited state (Figure 1.7). Similar to GSB signal the first pulse interaction creates coherence in the system (<g|e> or <e|g>). In contrast to GSB signal the second pulse interaction produce a population in the first excited state (<e|e>). The third pulse interaction drives a downwards coherence <g|e> or <e|g> in the system. This coherence emits a signal that can be detected as SE.

Excited-state absorption (ESA) signals generate from the coherence between two excited states (Figure 1.8). Similar to SE signal, for ESA the first pulse interaction makes a coherence <g|e> or <e|g> between ground state and first excited state and the second pulse interaction generate population <e|e> in the first excited state. In contrast to SE, the third pulse interaction drives an upwards coherence <f|e> or <e|f> in the system for ESA. The coherence emits a signal with the frequency of the energy difference between states *e* and *f*.

The direction of the signal can be calculated by applying the law of conservation of momentum. The signals from non-rephasing pathways would be along the direction $\boldsymbol{k_1 - k_2 + k_3}$ whereas for rephasing pathway signals the direction would be $\boldsymbol{-k_1 + k_2 + k_3}$ (here $\boldsymbol{k_1}$, $\boldsymbol{k_2}$, and $\boldsymbol{k_3}$ are the vector representation of the three pulses respectively). In practice, the laser beams are arranged in a boxcar geometry where the first three pulses are aligned in a fashion that they form the corners of a box, and the signal appears at the fourth corner of the box. For the detection of the rephasing and non-rephasing signals alignment of the instrument remains the same, only the ordering of the first two pulses is altered.

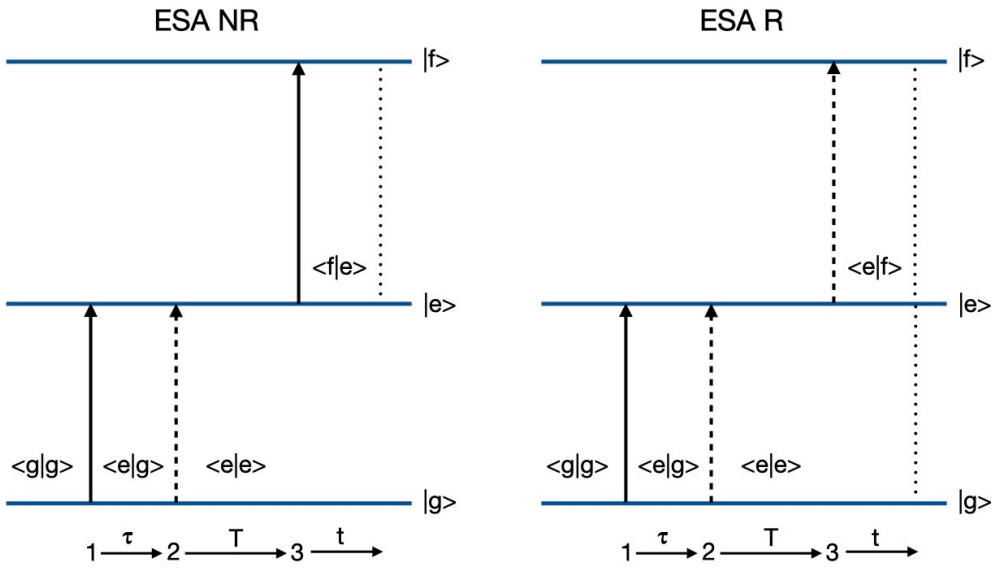

Figure 1.8. WMEL diagram of the excited-state absorption signal. The figure on the right correspond to the rephasing pathway, whereas the one on the left correspond to the non-rephasing pathway.

1.5.3 Quantum Coherences in 2DES

The broadband laser spectrum used in the 2DES with ultrashort laser pulses can cover a wide range of electronic and vibrational states within both excited and ground states. This raises the possibility to observe the evolution of the coherent wavepacket motions[96–99] and

detect the electronic, vibrational and vibronic coherences.[77,79,100,101] These coherences have distinct characteristics in damping times and position in the 2D spectrum.

Electronic coherences can be detected in strongly coupled chromophores where they share a common ground state and form exciton states. The electronic coherences can be characterized by their frequency of oscillations and crosspeak positions at the 2DES spectra. For example (Figure 1.9), consider an energy level diagram that contains two excited states *1* and *2* with a common ground state *g*. The first pulse creates coherence <1|g> and the second pulse drives the system to a new state <1|2>. In this case the new state is also a coherence state between two excited electronic states. This will evolve along the population time *T*. The frequency of this oscillating signal from the coherence will be equal to the energy difference between state *1* and *2*. The coherence signal will appear as crosspeaks symmetrical with respect to the diagonal in the 2DES spectra. The damping times of these coherences are typically in the order of tens of femtoseconds.

Vibrational coherences are observed between the vibrational energy levels in both the ground and excited states. Vibrational coherence peak patterns in the 2D spectrum depend on the Frank-Condon overlap of the excited state energy levels.[102,103] The peak patterns are spaced along the detection axis in the 2D spectrum according to the vibrational quanta. Higher intensity vibrational coherence peaks can be found along the lower energies of the excited states.[102,104,105] As an example of the origin of the vibrational coherence in the excited state (Figure 1.10), let's assume a two-level system, ground (*g*) and excited (*e*) state with two vibrational levels, v = 0 and 1. The first light-matter interaction drives the system to the second vibrational state of *e* represented by $\langle g_0|e_1\rangle$. The next interaction moves the system to $\langle e_0|e_1\rangle$ state. Therefore, it develops a coherence between two vibrational states

from the first excited state, *e*. This coherence evolves along the population time *T* and exhibits a frequency equal to the energy difference between two vibrational levels. The vibrational coherences in excited states provide information on the vibrational motions acting in the excited states upon excitation. The damping times of these coherences depends on the coupling between the electronic states and vibrational motions and the lifetime of the excited states.[106,107] Some of the vibrational coherences are long lived and detectable at the product states after the relaxation of excitation to the lower energy states.[108]

Vibrational coherences at the ground-state are observed when the two excitation pulses generate coherence between the ground vibrational states of the system. (Figure 1.11) The first interactions drives the system upwards to $<g_0|e_0>$ state. Then the second interaction steers the system downward to $<g_0|g_1>$ state. This produces a coherence between the two vibrational levels in the ground state. This coherence moves along the population time *T* with a frequency of the difference between two vibrational levels. The dephasing time of the vibrational coherence is about several hundreds of femtoseconds.

In real case scenarios like photosynthetic light-harvesting systems there are multiple electronic states with several vibrational levels in them. In those situations, it is very difficult to isolate a particular coherence. For most cases multiple coherences will be coupled together. A sophisticated multidimensional spectroscopy instrument with broadband ultrashort laser pulses required to identify all those coherences present in the system.

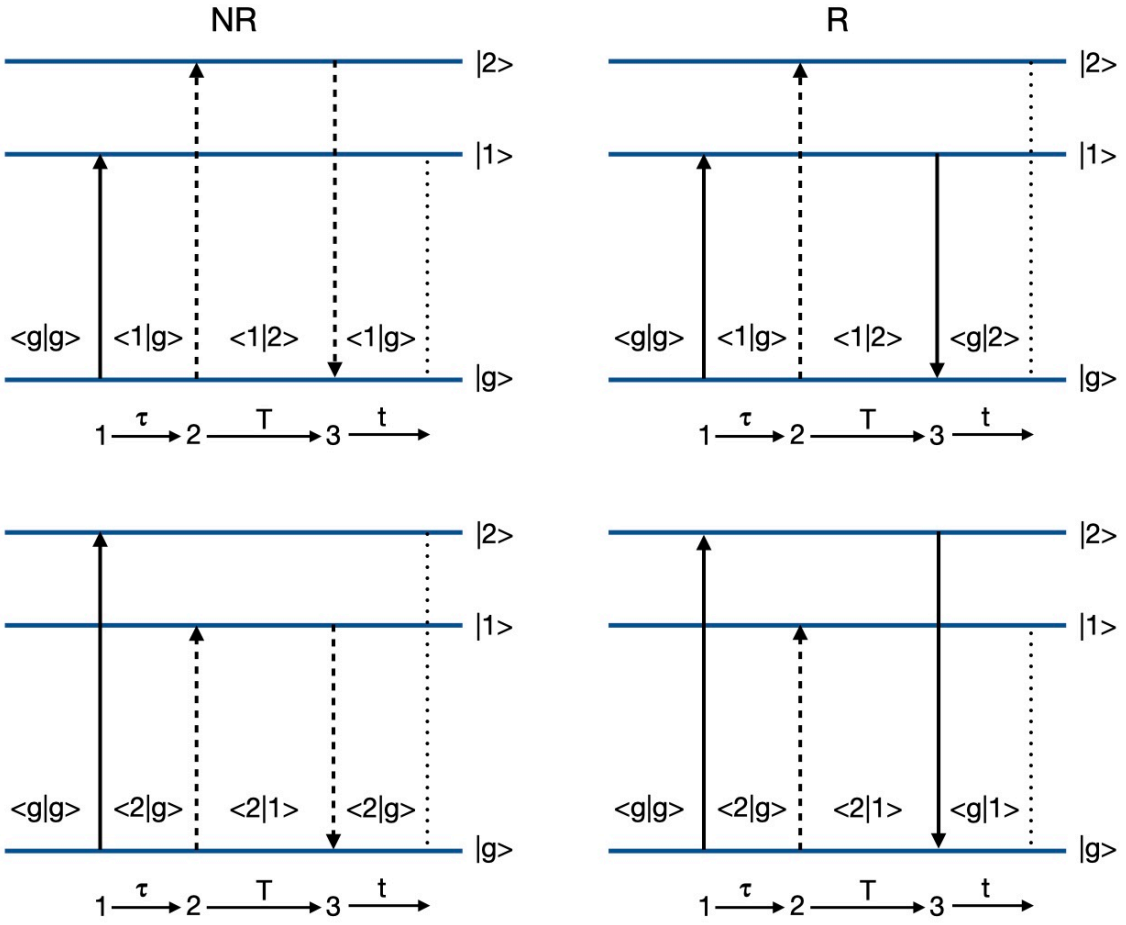

Figure 1.9. Example WMEL diagram for electronic coherences between excited electronic states, *1* and *2*. The figures on the right correspond to the rephasing pathway, whereas those on the left correspond to the non-rephasing pathway.

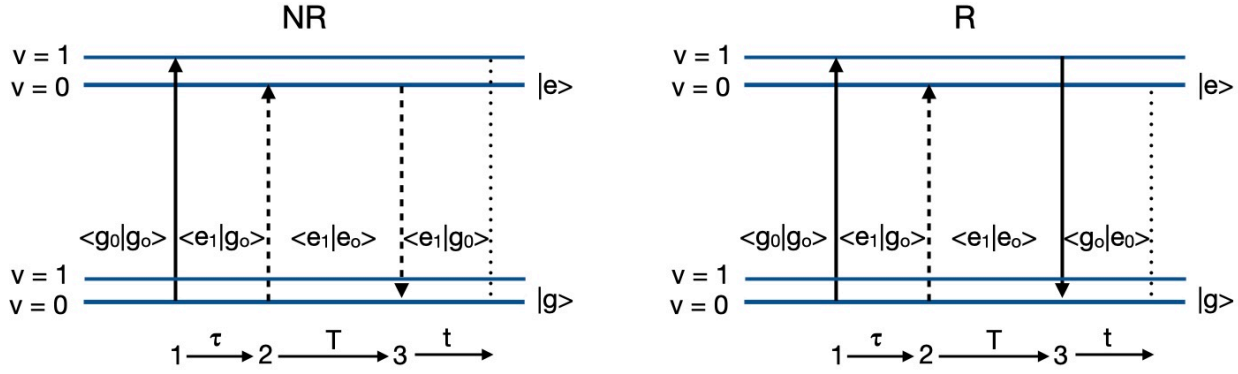

Figure 1.10. Example of WMEL diagram for vibrational coherences between vibrational levels (v = 0 and 1) in the excited electronic state, *e*. The figure on the right correspond to the rephasing pathway, whereas the one on the left correspond to the non-rephasing pathway.

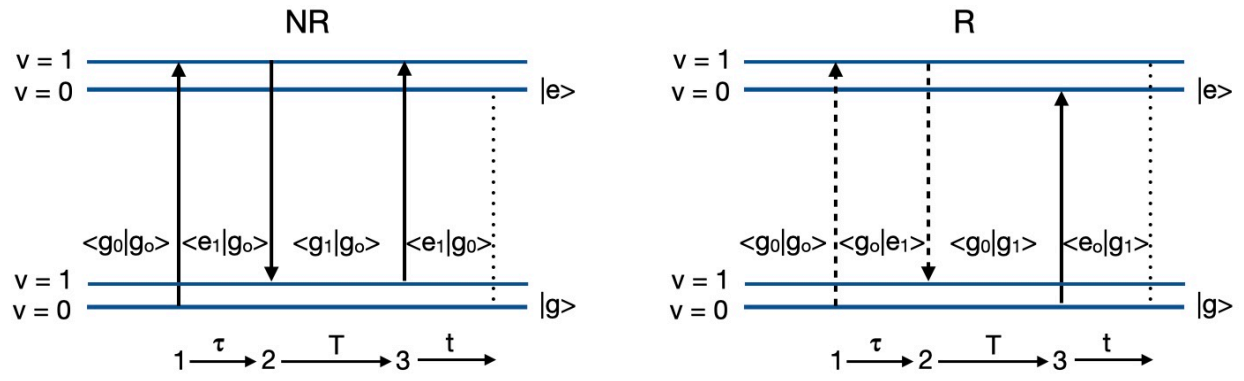

Figure 1.11. Example WMEL diagram for ground-state vibrational coherences (stimulated Raman) between ground and excited electronic state. Vibrational states are indicated by v = 0 and 1. The figure on the right correspond to the non-rephasing pathway, whereas the one on the left correspond to the rephasing pathway.

1.5.4 Interpretation of 2DES Spectra

Usually, 2DES signals at a particular population time, *T* are plotted as a contour diagram where x-axis is the excitation axis, and the y-axis is the detection axis. The excitation axis is created from the FT of the signals with respect to the coherence time, τ. The detected axis is produced directly from the CCD. Figure 1.12 shows a sample 2DES spectrum which is a correlated spectrum. It represents the pump induced change in the intensity of the probe beam. Both axes are in frequency unit. The red color peaks are coming from the positive signals and the blue color peaks are the negative signals. The signals are normalized with respect to the maximum signal at that population time, *T*.

At early time we would expect to observe mostly diagonal peaks due to ground state bleaching (GSB) and stimulated emission (SE) signals. The GSB and SE signals are positive in our setup shown in red color. The early time peaks contain inhomogeneous broadening. At later population time the peaks will have more homogeneous broadening lineshape. The diagonal diameter is coming from the homogeneous and inhomogeneous line broadening whereas the off-diagonal diameter is generating only from the homogeneous broadening.

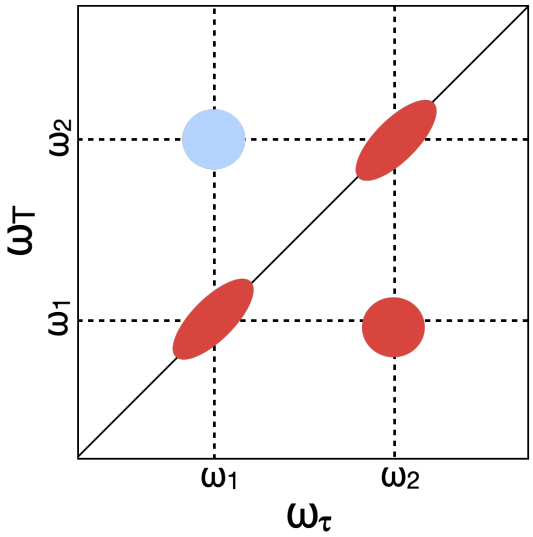

Figure 1.12. An example 2DES spectrum. Both axes are in frequency (ω) unit. The x-axis is excitation axis, and the y-axis is detection axis. The red color peaks are positive signals originating from GSB and SE whereas the blue peak represents negative signal from ESA.

Here Figure 1.12 shows that there are two different chromophores present in the system and they absorb ω_1 and ω_2. The above the diagonal blue peak represents an excited state absorption (ESA) peak which has a negative signal. The coordinate of the ESA peak is (ω_1, ω_2) which indicates that the excited state population was created using two pump pulses with ω_1- frequency and then the probe pulse with ω_2- frequency created a coherence between the first excited state and the higher excited state. The peak due to energy transfer would appear as below the diagonal positive peak. Figure 1.13 shows a WMEL diagram for an energy transfer process between two chromophores. Here first two pump pulses with ω_2- frequency creates a population at the excited state <2|2> of the chromophore 2. Before the probe pulse interacts with the system excitation population has been transferred to excited state <1|1> of the chromophore 1. Then probe pulse with ω_1 interacts with the sample and creates a coherence between excited state and the ground state of the chromophore 1. Therefore, we would observe a below the diagonal cross peak

at (ω_2, ω_1) in the 2DES spectra. The energy transfer peak has homogeneous ground state. This is because that the energy transfer peak is expected to appear at later population time.

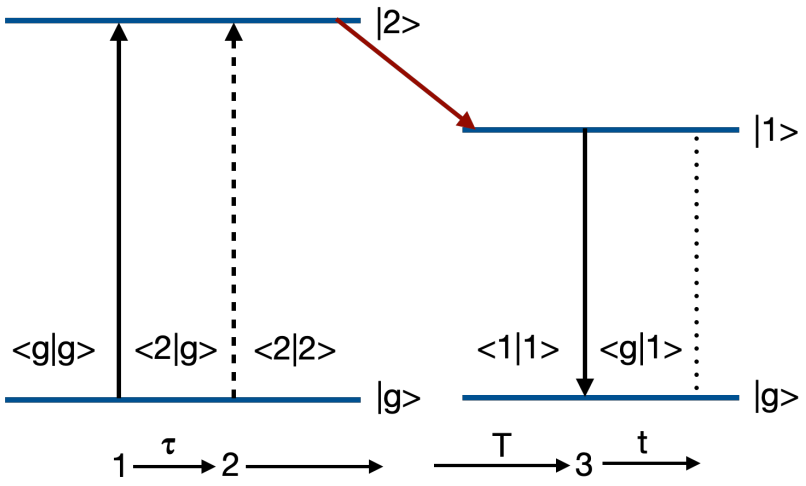

Figure 1.13. WMEL diagram for the energy transfer process between two chromophores. The red arrow represents the energy transfer from chromophore 2 to chromophore 1.

1.6 Data Processing and Analysis

A two-dimensional electronic spectroscopy (2DES) instrument (Figure 1.15) was used to acquire the data presented in this thesis. The details of the 2DES set up in Beck laboratory can be found in the next chapter section 2.2.3. The 2DES setup is based on the approach by Zanni and coworkers[109,110] and Ogilvie and coworkers[111] where they implemented a pump-probe geometry. The signal detected in pump-probe geometry is the sum of both nonrephasing and rephasing pathways.

In a 2DES experiment, a series of spectra are collected for each population time *T*. The population *T* spans from -3 ps to 300 ps. These spectra contain amplitudes detected at each binned pixel of the CCD for each coherence time, τ point. The time τ spans from 0 to 50 fs with 0.5 fs steps. So, there are 101 spectra for each time *T*. Data files for each spectrum contain 256 X 101 array of amplitudes where 256 is the total number of the binned CCD

pixels. The acquisition of the data is controlled by the home-built LabVIEW (National Instruments) scripts.

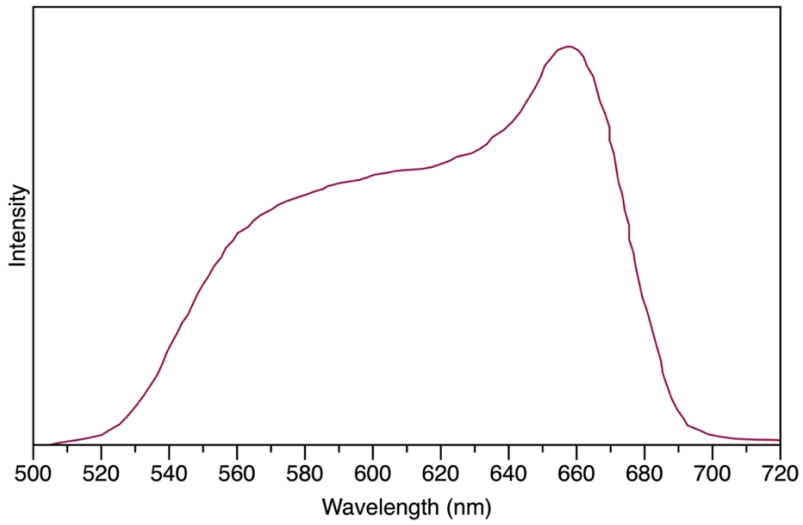

Figure 1.14. An example broadband laser spectrum in the range of 510-710 nm used in 2DES experiments. The full width at half maximum (FWHM) is 120 nm and the transform limited pulse duration was 6.7 fs.

The amplitude of FFT for pump-induced change in probe-transmission decays with time and damps out ~20 fs. An offset is subtracted to bring the oscillations centered around zero. The time points after the decay are removed and replaced with zeros. The amplitude at each detection wavelength is mirrored and concatenated since the signal oscillations are symmetrical. The data is further zero-padded to create 2^N data points for FFT analysis. The FFT output contains both real and imaginary components. The real components are extracted and plotted as a contour diagram that has excitation energy on the x-axis and detection energy on the y-axis. A series of 2D spectra is generated by repeating this process for each *T* point. Several iterations of data are taken for doing the average to get a better signal to noise ratio and calculate the 95% confidence interval at each data point. All these steps are performed using home-built MATLAB scripts.

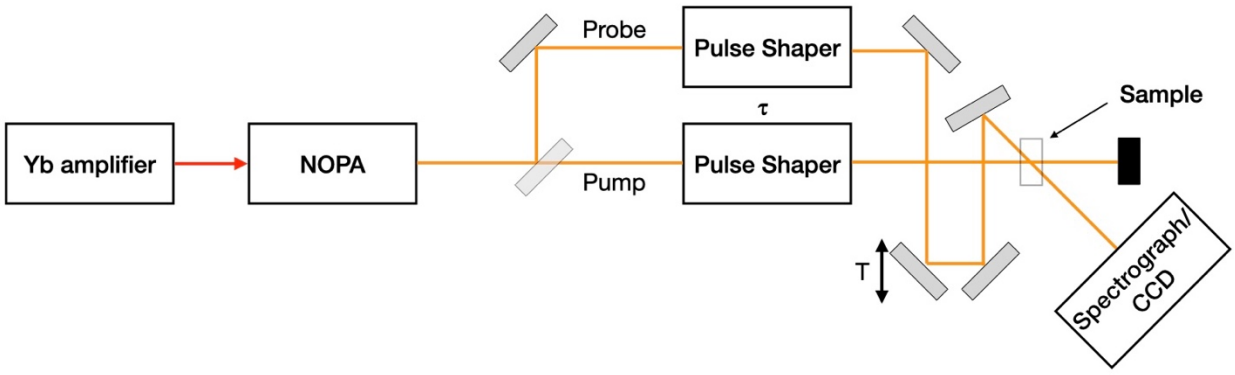

Figure 1.15. Instrumentation set up used in the 2DES experiments. The Yb laser (4W, 100 kHz, 1040 nm) is pumped to a NOPA to generate broadband visible pulses ranging from 500-700 nm. The adaptive pulse shapers compress the pulses. The pulse shaper on the pump beam creates the pulse pair and control the time (τ) between them. A time-of-flight delay stage is used to vary the time delay (T) between the pump and the probe beams. The emitted signals are collected using a home-built spectrograph and a fast CCD.

CarpetView software package (Light Conversion) is used to perform global and target models[112] that show the excitation energy transfer rates from one compartment to another for a multicompartment system. For 1D kinetic models, a part of the response along a desired excitation wavelength axis is averaged. This averaged data used as an input file that contains amplitude of the signals at all the detection wavelengths evolving with time *T*. The residuals are obtained at each data point by subtracting the response of the model from the actual signal. The residuals are used to perform FFT using Julia codes for obtaining the frequencies of the modulations. These modulation frequency data are used to prepare FT amplitude spectra and oscillation maps. The linear prediction singular value decomposition (LPSVD) analysis is performed to obtain the damping time of the modulation frequencies from the residual data using a MATLAB script.

REFERENCES

(1) Blankenship, R. E. *Molecular Mechanisms of Photosynthesis*; John Wiley & Sons, 2021.

(2) Mirkovic, T.; Ostroumov, E. E.; Anna, J. M.; van Grondelle, R.; Govindjee; Scholes, G. D. Light Absorption and Energy Transfer in the Antenna Complexes of Photosynthetic Organisms. *Chem. Rev.* **2017**, *117*, 249–293, DOI: 10.1021/acs.chemrev.6b00002.

(3) Wraight, C. A.; Clayton, R. K. The Absolute Quantum Efficiency of Bacteriochlorophyll Photooxidation in Reaction Centres of Rhodopseudomonas Spheroides. *Biochim. Biophys. Acta* **1974**, *333*, 246–260, DOI: 10.1016/0005-2728(74)90009-7.

(4) Engel, G. S.; Calhoun, T. R.; Read, E. L.; Ahn, T.-K.; Mančal, T.; Cheng, Y.-C.; Blankenship, R. E.; Fleming, G. R. Evidence for Wavelike Energy Transfer through Quantum Coherence in Photosynthetic Systems. *Nature* **2007**, *446*, 782–786, DOI: 10.1038/nature05678.

(5) Thyrhaug, E.; Tempelaar, R.; Alcocer, M. J. P.; Žídek, K.; Bína, D.; Knoester, J.; Jansen, T. L. C.; Zigmantas, D. Identification and Characterization of Diverse Coherences in the Fenna-Matthews-Olson Complex. *Nat. Chem.* **2018**, *10*, 780–786, DOI: 10.1038/s41557-018-0060-5.

(6) Hayes, D.; Engel, G. S. Extracting the Excitonic Hamiltonian of the Fenna-Matthews-Olson Complex Using Three-Dimensional Third-Order Electronic Spectroscopy. *Biophys. J.* **2011**, *100*, 2043–2052, DOI: 10.1016/j.bpj.2010.12.3747.

(7) Brixner, T.; Stenger, J.; Vaswani, H. M.; Cho, M.; Blankenship, R. E.; Fleming, G. R. Two-Dimensional Spectroscopy of Electronic Couplings in Photosynthesis. *Nature* **2005**, *434*, 625–628, DOI: 10.1038/nature03429.

(8) Polli, D.; Cerullo, G.; Lanzani, G.; De Silvestri, S.; Hashimoto, H.; Cogdell, R. J. Carotenoid-Bacteriochlorophyll Energy Transfer in LH2 Complexes Studied with 10-Fs Time Resolution. *Biophys. J.* **2006**, *90*, 2486–2497, DOI: 10.1529/biophysj.105.069286.

(9) Fidler, A. F.; Singh, V. P.; Long, P. D.; Dahlberg, P. D.; Engel, G. S. Timescales of Coherent Dynamics in the Light Harvesting Complex 2 (LH2) of Rhodobacter Sphaeroides. *J. Phys. Chem. Lett.* **2013**, *4*, 1404–1409, DOI: 10.1021/jz400438m.

(10) Ostroumov, E. E.; Mulvaney, R. M.; Anna, J. M.; Cogdell, R. J.; Scholes, G. D. Energy Transfer Pathways in Light-Harvesting Complexes of Purple Bacteria as Revealed by Global Kinetic Analysis of Two-Dimensional Transient Spectra. *J. Phys. Chem. B* **2013**, *117*, 11349–11362, DOI: 10.1021/jp403028x.

(11) Krueger, B. P.; Scholes, G. D.; Fleming, G. R. Calculation of Couplings and Energy-Transfer Pathways between the Pigments of LH2 by the Ab Initio Transition Density Cube Method. *J. Phys. Chem. B* **1998**, *102*, 5378–5386, DOI: 10.1021/jp9811171.

(12) Tian, L.; Gwizdala, M.; van Stokkum, I. H. M.; Koehorst, R. B. M.; Kirilovsky, D.; van Amerongen, H. Picosecond Kinetics of Light Harvesting and Photoprotective Quenching in Wild-Type and Mutant Phycobilisomes Isolated from the Cyanobacterium *Synechocystis* PCC 6803. *Biophys. J.* **2012**, *102*, 1692–1700, DOI: 10.1016/j.bpj.2012.03.008.

(13) van Stokkum, I. H. M.; Gwizdala, M.; Tian, L.; Snellenburg, J. J.; van Grondelle, R.; van Amerongen, H.; Berera, R. A Functional Compartmental Model of the Synechocystis PCC 6803 Phycobilisome. *Photosynth. Res.* **2018**, *135*, 87–102, DOI: 10.1007/s11120-017-0424-5.

(14) Nganou, C.; David, L.; Adir, N.; Mkandawire, M. Linker Proteins Enable Ultrafast Excitation Energy Transfer in the Phycobilisome Antenna System of Thermosynechococcus Vulcanus. *Photochem. Photobiol. Sci.* **2016**, *15*, 31–44, DOI: 10.1039/c5pp00285k.

(15) Sohoni, S.; Lloyd, L. T.; Hitchcock, A.; MacGregor-Chatwin, C.; Iwanicki, A.; Ghosh, I.; Shen, Q.; Hunter, C. N.; Engel, G. S. Phycobilisome's Exciton Transfer Efficiency Relies on an Energetic Funnel Driven by Chromophore-Linker Protein Interactions. *J. Am. Chem. Soc.* **2023**, *145*, 11659–11668, DOI: 10.1021/jacs.3c01799.

(16) Tronrud, D. E.; Wen, J.; Gay, L.; Blankenship, R. E. The Structural Basis for the Difference in Absorbance Spectra for the FMO Antenna Protein from Various Green Sulfur Bacteria. *Photosynth. Res.* **2009**, *100*, 79–87, DOI: 10.1007/s11120-009-9430-6.

(17) McDermott, G.; Prince, S. M.; Freer, A. A.; Hawthornthwaite-Lawless, A. M.; Papiz, M. Z.; Cogdell, R. J.; Isaacs, N. W. Crystal Structure of an Integral Membrane Light-Harvesting Complex from Photosynthetic Bacteria. *Nature* **1995**, *374*, 517–521, DOI: 10.1038/374517a0.

(18) Papiz, M. Z.; Prince, S. M.; Howard, T.; Cogdell, R. J.; Isaacs, N. W. The Structure and Thermal Motion of the B800–850 LH2 Complex from Rps.Acidophila at 2.0Å Resolution and 100K: New Structural Features and Functionally Relevant Motions. *J. Mol. Biol.* **2003**, *326*, 1523–1538, DOI: 10.1016/s0022-2836(03)00024-x.

(19) Scholes, G. D.; Fleming, G. R. On the Mechanism of Light Harvesting in Photosynthetic Purple Bacteria: B800 to B850 Energy Transfer. *J. Phys. Chem. B* **2000**, *104*, 1854–1868, DOI: 10.1021/jp993435l.

(20) Glazer, A. N. Phycobilisomes: Structure and Dynamics. *Annu. Rev. Microbiol.* **1982**, *36*, 173–198, DOI: 10.1146/annurev.mi.36.100182.001133.

(21) Glazer, A. N. Light Harvesting by Phycobilisomes. *Annu. Rev. Biophys. Biophys. Chem.* **1985**, *14*, 47–77, DOI: 10.1146/annurev.bb.14.060185.000403.

(22) Gantt, E. Phycobilisomes: Light-Harvesting Pigment Complexes. *Bioscience* **1975**, *25*, 781–788, DOI: 10.2307/1297221.

(23) Rosinski, J.; Hainfeld, J. F.; Rigbi, M.; Siegelman, H. W. Phycobilisome Ultrastructure and Chromatic Adaptation in Fremyella Diplosiphon. *Ann. Bot.* **1981**, *47*, 1–12, DOI: 10.1093/oxfordjournals.aob.a085984.

(24) Bryant, D. A.; Guglielmi, G.; de Marsac, N. T.; Castets, A.-M.; Cohen-Bazire, G. The Structure of Cyanobacterial Phycobilisomes: A Model. *Arch. Microbiol.* **1979**, *123*, 113–127, DOI: 10.1007/BF00446810.

(25) Domínguez-Martín, M. A.; Sauer, P. V.; Kirst, H.; Sutter, M.; Bína, D.; Greber, B. J.; Nogales, E.; Polívka, T.; Kerfeld, C. A. Structures of a Phycobilisome in Light-Harvesting and Photoprotected States. *Nature* **2022**, *609*, 835–845, DOI: 10.1038/s41586-022-05156-4.

(26) Zheng, L.; Zheng, Z.; Li, X.; Wang, G.; Zhang, K.; Wei, P.; Zhao, J.; Gao, N. Structural Insight into the Mechanism of Energy Transfer in Cyanobacterial Phycobilisomes. *Nat. Commun.* **2021**, *12*, 5497, DOI: 10.1038/s41467-021-25813-y.

(27) Zhang, J.; Ma, J.; Liu, D.; Qin, S.; Sun, S.; Zhao, J.; Sui, S.-F. Structure of Phycobilisome from the Red Alga Griffithsia Pacifica. *Nature* **2017**, *551*, 57–63, DOI: 10.1038/nature24278.

(28) Harris, D.; Bar-Zvi, S.; Lahav, A.; Goldshmid, I.; Adir, N. The Structural Basis for the Extraordinary Energy-Transfer Capabilities of the Phycobilisome. *Subcell. Biochem.* **2018**, *87*, 57–82, DOI: 10.1007/978-981-10-7757-9_3.

(29) Liu, L.-N.; Chen, X.-L.; Zhang, Y.-Z.; Zhou, B.-C. Characterization, Structure and Function of Linker Polypeptides in Phycobilisomes of Cyanobacteria and Red Algae: An Overview. *Biochim. Biophys. Acta* **2005**, *1708*, 133–142, DOI: 10.1016/j.bbabio.2005.04.001.

(30) Chang, L.; Liu, X.; Li, Y.; Liu, C.-C.; Yang, F.; Zhao, J.; Sui, S.-F. Structural Organization of an Intact Phycobilisome and Its Association with Photosystem II. *Cell Res.* **2015**, *25*, 726–737, DOI: 10.1038/cr.2015.59.

(31) Glazer, A. N. Phycobilisome a Macromolecular Complex Optimized for Light Energy Transfer. *Biochimica et Biophysica Acta (BBA) - Reviews on Bioenergetics* **1984**, *768*, 29–51, DOI: 10.1016/0304-4173(84)90006-5.

(32) Montgomery, B. L. Seeing New Light: Recent Insights into the Occurrence and Regulation of Chromatic Acclimation in Cyanobacteria. *Curr. Opin. Plant Biol.* **2017**, *37*, 18–23, DOI: 10.1016/j.pbi.2017.03.009.

(33) Kehoe, D. M.; Gutu, A. Responding to Color: The Regulation of Complementary Chromatic Adaptation. *Annu. Rev. Plant Biol.* **2006**, *57*, 127–150, DOI: 10.1146/annurev.arplant.57.032905.105215.

(34) Chenu, A.; Scholes, G. D. Coherence in Energy Transfer and Photosynthesis. *Annu. Rev. Phys. Chem.* **2015**, *66*, 69–96, DOI: 10.1146/annurev-physchem-040214-121713.

(35) Förster, T. Zwischenmolekulare Energiewanderung Und Fluoreszenz. *Ann. Phys.* **1948**, *437*, 55–75, DOI: 10.1002/andp.19484370105.

(36) Cantor, C. R.; Schimmel, P. R. *Biophysical Chemistry: Part II: Techniques for the Study of Biological Structure and Function*; Macmillan, 1980.

(37) Ohad, I.; CLAYTONt, R. K.; Bogorad, L. Purified from Fremyella Diplosiphon: Temperature Dependence and Quantum Efficiency. *Proceedings of the National Academy of Sciences of the United States of America* **1979**, *76*, 5655–5659, DOI: 10.1073/pnas.76.11.5655.

(38) Brody, S. S.; Rabinowitch, E. Excitation Lifetime of Photosynthetic Pigments in Vitro and in Vivo. *Science* **1957**, *125*, 555, DOI: 10.1126/science.125.3247.555.

(39) Tomita, G.; Rabinowitch, E. Excitation Energy Transfer between Pigments in Photosynthetic Cells. *Biophys. J.* **1962**, *2*, 483–499, DOI: 10.1016/s0006-3495(62)86869-6.

(40) Singhal, G. S.; Rabinowitch, E. Measurement of the Fluorescence Lifetime of Chlorophyll a in Vivo. *Biophys. J.* **1969**, *9*, 586–591, DOI: 10.1016/S0006-3495(69)86405-2.

(41) Grabowski, J.; Gantt, E. PHOTOPHYSICAL PROPERTIES OF PHYCOBILIPROTEINS FROM PHYCOBILISOMES: FLUORESCENCE LIFETIMES, QUANTUM YIELDS, AND POLARIZATION SPECTRA. *Photochem. Photobiol.* **1978**, *28*, 39–45, DOI: 10.1111/j.1751-1097.1978.tb06927.x.

(42) Kobayashi, T.; Degenkolb, E. O.; Bersohn, R.; Rentzepis, P. M.; MacColl, R.; Berns, D. S. Energy Transfer among the Chromophores in Phycocyanins Measured by Picosecond Kinetics. *Biochemistry* **1979**, *18*, 5073–5078, DOI: 10.1021/bi00590a008.

(43) Wong, D.; Pellegrino, F.; Alfano, R. R.; Zilinskas, B. A. FLUORESCENCE RELAXATION KINETICS AND QUANTUM YIELD FROM THE ISOLATED PHYCOBILIPROTEINS OF THE BLUE-GREEN ALGA *NOSTOC* SP. MEASURED AS A FUNCTION OF SINGLE PICOSECOND PULSE INTENSITY, *I. Photochem. Photobiol.* **1981**, *33*, 651–662, DOI: 10.1111/j.1751-1097.1981.tb05471.x.

(44) Holzwarth, A. R.; Wendler, J.; Wehrmeyer, W. Studies on Chromophore Coupling in Isolated Phycobiliproteins. I. Picosecond Fluorescence Kinetics of Energy Transfer in Phycocyanin 645 from Chroomonas Sp. *Biochim. Biophys. Acta* **1983**.

(45) Holzwarth, A. R.; Wendler, J.; Suter, G. W. Studies on Chromophore Coupling in Isolated Phycobiliproteins: II. Picosecond Energy Transfer Kinetics and Time-Resolved Fluorescence Spectra of C-Phycocyanin …. *Biophys. J.* **1987**.

(46) Holzwarth, A. R.; Bittersmann, E.; Reuter, W.; Wehrmeyer, W. Studies on Chromophore Coupling in Isolated Phycobiliproteins: III. Picosecond Excited State Kinetics and Time-Resolved Fluorescence Spectra of Different Allophycocyanins from Mastigocladus Laminosus. *Biophys. J.* **1990**, *57*, 133–145, DOI: 10.1016/S0006-3495(90)82514-5.

(47) Wendler, J.; John, W.; Scheer, H.; Hoezwarth, A. R. Energy Transfer in Trimeric C-Phycocyanin Studied by Picosecond Fluorescence Kinetics. *Photochem. Photobiol.* **1986**, *44*, 79–85.

(48) Sauer, K.; Scheer, H.; Sauer, P. FÖRSTER TRANSFER CALCULATIONS BASED ON CRYSTAL STRUCTURE DATA FROM Agmenellum Quadruplicatum C-PHYCOCYANIN. *Photochem. Photobiol.* **1987**, *46*, 427–440, DOI: 10.1111/j.1751-1097.1987.tb04790.x.

(49) Sauer, K.; Scheer, H. Excitation Transfer in C-Phycocyanin. Förster Transfer Rate and Exciton Calculations Based on New Crystal Structure Data for C-Phycocyanins from Agmenellum Quadruplicatum and Mastigocladus Laminosus. *Biochimica et Biophysica Acta (BBA) - Bioenergetics* **1988**, *936*, 157–170, DOI: 10.1016/0005-2728(88)90232-0.

(50) Porter, G.; Tredwell, C. J.; Searle, G. F.; Barber, J. Picosecond Time-Resolved Energy Transfer in Porphyridium Cruentum. Part I. In the Intact Alga. *Biochim. Biophys. Acta* **1978**, *501*, 232–245, DOI: 10.1016/0005-2728(78)90029-4.

(51) Searle, G. F.; Barber, J.; Porter, G.; Tredwell, C. J. Picosecond Time-Resolved Energy Transfer in Porphyridium Cruentum. Part II. In the Isolated Light Harvesting Complex (Phycobilisomes). *Biochim. Biophys. Acta* **1978**, *501*, 246–256, DOI: 10.1016/0005-2728(78)90030-0.

(52) Holzwarth, A. R.; Wendler, J.; Wehrmeyer, W. Picosecond Time Resolved Energy Transfer in Isolated Phycobilisomes from Rhodella Violacea (Rhodophyceae). *Photochem. Photobiol.* **1982**, *36*, 479–487, DOI: 10.1111/j.1751-1097.1982.tb04405.x.

(53) Wendler, J.; Holzwarth, A. R.; Wehrmeyer, W. Picosecond Time-Resolved Energy Transfer in Phycobilisomes Isolated from the Red Alga Porphyridium Cruentum. *Biochimica et Biophysica Acta (BBA) - Bioenergetics* **1984**, *765*, 58–67, DOI: 10.1016/0005-2728(84)90157-9.

(54) Suter, G. W.; Mazzola, P.; Wendler, J. Fluorescence Decay Kinetics in Phycobilisomes Isolated from the Bluegreen Alga Synechococcus 6301. *Biochim. Biophys. Acta* **1984**.

(55) Glazer, A. N.; Yeh, S. W.; Webb, S. P.; Clark, J. H. Disk-to-Disk Transfer as the Rate-Limiting Step for Energy Flow in Phycobilisomes. *Science* **1985**, *227*, 419–423.

(56) Glazer, A. N.; Chan, C.; Williams, R. C.; Yeh, S. W.; Clark, J. H. Kinetics of Energy Flow in the Phycobilisome Core. *Science*. 1985, pp 1051–1053.

(57) Pellegrino, F.; Wong, D.; Alfano, R. R.; Zilinskas, B. A. Fluorescence Relaxation Kinetics and Quantum Yield from the Phycobilisomes of the Blue-Green Alga Nostoc Sp. Measured as a Function of Single Picosecond Pulse Intensity. *Photochem. Photobiol.* **1981**, *34*, 691–696, DOI: 10.1111/j.1751-1097.1981.tb09065.x.

(58) Yamazaki, I.; Mimuro, M.; Murao, T.; Yamazaki, T.; Yoshihara, K.; Fujita, Y. EXCITATION ENERGY TRANSFER IN THE LIGHT HARVESTING ANTENNA SYSTEM OF THE RED ALGA *Porphyridium Cruentum* AND THE BLUE-GREEN ALGA *Anacystis Nidulans*: ANALYSIS OF TIME-RESOLVED FLUORESCENCE SPECTRA. *Photochem. Photobiol.* **1984**, *39*, 233–240, DOI: 10.1111/j.1751-1097.1984.tb03432.x.

(59) Mimuro, M.; Yamazaki, I.; Tamai, N.; Katoh, T. Excitation Energy Transfer in Phycobilisomes at −196°C Isolated from the Cyanobacterium Anabaena Variabilis (M-3): Evidence for the Plural Transfer Pathways to the Terminal Emitters. *Biochimica et Biophysica Acta (BBA) - Bioenergetics* **1989**, *973*, 153–162, DOI: 10.1016/S0005-2728(89)80416-5.

(60) Beck, W. F.; Sauer, K. Energy-Transfer and Exciton-State Relaxation Processes in Allophycocyanin. *J. Phys. Chem.* **1992**, *96*, 4658–4666, DOI: 10.1021/j100190a094.

(61) Edington, M. D.; Riter, R. E.; Beck, W. F. Evidence for Coherent Energy Transfer in Allophycocyanin Trimers. *J. Phys. Chem.* **1995**, *99*, 15699–15704, DOI: 10.1021/j100043a001.

(62) Edington, M. D.; Riter, R. E.; Beck, W. F. Interexciton-State Relaxation and Exciton Localization in Allophycocyanin Trimers. *J. Phys. Chem.* **1996**, *100*, 14206–14217, DOI: 10.1021/jp960454b.

(63) Riter, R. E.; Edington, M. D.; Beck, W. F. Isolated-Chromophore and Exciton-State Photophysics in C-Phycocyanin Trimers. *J. Phys. Chem. B* **1997**, *101*, 2366–2371, DOI: 10.1021/jp962609l.

(64) Homoelle, B. J.; Edington, M. D.; Diffey, W. M.; Beck, W. F. Stimulated Photon-Echo and Transient-Grating Studies of Protein-Matrix Solvation Dynamics and Interexciton-State Radiationless Decay in α Phycocyanin and Allophycocyanin. *The Journal of Physical Chemistry B*. 1998, pp 3044–3052.

(65) Edington, M. D.; Riter, R. E.; Beck, W. F. Femtosecond Transient Hole-Burning Detection of Interexciton-State Radiationless Decay in Allophycocyanin Trimers. *J. Phys. Chem. B* **1997**, *101*, 4473–4477, DOI: 10.1021/jp970424o.

(66) Ying, L.; Xie, X. S. Fluorescence Spectroscopy, Exciton Dynamics, and Photochemistry of Single Allophycocyanin Trimers. *J. Phys. Chem. B* **1998**, *102*, 10399–10409, DOI: 10.1021/jp983227d.

(67) Womick, J. M.; Moran, A. M. Exciton Coherence and Energy Transport in the Light-Harvesting Dimers of Allophycocyanin. *J. Phys. Chem. B* **2009**, *113*, 15747–15759, DOI: 10.1021/jp907644h.

(68) Womick, J. M.; Moran, A. M. Vibronic Enhancement of Exciton Sizes and Energy Transport in Photosynthetic Complexes. *J. Phys. Chem. B* **2011**, *115*, 1347–1356, DOI: 10.1021/jp106713q.

(69) Womick, J. M.; Moran, A. M. Nature of Excited States and Relaxation Mechanisms in C-Phycocyanin. *J. Phys. Chem. B* **2009**, *113*, 15771–15782, DOI: 10.1021/jp908093x.

(70) Womick, J. M.; Liu, H.; Moran, A. M. Exciton Delocalization and Energy Transport Mechanisms in R-Phycoerythrin. *J. Phys. Chem. A* **2011**, *115*, 2471–2482, DOI: 10.1021/jp111720a.

(71) Wang, Q.; Moerner, W. E. Dissecting Pigment Architecture of Individual Photosynthetic Antenna Complexes in Solution. *Proc. Natl. Acad. Sci. U. S. A.* **2015**, *112*, 13880–13885, DOI: 10.1073/pnas.1514027112.

(72) Tian, L.; van Stokkum, I. H. M.; Koehorst, R. B. M.; Jongerius, A.; Kirilovsky, D.; van Amerongen, H. Site, Rate, and Mechanism of Photoprotective Quenching in Cyanobacteria. *J. Am. Chem. Soc.* **2011**, *133*, 18304–18311, DOI: 10.1021/ja206414m.

(73) Akhtar, P.; Biswas, A.; Petrova, N.; Zakar, T.; van Stokkum, I. H. M.; Lambrev, P. H. Time-Resolved Fluorescence Study of Excitation Energy Transfer in the Cyanobacterium Anabaena PCC 7120. *Photosynth. Res.* **2020**, *144*, 247–259, DOI: 10.1007/s11120-020-00719-w.

(74) Lee, H.; Cheng, Y.-C.; Fleming, G. R. Coherence Dynamics in Photosynthesis: Protein Protection of Excitonic Coherence. *Science* **2007**, *316*, 1462–1465, DOI: 10.1126/science.1142188.

(75) Collini, E.; Wong, C. Y.; Wilk, K. E.; Curmi, P. M. G.; Brumer, P.; Scholes, G. D. Coherently Wired Light-Harvesting in Photosynthetic Marine Algae at Ambient Temperature. *Nature* **2010**, *463*, 644–647, DOI: 10.1038/nature08811.

(76) Ghosh, S.; Bishop, M. M.; Roscioli, J. D.; LaFountain, A. M.; Frank, H. A.; Beck, W. F. Excitation Energy Transfer by Coherent and Incoherent Mechanisms in the Peridinin–Chlorophyll a Protein. *J. Phys. Chem. Lett.* **2017**, *8*, 463–469, DOI: 10.1021/acs.jpclett.6b02881.

(77) Jonas, D. M. Two-Dimensional Femtosecond Spectroscopy. *Annu. Rev. Phys. Chem.* **2003**, *54*, 425–463, DOI: 10.1146/annurev.physchem.54.011002.103907.

(78) Brixner, T.; Mancal, T.; Stiopkin, I. V.; Fleming, G. R. Phase-Stabilized Two-Dimensional Electronic Spectroscopy. *J. Chem. Phys.* **2004**, *121*, 4221–4236, DOI: 10.1063/1.1776112.

(79) Cho, M. Coherent Two-Dimensional Optical Spectroscopy. *Chem. Rev.* **2008**, *108*, 1331–1418, DOI: 10.1021/cr078377b.

(80) Ginsberg, N. S.; Cheng, Y.-C.; Fleming, G. R. Two-Dimensional Electronic Spectroscopy of Molecular Aggregates. *Acc. Chem. Res.* **2009**, *42*, 1352–1363, DOI: 10.1021/ar9001075.

(81) Cowan, M. L.; Ogilvie, J. P.; Miller, R. J. D. Two-Dimensional Spectroscopy Using Diffractive Optics Based Phased-Locked Photon Echoes. *Chem. Phys. Lett.* **2004**, *386*, 184–189, DOI: 10.1016/j.cplett.2004.01.027.

(82) Roscioli, J. D.; Ghosh, S.; LaFountain, A. M.; Frank, H. A.; Beck, W. F. Quantum Coherent Excitation Energy Transfer by Carotenoids in Photosynthetic Light Harvesting. *J. Phys. Chem. Lett.* **2017**, *8*, 5141–5147, DOI: 10.1021/acs.jpclett.7b01791.

(83) Roscioli, J. D.; Ghosh, S.; LaFountain, A. M.; Frank, H. A.; Beck, W. F. Structural Tuning of Quantum Decoherence and Coherent Energy Transfer in Photosynthetic Light Harvesting. *J. Phys. Chem. Lett.* **2018**, *9*, 5071–5077, DOI: 10.1021/acs.jpclett.8b01919.

(84) Tilluck, R. W.; Ghosh, S.; Guberman-Pfeffer, M. J.; Roscioli, J. D.; Gurchiek, J. K.; LaFountain, A. M.; Frank, H. A.; Gascón, J. A.; Beck, W. F. Interexciton Nonradiative Relaxation Pathways in the Peridinin-Chlorophyll Protein. *CR-PHYS-SC* **2021**, *2*, DOI: 10.1016/j.xcrp.2021.100380.

(85) Tilluck, R. W.; Mohan T M, N.; Hetherington, C. V.; Leslie, C. H.; Sil, S.; Frazier, J.; Zhang, M.; Levine, B. G.; Van Patten, P. G.; Beck, W. F. Vibronic Excitons and Conical Intersections in Semiconductor Quantum Dots. *J. Phys. Chem. Lett.* **2021**, *12*, 9677–9683, DOI: 10.1021/acs.jpclett.1c02630.

(86) Turner, D. B.; Hassan, Y.; Scholes, G. D. Exciton Superposition States in CdSe Nanocrystals Measured Using Broadband Two-Dimensional Electronic Spectroscopy. *Nano Lett.* **2012**, *12*, 880–886, DOI: 10.1021/nl2039502.

(87) Cassette, E.; Dean, J. C.; Scholes, G. D. Two-Dimensional Visible Spectroscopy For Studying Colloidal Semiconductor Nanocrystals. *Small* **2016**, *12*, 2234–2244, DOI: 10.1002/smll.201502733.

(88) Collini, E.; Gattuso, H.; Levine, R. D.; Remacle, F. Ultrafast Fs Coherent Excitonic Dynamics in CdSe Quantum Dots Assemblies Addressed and Probed by 2D Electronic Spectroscopy. *J. Chem. Phys.* **2021**, *154*, 014301, DOI: 10.1063/5.0031420.

(89) Wong, C. Y.; Scholes, G. D. Using Two-Dimensional Photon Echo Spectroscopy to Probe the Fine Structure of the Ground State Biexciton of CdSe Nanocrystals. *J. Lumin.* **2011**, *131*, 366–374, DOI: 10.1016/j.jlumin.2010.09.015.

(90) Seiler, H.; Palato, S.; Sonnichsen, C.; Baker, H.; Kambhampati, P. Seeing Multiexcitons through Sample Inhomogeneity: Band-Edge Biexciton Structure in CdSe Nanocrystals Revealed by Two-Dimensional Electronic Spectroscopy. *Nano Lett.* **2018**, *18*, 2999–3006, DOI: 10.1021/acs.nanolett.8b00470.

(91) Gallagher Faeder, S. M.; Jonas, D. M. Two-Dimensional Electronic Correlation and Relaxation Spectra: Theory and Model Calculations. *J. Phys. Chem. A* **1999**, *103*, 10489–10505, DOI: 10.1021/jp9925738.

(92) Hybl, J. D.; Albrecht, A. W.; Gallagher Faeder, S. M.; Jonas, D. M. Two-Dimensional Electronic Spectroscopy. *Chem. Phys. Lett.* **1998**, *297*, 307–313, DOI: 10.1016/S0009-2614(98)01140-3.

(93) Mukamel, S. Principles of Nonlinear Optical Spectroscopy. **1995**.

(94) Hamm, P.; Zanni, M. *Concepts and Methods of 2D Infrared Spectroscopy*; Cambridge University Press, **2011**.

(95) Wilkinson, G. R. R. J. H. Clark and R. E. Hester (Editors). Advances in Infrared and Raman Spectroscopy, Vol. 12. Wiley, New York. 1985. *J. Raman Spectrosc.* **1986**, *17*, 487–487, DOI: 10.1002/JRS.1250170613.

(96) Fragnito, H. L.; Bigot, J.-Y.; Becker, P. C.; Shank, C. V. Evolution of the Vibronic Absorption Spectrum in a Molecule Following Impulsive Excitation with a 6 Fs Optical Pulse. *Chem. Phys. Lett.* **1989**, *160*, 101–104, DOI: 10.1016/0009-2614(89)87564-5.

(97) Pollard, W. T.; Fragnito, H. L.; Bigot, J.-Y.; Shank, C. V.; Mathies, R. A. Quantum-Mechanical Theory for 6 Fs Dynamic Absorption Spectroscopy and Its Application to Nile Blue. *Chem. Phys. Lett.* **1990**, *168*, 239–245.

(98) Dexheimer, S. L.; Wang, Q.; Peteanu, L. A.; Pollard, W. T.; Mathies, R. A.; Shank, C. V. Femtosecond Impulsive Excitation of Nonstationary Vibrational States in Bacteriorhodopsin. *Chem. Phys. Lett.* **1992**, *188*, 61–66, DOI: 10.1016/0009-2614(92)85089-S.

(99) Ruhman, S.; Joly, A. G.; Nelson, K. A. Time-resolved Observations of Coherent Molecular Vibrational Motion and the General Occurrence of Impulsive Stimulated Scattering. *J. Chem. Phys.* **1987**, *86*, 6563–6565, DOI: 10.1063/1.452400.

(100) Tian, P.; Keusters, D.; Suzaki, Y.; Warren, W. S. Femtosecond Phase-Coherent Two-Dimensional Spectroscopy. *Science* **2003**, *300*, 1553–1555, DOI: 10.1126/science.1083433.

(101) Ogilvie, J. P.; Kubarych, K. J. Chapter 5 Multidimensional Electronic and Vibrational Spectroscopy: An Ultrafast Probe of Molecular Relaxation and Reaction Dynamics. In *Advances In Atomic, Molecular, and Optical Physics*; Academic Press, **2009;** Vol. 57, pp 249–321.

(102)Butkus, V.; Zigmantas, D.; Valkunas, L.; Abramavicius, D. Vibrational vs. Electronic Coherences in 2D Spectrum of Molecular Systems. *Chem. Phys. Lett.* **2012**, *545*, 40–43, DOI: 10.1016/j.cplett.2012.07.014.

(103)Turner, D. B.; Wilk, K. E.; Curmi, P. M. G.; Scholes, G. D. Comparison of Electronic and Vibrational Coherence Measured by Two-Dimensional Electronic Spectroscopy. *J. Phys. Chem. Lett.* **2011**, *2*, 1904–1911, DOI: 10.1021/jz200811p.

(104)Butkus, V.; Alster, J.; Bašinskaitė, E.; Augulis, R. N.; Neuhaus, P.; Valkunas, L.; Anderson, H. L.; Abramavicius, D.; Zigmantas, D. Discrimination of Diverse Coherences Allows Identification of Electronic Transitions of a Molecular Nanoring. *J. Phys. Chem. Lett.* **2017**, *8*, 2344–2349, DOI: 10.1021/acs.jpclett.7b00612.

(105)Butkus, V.; Zigmantas, D.; Abramavicius, D.; Valkunas, L. Distinctive Character of Electronic and Vibrational Coherences in Disordered Molecular Aggregates. *Chem. Phys. Lett.* **2013**, *587*, 93–98, DOI: 10.1016/j.cplett.2013.09.043.

(106)Chenu, A.; Christensson, N.; Kauffmann, H. F.; Mančal, T. Enhancement of Vibronic and Ground-State Vibrational Coherences in 2D Spectra of Photosynthetic Complexes. *Sci. Rep.* **2013**, *3*, 2029, DOI: 10.1038/srep02029.

(107)McHale, J. L. *Molecular Spectroscopy*; CRC Press, 2017.

(108)Pollard, W. T.; Mathies, R. A. Analysis of Femtosecond Dynamic Absorption Spectra of Nonstationary States. *Annu. Rev. Phys. Chem.* **1992**, *43*, 497–523, DOI: 10.1146/annurev.pc.43.100192.002433.

(109)Shim, S.-H.; Zanni, M. T. How to Turn Your Pump-Probe Instrument into a Multidimensional Spectrometer: 2D IR and Vis Spectroscopies via Pulse Shaping. *Phys. Chem. Chem. Phys.* **2009**, *11*, 748–761, DOI: 10.1039/b813817f.

(110)Grumstrup, E. M.; Shim, S.-H.; Montgomery, M. A.; Damrauer, N. H.; Zanni, M. T. Facile Collection of Two-Dimensional Electronic Spectra Using Femtosecond Pulse-Shaping Technology. *Opt. Express, OE* **2007**, *15*, 16681–16689, DOI: 10.1364/OE.15.016681.

(111)Myers, J. A.; Lewis, K. L. M.; Tekavec, P. F.; Ogilvie, J. P. Two-Color Two-Dimensional Fourier Transform Electronic Spectroscopy with a Pulse-Shaper. *Opt. Express* **2008**, *16*, 17420–17428, DOI: 10.1364/oe.16.017420.

(112)van Stokkum, I. H. M.; Larsen, D. S.; van Grondelle, R. Global and Target Analysis of Time-Resolved Spectra. *Biochim. Biophys. Acta* **2004**, *1657*, 82–104, DOI: 10.1016/j.bbabio.2004.04.011.

APPENDIX

CURRENT LIST OF PUBLICATIONS

By

Sourav Sil

1. Sil, S.; Tilluck, R. W.; Mohan T M, N.; Leslie, C. H.; Rose, J. B.; Domingues-Martin, M. A.; Lou, W.; Kerfeld, C. A.; Beck, W. F. Excitation energy transfer and vibronic coherence in intact phycobilisomes. *Nat. Chem.* **2022**, *14*, 1286-1294, DOI: 10.1038/s41557-022-01026-8.
2. Tilluck, R. W.; Mohan T M, N.; Hetherington, C. V.; Leslie, C. H.; Sil, S.; Frazier, J.; Zhang, M.; Levine, B. G.; Van Patten, P. G.; Beck, W. F. Vibronic excitons and conical intersections in semiconductor quantum dots. *J. Phys. Chem. Lett.* **2021**, *12*, 9677–9683, DOI: 10.1021/acs.jpclett.1c02630.
3. Mohan T M, N.; Leslie, C. H.; Sil, S.; Rose, J. B.; Tilluck, R. W.; Beck, W. F. Broadband 2DES detection of vibrational coherence in the S_x state of canthaxanthin. *J. Chem. Phys.* **2021**, *155*, 035103, DOI: 10.1063/5.0055598.

Chapter 2: Excitation Energy Transfer and Vibronic Coherence in Intact Phycobilisomes

Phycobilisome is the primary light-harvesting protein complex in cyanobacteria and red algae. It contains bilin (open chain tetrapyrrole) chromophores that absorb mid-visible solar photons and channel that energy to the Photosystem II. Broadband two-dimensional electronic spectroscopy with 6.7-fs laser pulses were employed to detect the excitation energy transfer pathways in intact phycobilisomes isolated from *Fremyella diplosiphon* grown under white light. The experimental results strongly indicate that the delocalized excitons are present in the rod of the phycobilisomes involving bilin chromophores. The kinetic model suggests that the excitation energy absorbed by phycoerythrin disks at the end of the rods moves to the C-phycocyanin disks along their length less than 600 fs. Oscillation maps show that the relaxation of a manifold of vibronic exciton states is mediated via coherent wavepacket motions predominantly involving the Hydrogen out-of-plane (HOOP) vibrations of the bilins. However, the charge transfer character of the bilin chromophores in the allophycocyanin disks localizes the excitation energy in the core of the phycobilisomes. The energy localization slows down energy transfer rate that allows photoregulatory processes to occur efficiently on the higher than 10-ps timescale. The work presented in this chapter has been adapted from *Nat. Chem.* **2022**, *14*, 1286-1294 (DOI: 10.1038/s41557-022-01026-8).

2.1 Introduction

The phycobilisome (Figure 2.1) is the principal peripheral light-harvesting antenna complex in cyanobacteria and red algae.[1–3] Phycobilisomes contain triangular core structure and rod-like structures attached to the core. The core and rods are made of disk-shaped $(\alpha\beta)_3$ trimeric or $(\alpha\beta)_6$ hexameric phycobiliproteins along with linker proteins.[4] The bilin chromophores covalently attached at a specific position of the phycobiliproteins constitute a funnel-shaped energy landscape. The phycobiliprotein allophycocyanin (APC) in the core of phycobilisomes absorb red light (λ_{max} = 650 nm) whereas the core-proximal disks of the rod C-phycocyanin (CPC) absorb shorter wavelengths (λ_{max} = 620 nm) than APC. Some cyanobacteria can produce another phycobiliprotein phycoerythrin (PE) as core-distal disks of the rod that absorb even shorter wavelengths (λ_{max} = 565 nm). This way structure of phycobilisomes promotes a downhill flow of excitation energy from rods to the redshifted bilins in the core, which then transfer energy to chlorophyll in the membrane protein PS I and PS II.[5]

So far, van Stokkum et al. reported the most detailed model for excitation energy transfer processes in intact phycobilisomes from *Synechocystis* sp. PCC 6803.[6] In that report they combined the results from their 200-fs pump-probe transient absorption studies and 10-ps streak-camera fluorescence measurements.[7] Their kinetic model has more than ten compartments where excitation energy transfer occurs in hopping style in ~2-ps or longer steps between a given CPC or APC disk following the Förster mechanism.[8–10]

In contrast with this model, a number of nonlinear femtosecond spectroscopy studies have detected much faster (< 1 ps) excitation energy transfer processes in isolated phycobiliproteins[13–17] and in the rod of the intact phycobilisomes[18–20] from several

cyanobacteria species. These results suggest that the delocalized excitons might be present due to the electronic interactions between bilins in adjacent phycobiliprotein disks in the intact phycobilisome. A few published cryo-electron microscopy structures of the intact phycobilisomes from cyanobacteria[21,22] and red algae[23,24] show the arrangement of the bilin chromophores in the phycobiliprotein subunits with atomic details.

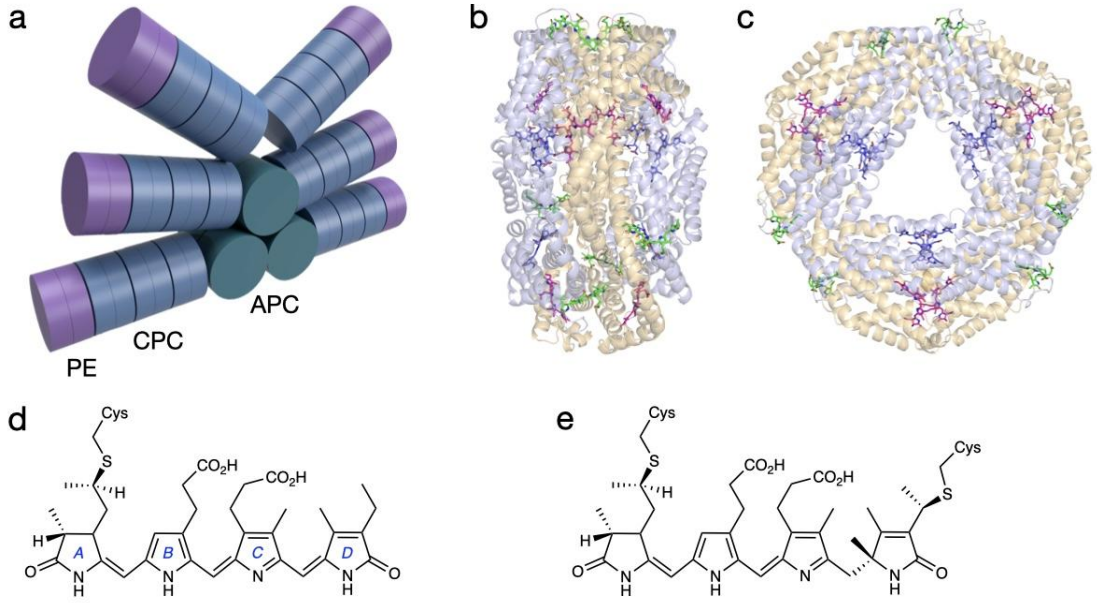

Figure 2.1 Structure of phycobilisome, phycobiliprotein and bilin molecules from *Fremyella diplosiphon*. a, Model for phycobilisome[11] that includes PE and CPC in the rods and APC in the core. b and c, Side view (b) and planar view (c) of the X-ray crystal structure of $(\alpha\beta)_6$ hexameric CPC from *F. diplosiphon* (PDB structure 1CPC).[12] The α and β subunits are shown as yellow and blue ribbons, respectively. The bilin chromophores are represented as stick structures: α84 in red, β84 in blue and β155 in green color. The numbers are the cysteine residue to which the chromophores are linked. d, the structure of phycocyanobilin that binds with CPC and APC. The rings are numbered as A to D starting from the ring that is attached to cysteine residue. e, the structure of phycoerythrobilin that can be found in PE.

In contrast with this model, a number of nonlinear femtosecond spectroscopy studies have detected much faster (< 1 ps) excitation energy transfer processes in isolated phycobiliproteins[13–17] and in the rod of the intact phycobilisomes[18–20] from several cyanobacteria species. These results suggest that the delocalized excitons might be present

due to the electronic interactions between bilins in adjacent phycobiliprotein disks in the intact phycobilisome. A few published cryo-electron microscopy structures of the intact phycobilisomes from cyanobacteria[21,22] and red algae[23,24] show the arrangement of the bilin chromophores in the phycobiliprotein subunits with atomic details.

Here we employed multidimensional electronic spectroscopy[25,26] to characterize the excitation energy transfer processes in intact phycobilisomes isolated from WT filamentous cyanobacterium *Fremyella diplosiphon* UTEX 481. The phycobilisomes from *Fremyella* incorporate PE disks at the end of the rod. We detected the mechanisms of excitation energy transfer processes down the rods to the core of the phycobilisome by isolating the responses following excitation of the PE in two-dimensional electronic spectra. Additionally, the broadband excitation pulses help us to identify the role of vibronic coherence in excitation energy transfer processes. Our results indicate that the absorption of light generates delocalized pathways of bilins that channels excitation energy down the rods on sub-picosecond timescale via coherent non-adiabatic mechanism. The intramolecular charge-transfer (ICT) character of the bilins in the core promotes the localization of excitation in a single chromophore and that makes the delocalized pathways short-lived. Localization of the excitation in the core of the phycobilisome forces the energy transfer process to become slow and helps photoregulatory mechanisms to occur efficiently.

2.2 Experimental Methods

2.2.1 Sample Preparation

Cultures of wild-type *Fremyella diplosiphon* were grown in BG11 media (Table 2.1) under continuous illumination of medium intensity (50 μE $m^{-2}s^{-1}$) fluorescent white light at

a constant temperature of 30 ^{0}C and in presence of 3% CO_2. Intact phycobilisomes were isolated from these cultures following the procedure described by Gantt et al.[27,28] with some modifications. Cells were collected at OD_{750} of ~1.0 using a centrifuge at 19000 *g* for 20 min. Then cells were resuspended in a PBS isolation buffer solution (0.8 M Potassium Phosphate buffer, 1 mM EDTA, 0.5 mM PMSF, pH 7) and collected again in a centrifuge at 30000 *g* for 15 min. Then the cells were resuspended in PBS buffer solution again and passed through the French press three times at 1000 psi to break the cells. Triton X-100 (2%) was added in the broken cells to remove the cellular debris. After 30 min the cellular extracts were loaded in the centrifuge at 40000 *g* for 30 min to isolate the intact phycobilisomes from the cellular debris. The supernatant was collected and loaded in the sucrose gradient (Table 2.2) to remove the remaining soluble proteins. The gradient was spun overnight (~16-18 hrs.) in an ultracentrifuge at 77000 *g*. Then isolated intact phycobilisomes were taken out from the 0.75 M/ 1 M interface of the sucrose gradient. The sucrose was removed from the phycobilisomes by using chromatography technique. The concentration of phycobilisomes was adjusted to the requirement of the experiments by adding 0.8 M potassium phosphate buffer solution.

2.2.2 Linear Spectroscopy

Linear absorption spectra of intact phycobilisomes samples were recorded using a Shimadzu UV-2600 spectrophotometer at room temperature (23 °C). For the 2DES study the concentration of the phycobilisome sample was adjusted to obtain 0.3 OD (in 1 mm cuvette) by adding 0.8 M potassium phosphate buffer (pH 7). For the fluorescence experiments the OD value of the sample was adjusted to obtain 0.1 for a 1 cm path length at the excitation wavelength.

The fluorescence spectra were recorded with a home-built fluorescence spectrometer, which was described previously.[29,30] A broadband LED and a compact double monochromator (2 nm bandpass) was used in the fluorescence instrument as an excitation light source. A grating spectrograph and a CCD detector were used as the detection system. There were two polarizers before and after the sample position to select the orientation of the excitation and emission beam respectively. The emission spectra were corrected for the wavelength dependency of the emission optics, spectrograph, and CCD detector.

2.2.3 Two-Dimensional Electronic Spectroscopy (2DES)

The 2DES spectra were recorded with a two beam pump-probe optical configuration[31] at room temp (23 °C). The laser pulses were obtained from a noncollinear optical parametric amplifier (NOPA, Spectra-Physics) which was pumped by a Yb laser (Spectra-Physics, 100 kHz repetition rate, 4 W average power). The NOPA output was split by a broadband dielectric beamsplitter to generate a pump and probe beam. A pair of chirped mirrors and adaptive pulse shaper (FemtoJock and FemtoJock P, respectively, Biophotonic Solutions) were employed in each beam to compress the laser pulses. The laser pulse duration was measured at the sample position by MIIPS scans.[32] For this set of experiments NOPA's output beam spectrum was centered at 600 nm (spectral width 520-700 nm). The excitation energy was attenuated to 2.4 nJ per pulse and the pulse duration was 6.7 fs at the sample's position. The polarization of the pump beam was rotated to magic angle (54.7^{o}) from that of the probe beam. Both beams were focused by off-axis parabolic mirrors overlapped spatially at the sample position. The pump-induced change in the probe transmission through the sample was recorded with a spectrograph and a fast CCD detector (Andor Newton 940) using a phase-sensitive detection protocol with amplitude modulation

of the pump pulses.[33] A polarizer with the set polarization along the polarization of the probe beam was placed before the spectrograph to block any scatter light that originated from the pump beam.

In the 2DES experiment with pump-probe geometry the pulse sequence was pump pulse 1 - τ (coherence time) - pump pulse 2 - T (population time) - probe pulse. The pump beam's pulse shaper was programmed to control the coherence time (τ), time interval between two pump pulses, ranging from 0 to 50 fs with 0.5 fs steps. The excitation axis was obtained from the Fourier transformation of the τ axis. The detection axis was generated directly from the CCD. The population time (T) was controlled by the conventional time-of-flight delay stages ranging from -3 ps to 300 ps with steps varying from 2.5 fs to 10 ps. Each 2DES spectrum was an average of 5 successive T scans. Using this approach, the obtained spectra are the sum of the rephasing and non-rephasing nonlinear optical pathways.[33]

For 2DES experiments the phycobilisome samples (8 ml) were recirculated by using a peristaltic pump (Bio-Rad) with a speed of 3.84 ml/minute. Instead of a static cuvette a 1 mm flow cell was used. During the experiment, the absorption spectrum of the phycobilisomes sample was checked periodically to monitor the permanent photobleaching and photodamage of the sample.

2.3 Results

2.3.1 Linear Spectroscopy

Figure 2.2 shows the absorption and fluorescence spectra at room temperature (23 ^{0}C) from intact phycobilisomes isolated from *Fremyella diplosiphon* grown under continues illumination of medium intensity white light. The spectrum is plotted as oscillator strength vs wavenumber (ν). For absorption, the oscillator strength, ε/ν is calculated from the

absorption spectrum, $\varepsilon(\nu)$ and for fluorescence, the expression for oscillator strength is $\lambda^2 F(\nu)/\nu^3$ where λ is wavelength and $F(\nu)$ is the fluorescence intensity. The absorption spectrum of phycobilisomes contains two peaks from PE and CPC at 570 and 620 nm respectively. Also, there is a shoulder peak at 650 nm originating from APC. The fluorescence spectrum shows maximum intensity at 672 nm after exciting the sample at 550 nm. The terminal emitter is emitting the fluorescence after exciting mostly PE in the phycobilisome that indicates the phycobilisomes are intact.

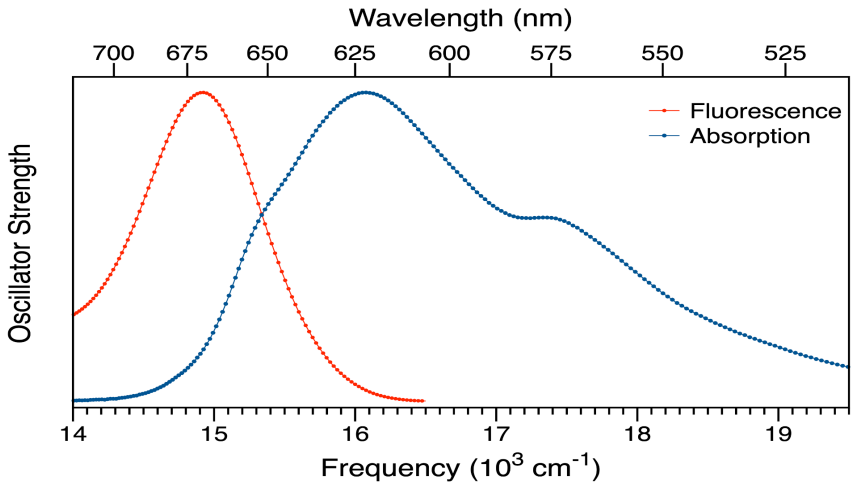

Figure 2.2 Absorption (ε/ν) and fluorescence ($\lambda^2 F(\nu)/\nu^3$) oscillator strength spectra of the intact phycobilisomes from *Fremyella diplosiphon* with respect to frequency in wavenumber (ν) scale at room temperature (23 ^{0}C). The sample was excited at 550 nm for fluorescence spectrum.

Figure 2.3 represents a deconvolution plot. A model absorption spectrum of intact phycobilisomes was prepared by adding the phycobiliprotein (PE, CPC, APC_{660}, APC_{680}) spectrum. All the phycobiliprotein spectra were shifted along the x-axis and varied their relative intensities to match the model spectrum with the actual absorption spectrum. For APC_{680} spectrum the absorption spectrum of APC_{660} was used with a 10 nm redshift.

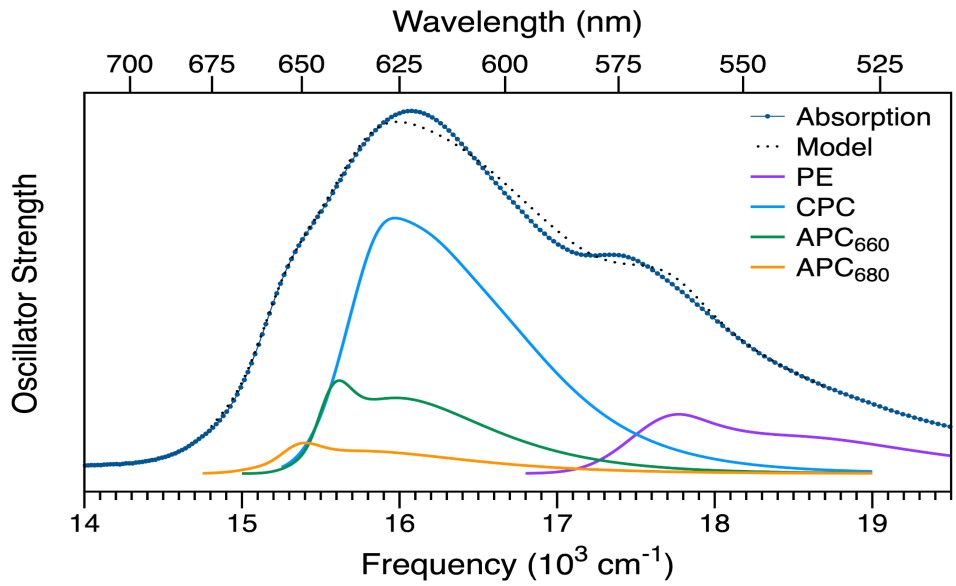

Figure 2.3 Spectral deconvolution Plot. Absorption spectrum is superimposed with the model spectrum of the intact phycobilisomes. The model spectrum is a sum of phycobiliprotein (PE, CPC, APC_{660} and APC_{680}) spectra.

Figure 2.4 shows the continues excitation-emission spectra collected from intact and broken phycobilisomes plotted a contour diagram. The spectrum of intact phycobilisome shows the maximum intensity at ~670 nm which is not a function of excitation wavelength. Also, there is no peak from PE at 580 nm. Intact phycobilisomes were added into low ionic strength phosphate buffer solution to break them intentionally. For the broken phycobilisomes there is a separate peak for PE at 580 nm and the main peak has blue-shifted to 650 nm which the emission maxima of CPC in the rods. In this was every phycobilisome samples were tested before and after 2DES experiments.

2.3.2 2DES Spectra

Figure 2.5 shows a series of 2DES spectra recorded with intact phycobilisomes isolated from F. *diplosiphon* at room temp (23 ^{0}C) using 6.7-fs laser pulses. The laser spectrum of this experiment has a central wavelength ~600 nm (Figure A2.5) and expands from 520 nm to 700 nm that covers the absorption of the blue-most phycobiliprotein PE and red-most

emission from the phycobiliprotein APC. The continuous excitation-emission spectrum (Figure 2.4) confirms that the phycobilisomes used in the experiment were intact.

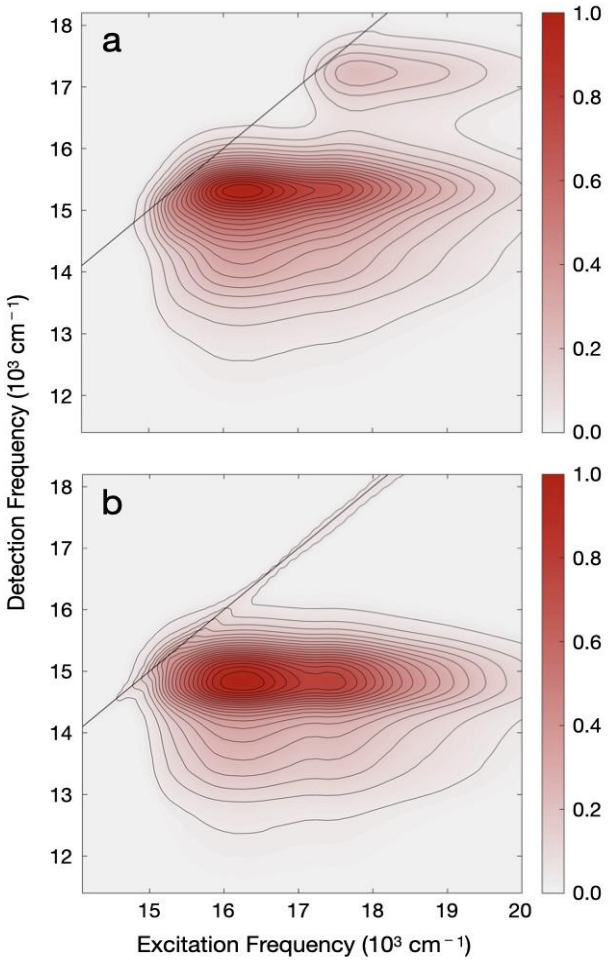

Figure 2.4. Continuous fluorescence excitation-emission spectra at room temperature (23 ^{0}C) from phycobilisomes isolated from *Fremyella diplosiphon*. a, for broken phycobilisomes which were prepared by adding intact phycobilisomes in 80 mM phosphate buffer solution at pH 7; b, for intact phycobilisomes in 0.8 M phosphate buffer solution at pH 7.

The 2DES spectrum shows the pump pulse induced change in the intensity of the delayed probe pulse as it passes through the sample after a delay time T. The prominent below-diagonal cross peak of stimulated emission (SE) character indicates the excitation energy transfer processes in phycobilisomes. That cross-peak progresses down the detection axis with population time *T* and finally lines up with the emission maximum of

APC_{680}. At early population time *T*, partially resolved cross peaks are present above and below the diagonal that display very rapidly damped amplitude modulation.

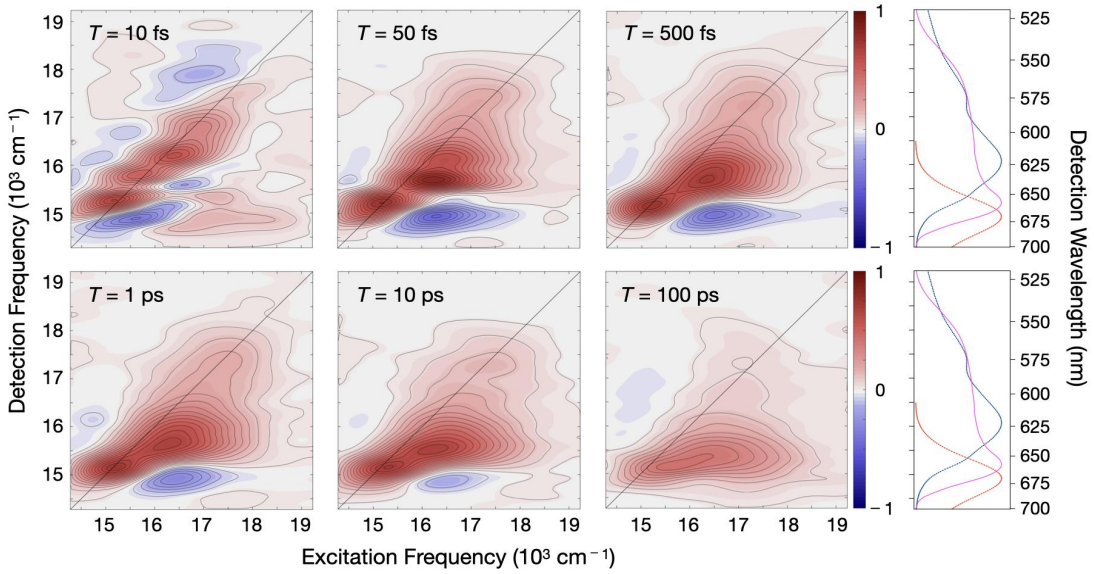

Figure 2.5. A series of 2DES spectra from intact phycobilisomes isolated from *Fremyella diplosiphon* ranging from T = 10 fs to 100 ps. The plotted signals are the sum of the rephasing and non-rephasing nonlinear optical responses. Each spectrum is normalized with respect to the maximum amplitude observed in the entire dataset. The side panels contain the absorption (blue) and fluorescence (red) oscillator strength spectra and laser spectrum (magenta) that were used in the 2DES experiments.

2.3.3 Global and Target Model

A global and target model can approximately describe the time evolution of the non-oscillatory signals in the 2DES spectra.[34] Using this method we can determine the average time required to transfer excitation energy between the phycobiliprotein components of the phycobilisome. For the global and target modeling, 550-580-nm excitation strip in the 2DES spectra was selected. This was because PE has maximum absorption in that spectral range and our goal was to determine the excitation energy transfer process from the end of the rod to the core of the phycobilisome. A kinetic model (Figure 2.6A) with five compartments including two distinct CPC segments (CPC_1 and CPC_2) is capable of

describing the excitation energy transfer process to the core sufficiently. Each compart is an ensemble of bilin chromophores in phycobiliprotein disks. The excited-state population moves from PE to CPC_1 with a 62±3-fs time constant. This time constant corresponds to the rising amplitude of the cross peak detected below the diagonal at 620 nm. In the T=10 fs spectrum a partially resolved peak appears from the SE of PE as below the diagonal cross peak at 580-600 nm region. Similar processes were reported in the transient grating measurements of isolated PE on the <100-fs timescale by Womick et al.[17] The cross peak due to excitation energy transfer moves further down the detection axis to 640 nm in 560±50 fs. This process corresponds to the energy transfer step CPC_1 to CPC_2 in the kinetic model. Similar time-constants have been reported in hexameric CPC[13,16] and in intact phycobilisomes.[18–20]

Then the cross peak moves down to the 650-680-nm range in the detection axis that corresponds to the core of the phycobilisome.[7,35] Excitation reaches to APC_{660} in 13±2 ps and travels then to APC_{680} in 58±3 ps (the subscripts of APC refers to the emission maximum). Excitation energy transfer rate in the core (APC_{660} to APC_{680}) is 50 times slower than that in the rods (CPC_1 to CPC_2). A kinetic model (Figure A2.1) with four compartments for the 645-660 nm excitation strip of the 2DES spectra produces a lower time constant 29±2 ps for APC_{660} to APC_{680} energy transfer step. Two kinetically different APC_{660} compartments are required for this model. In both models, the terminal emitter APC_{680} relaxes non-radiatively to ground state in ~400 ps. This lifetime is significantly shorter than ~1.5-ns intrinsic lifetime of the first excited state for a bilin chromophore. These results might suggest that bilin excited states in the terminal emitter are quenched by exciton-exciton annihilation[6] at the excitation pulses used in the 2DES experiment. Another

possible explanation would be that these phycobilisomes photoaccumulated redshifted bilins in the core that act as excitation energy traps.[36,37]

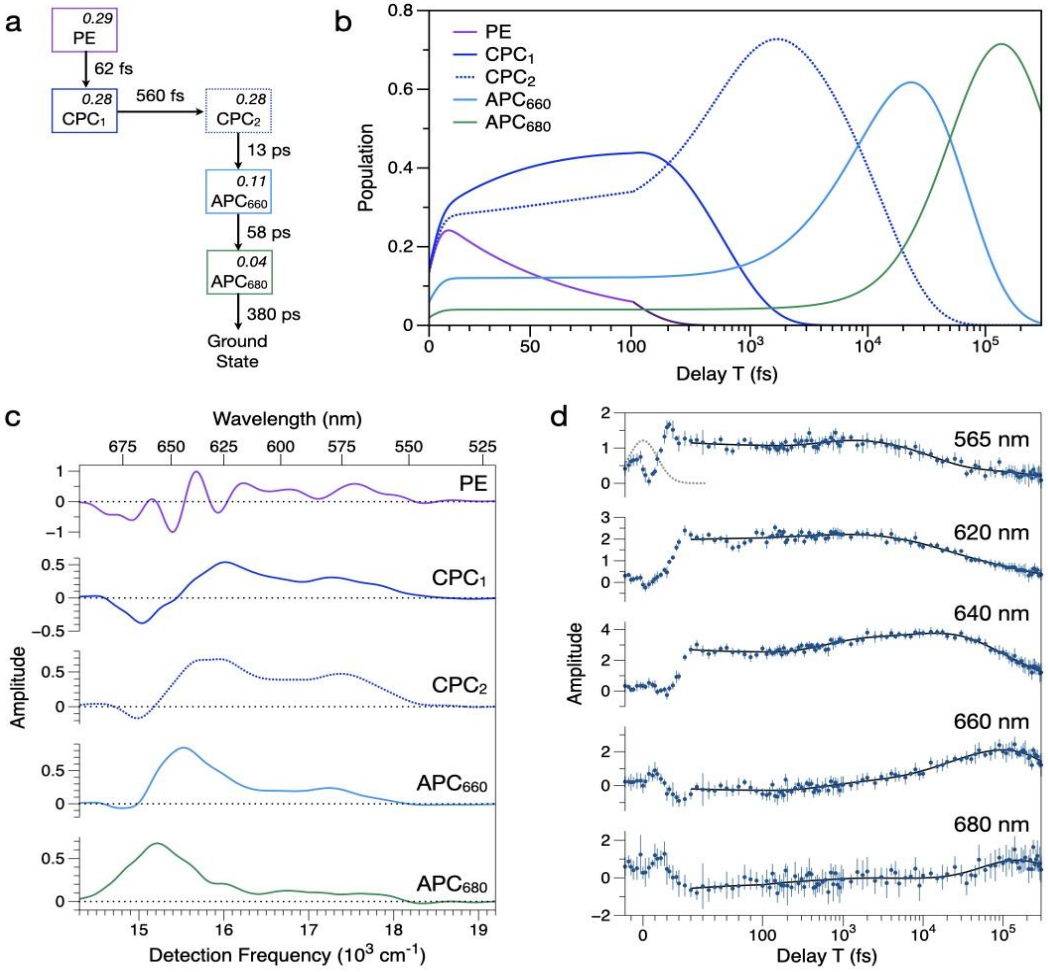

Figure 2.6. Global and target model for the 550-580 nm strip of the excitation axis of the 2DES spectrum. The <40-fs region of the T axis was excluded during modeling. a, Five-compartment spectrokinetic scheme with the time constants for each excitation energy transfer step. Each box is labeled with the initial fractional excitation that was calculated from the spectral deconvolution plot (Figure 2.3). b, Time (T) evolution of population for each compartment. c, Evolution-associated difference spectra (EADS). d, Amplitude transients sampled at five different detection wavelengths. The fitted global model is shown in black curve for T>40 fs. The bar at each data point represents the 95% confidence interval. The instrument-response function with 12-fs full width at half-maximum is shown with 565-nm transients as a Gaussian peak in a gray dotted curve centered at T = 0 fs. A semilogarithmic T axis with the linear-log split at 100 fs is used for b and d.

The evolution-associated difference spectra (EADS, Figure 2.6C) from global models indicate the presence of the delocalized excited states for the sub-picosecond processes in the rod of the phycobilisomes. EADS is the average of the third-order nonlinear optical responses from the bilin chromophores in a specific kinetic compartment. The EADS from PE box shows positive signals due to Ground-state bleaching (GSB) and SE over the 550-640-nm range. It also includes a set of negative peaks from excited-state absorption (ESA) transitions detected at 625 nm, 650 nm and 670 nm. These detection wavelengths also the absorption maximum of CPC, APC_{660} and APC_{680} respectively. This observation indicates that the bilin chromophores in the phycobilisome have a shared electronic ground-state character due to the presence of delocalized excitons. The ESA peak appears due to the absorption transitions from a singly excited exciton state to one of the higher energy states in a manifold of doubly excited exciton states.[38] This assignment is consistent with the other studies[15,16,38] where an excitonic model was considered for the pair of α84 and β84 chromophores from CPC and APC. The exciton ESA bands are sharper and deeper whereas the ESA bands of a single bilins are broad that spans the ground-state absorption region due to independent transitions to higher excited states.[38]

The EADS from the subsequent compartments of the global model show broader lineshape. The GSB and SE peaks are progressively red-shifted, and ESA peaks are decreasing in intensity (Figure 2.6C). These findings suggest that the excitation is increasingly localized on a single chromophore in the core of the phycobilisome. The ESA signal in the 2DES spectra decreases rapidly as compared to the GSB signal on the diagonal (Figure A2.2). After localization, the diagonal signal incorporates a long-lived component. This is due to the superimposition of the broad GSB lineshape of the APC in the core. Then

the diagonal signal moves to the farther red as excitation travels to the terminal emitter APC_{680} from APC_{660} mainly via the Förster mechanism.

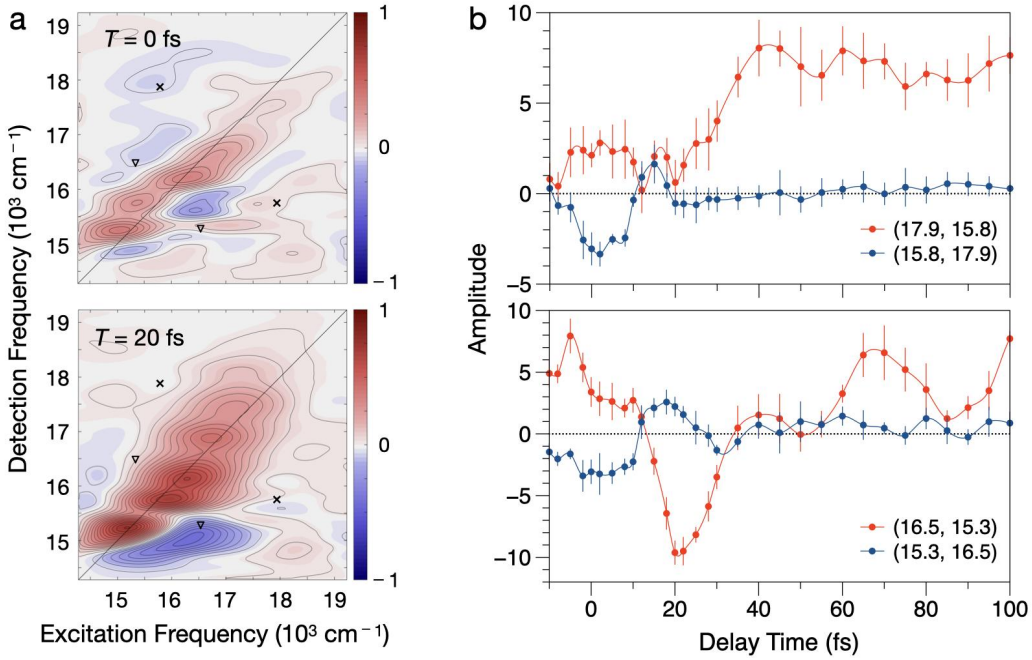

Figure 2.7. Oppositely phased oscillations from amplitude transients positioned symmetrically above and below the diagonal of the 2DES spectra. a, 2DES spectra from intact phycobilisomes isolated from *Fremyella diplosiphon* at T = 0 and 20 fs with normalized amplitude with respect to the maximum in the entire dataset. Markers 'x' and '▾' indicate the coordinates of the transients shown in figure b. b, Amplitude transients at the marked coordinates (in 10^3 cm^{-1}) and the bars are indicating the 95% confidence interval.

2.3.4 Coherence and Oscillation Maps

The global model predicted the presence of delocalized exciton in the phycobilisome upon photoexcitation. That prediction inspired us to do the coherence analysis on the rapidly damped oscillations in the 2DES spectra. Figure 2.7 represents a pair of amplitude transients positioned symmetrically across the diagonal of the 2DES spectrum. The transients are showing the modulation of the cross peaks that have an energy gap of 2100 cm^{-1} and 1200 cm^{-1}. The transients have oppositely phased oscillations till T<30 fs. Then a

more complicated oscillation pattern continues at least to T = 100 fs. Previous studies of the system with intermediate-to-strong electronic coupling between chromophores have discussed extensively the in-phase oscillatory signals due to delocalized electronic excitations.[39–43] Tiwari et al. predicted that the antiphase character can appear due to the delocalization of anticorrelated vibrations for paired chromophores.[44] This indicates that the oscillatory signals in the phycobilisome might have a vibronic character that involves mixing of electronic and vibrational states.

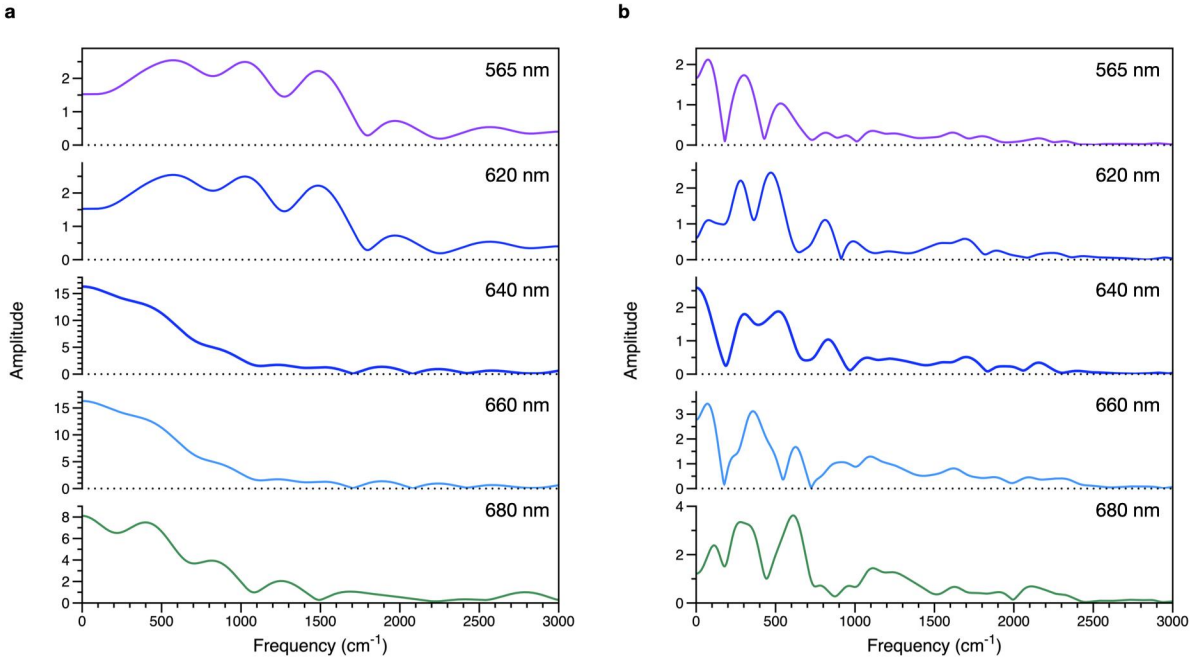

Figure 2.8. Fourier amplitude spectra. a and b, Fourier amplitude spectra calculated from T = 0-100 fs (a) and T = 50-500 fs (b) range of the amplitude transients presented in Figure 2.6d after subtracting the fitted global model. The effective resolution of these spectra is ~300 cm^{-1} and 75 cm^{-1} respectively.

At vibrational frequencies of bilins in phytochromes[45–48] and cyanobacteriochromes,[49] the strongest oscillatory signals from the phycobilisome have been observed asymmetrically below the diagonal of the 2DES spectrum.[42,50] These observations provide additional evidence that the vibrations contribute to the coherence. Figure 2.8 exhibits the

Fourier-transform (FT) amplitude spectra over T = 0-100 fs and Hann-windowed T = 50-500 fs range of the transients shown in Figure 2.6D. The C=C stretching vibrations, in-plane N-H rocking mode (from the B and C ring) are expected to show up in the ~1550-1700-cm^{-1} range in the FT spectra. The C-C and C-N stretching modes, in-plane vinyl C-H wagging mode appear at ~1300 cm^{-1}. The vinyl C-H out-of-plane wagging (HOOP) modes are observed in the ~800-900 cm^{-1} range. There are some additional peaks in the ~400-600 cm^{-1} region originating from the torsional vibrations which don't have the strong resonance Raman activity in single bilins.[47] The effective damping times for these oscillations are in the range of 50-100 fs.

An oscillation map can show the contribution of a particular coherence to the 2DES spectrum. The 3D spectrum[26,42] obtained by Fourier transformation with respect to T, is sliced at a particular oscillation frequency to create an oscillation map. Figure 2.9 shows the oscillation maps with the strongest peaks from the T = 0-100 fs of data. Additional oscillation maps shown in Figure A2.3 and Figure A2.4 are obtained from Hann-windowed T = 50-500 fs data. The oscillation maps obtained from later population time (T= 50-500 fs) are useful to identify the vibrational coherences that operate after the fast non-radiative decay processes.

The peak patterns in the oscillation maps for rapidly damped modulations can be explained in terms of coherent wavepacket motions proposed by Pollard and Mathies[51] in a theory for broadband femtosecond spectroscopy. The elongated peaks appear slightly above and parallel to the diagonal in several oscillation maps originating from the coherence oscillatory motion of the wavepacket in the ground state which are created by stimulated Raman transitions. The oscillation map for the 520-cm^{-1} does not have a

diagonal peak whereas the 1670-cm-1 map has a relatively strong diagonal peak due to the C=C stretching modes (Figure 2.9). Several oscillation maps exhibit a series of intense peaks near the fluorescence maxima in the detection axis. The coherent motion of the excited-state wavepackets are creating these peaks while evolving to the lower energy via a coherent non-adiabatic mechanism.[52] In the wavepacket motion the vibrational modes are strongly coupled with interexciton electronic transitions. In this picture the complex peak pattern in oscillation maps appear due to interference of the GSB signals from the ground-state wavepackets with SE and exciton ESA signals from the excited-state wavepackets. In contrast, an evenly spaced 'chair-shaped' peak pattern can be observed due to superimposed GSB and SE peaks for vibrational coherences in the Born-Oppenheimer regime, where the periods of the vibrational modes are much shorter than the electronic relaxation times.

2.4 Discussion

Womick and Moran[15,53] first proposed the vibronic exciton scheme for the α84-β84 bilin pairs in APC trimers. That scheme could explain the prominence of the HOOP mode at ~800-900 cm^{-1} in the phycobilisomes as compared to that in the resonance Raman spectra of single bilin chromophore. Figure 2.10A shows a four-exciton energy level diagram (X1 to X4) obtained by quantum-coherent mixing of the first two vibrational energy levels ($\nu = 0$ and 1) of the singly excited electronic states of a α84-β84 pair. This representation is an extension of the quantum-coherent mixing of the purely electronic states of a pair of chromophores. The delocalized character and the speed of non-radiative decay between the exciton states increased in the APC trimer because the difference in energy between the bilin sites matches with the HOOP quantum, the so-called vibrational resonance

condition.[54,55] For the isolated CPC hexamers, the degree of delocalization is less since energy difference between the α84 and β84 chromophores does not match the HOOP quantum.[16,53] The energy gap between X1 and X4 is twice of HOOP quanta. Therefore, the coherence related to X1-X4 would contribute to the 1600-1700 cm^{-1} range in the oscillation maps.

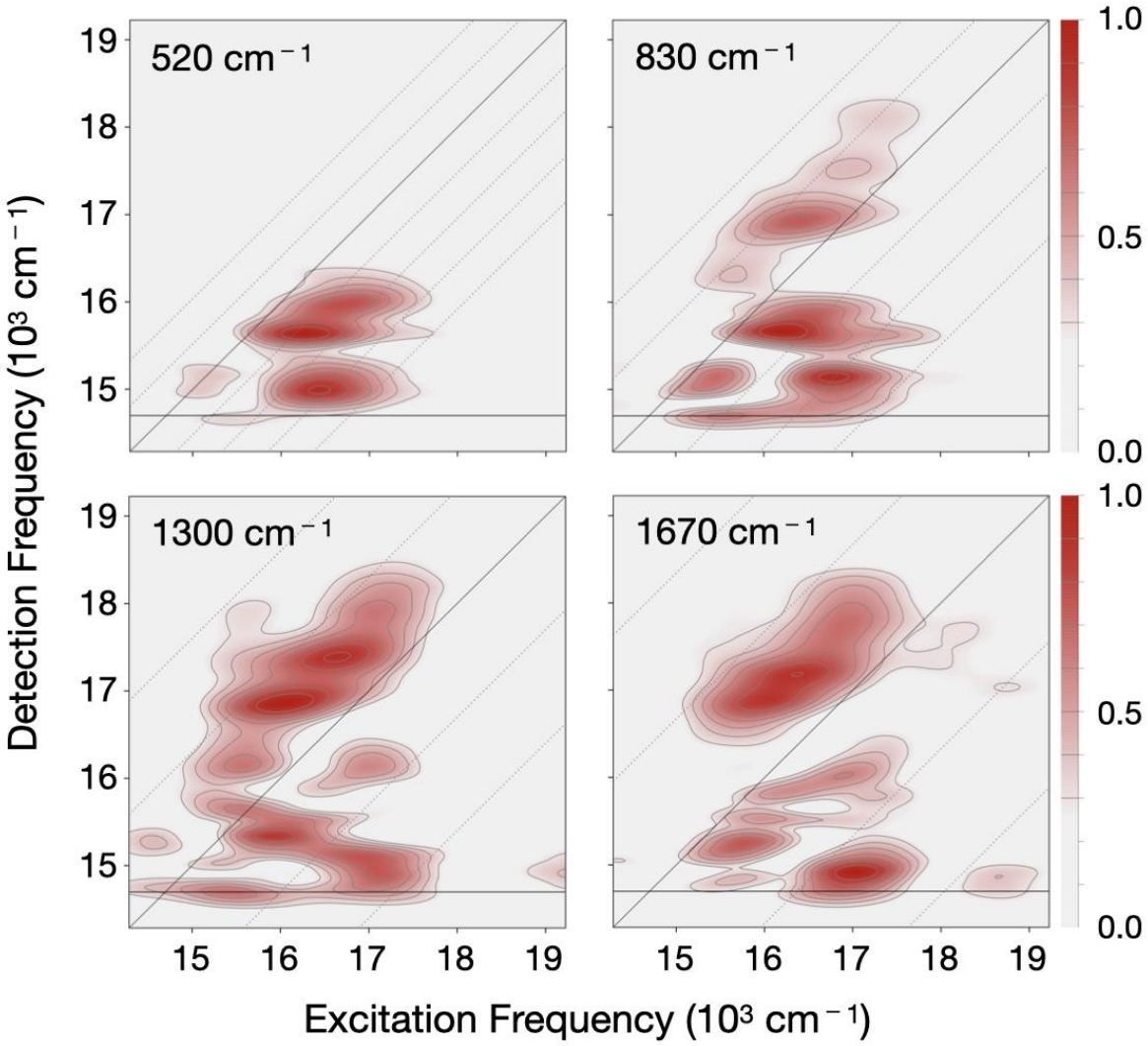

Figure 2.9. Oscillation maps for the principal components observed in Figure 2.8 centered at 520, 830, 1300 and 1670 cm^{-1}, as calculated by Fourier transformation of the 2DES spectrum over the T = 0-100 fs range. The non-oscillatory part was removed by subtracting an overdetermined 2D global model. Several equispaced dashed lines have been drawn parallel to the diagonal line by the selected modulation frequency. The black horizontal line along the detection axis represents the peak of the fluorescence-oscillator spectrum.

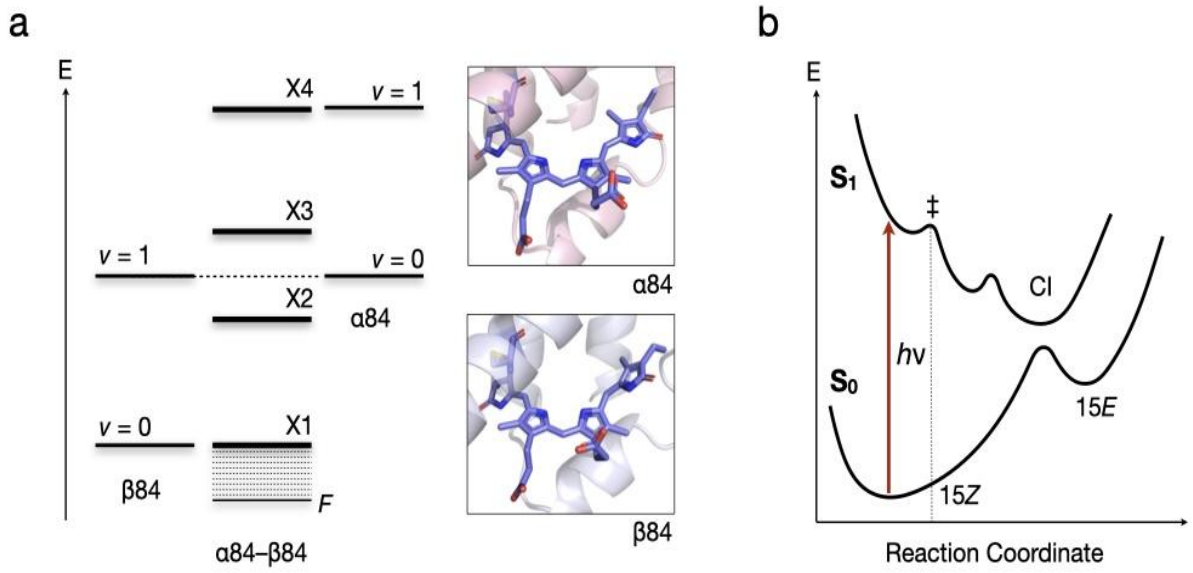

Figure 2.10. Energy level and potential energy diagrams for bilin chromophores. a, Vibronic excitons for a pair of α84-β84 bilin chromophores in APC trimers, as proposed by Womick and Moran.[53] 'F' labels the fluorescence state reached after localization from the X1 level. The insets show a close look of the confirmation of the α84 and β84 chromophores in the X-ray crystal structure of APC trimer (PDB - 1ALL)[56] where ring A is attached with cysteine residue in the left-hand side. b, Potential energy plot for the ground state (S_0) and first excited (S_1) singlet electronic state of the bilins with respect to a reaction coordinate due to a sequential in-plane and out-of-plane motions. Near a seam of conical intersections (CI) the S_0 and S_1 states are mixed in character where decay to the original 15Z or to the D-ring-flipped 15E configuration occurs. There is a local barrier in the S_1 state prior to the out-of-plane motions.[57]

The out-of-plane distortions and the resulting coupling[47] to torsional modes of the bilin chromophores in the phycobilisome would make the HOOP mode more prominent in the vibronic exciton scheme. Figure 2.10B represents the potential energy level diagram including the ground state (S_0) and the first singlet excited state (S_1) with respect to the out-of-plane distortions.[57] The resonance Raman-active stretching modes[58] can create the out-of-plane distortion in a bilin chromophore from a planar ground-state conformation. If a vibrational mode twists or bends the conjugated region of a chromophore then it can cause a large modulation in the potential energies of the S_1 and S_2. In that situation ICT

character can be created.[59–61] So, the torsional modes could act as a promoting modes in a coherent non-adiabatic relaxation mechanism[52,62,63] along with the HOOP modes. This HOOP mode would accept energy at each interexciton relaxation step through vibrational resonance. The torsional modes behave as a branching mode that helps to lift the degeneracy at conical intersection (CTs) of the potential energy surfaces of two exciton states.[62,64] Figure 2.11A is a cartoon representation of how a cascade of CIs between the exciton potential energy surfaces for a pair of bilins could mediate coherent non-radiative passage of a wavepacket to the lowest exciton level. In APC, the interexciton relaxation takes about 30 fs[15,38,53] and similar time constant has been reported for PE[17] also. Other studies on cryptophyte phycobiliproteins proposed similar fast non-adiabatic vibronic processes.[65,66]

Figure 2.11B shows the electronic and vibronic exciton energy level diagram in the intact phycobilisome. Here a simplified picture has been shown that was derived only from the singly excited excitons due to a pair of bilin chromophores. If we consider more than a pair of chromophores are collectively excited, then the manifold of exciton states would be denser. The twisting of the bilins in the S_1 state would promote the localization[67,68] because the reorganization energy (or system-bath coupling) λ[69] increases with the increase on permanent dipole moment of a chromophore. Therefore, there is a kinetic competition going on between the fast interexciton relaxation mechanisms and localization on a single bilin. This was observed recently in the peridinin-chlorophyll protein that exhibits out-of-plane motion of the carotenoid peridinin.[68,70]

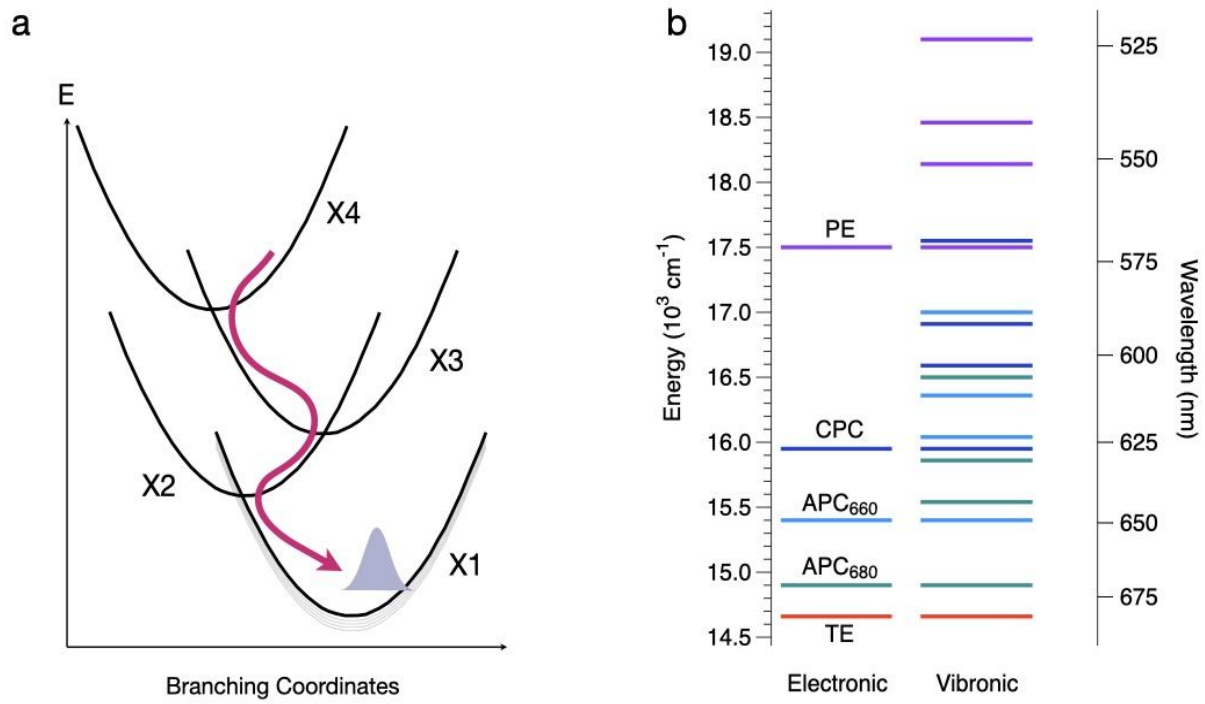

Figure 2.11. Non-adiabatic interexciton relaxation mechanism and energy states in intact phycobilisome. a, Schematic representation of coherent wavepacket motions after optically prepared X4 state for a pair of bilins via a cascade of conical intersections between exciton potential surfaces. b, Simplified energy level (electronic and vibronic) scheme for intact phycobilisome. Energy state of the phycobiliprotein was taken from Figure 2.3. TE is the fluorescence maxima for APC_{680} terminal emitters. The vibronic levels shown for each component are as in Figure 2.10a. The electronic coupling J is 160 cm^{-1} and the energy of the two vibrational level $E_{v=1}$ and $E_{v=0}$ has a difference of 800 cm^{-1} for the HOOP mode of bilin was considered for the vibronic levels.

The localization of the excitation energy could occur at any bilin chromophore in the phycobilisome, but the lower energy β84 chromophore in APC has higher probability for this. The crystal structure of APC trimer (PDB structure 1ALL)[56] shows that the β84 chromophore has an additional rotation of ring C and ring D is out of plane compared to those of the α84 chromophore (Figure 2.10A). Therefore, even in the ground-state α84 possesses a higher permanent dipole moment. The lowest-energy excitons have higher contributions from the lower energy levels of the chromophore. Also, delocalization decreases with increase in λ compared to electronic coupling J.[67,68]. Therefore, the lower

exciton state would be very likely to be localized on the β84 chromophore in the APC. This proposal is supported by the findings in the oscillation map (Figure A2.4) of coherences at ~1100 cm^{-1} that have peaks mainly in the APC region. This oscillation is occurring due to the in-plane wagging mode of the vinyl C-H for a localized bilin excitation in a twisted conformation for ring D. The in-plane and out-of-plane vinyl C-H wagging modes are becoming mixed due to ICT character. This mixing is redshing the in-plane mode to ~1300 cm^{-1} and blueshifting the HOOP mode to ~830 cm^{-1} range.[48]

The excitation energy transfer rate from the rods to the APC_{660} in the core is very slow as compared to that in the rods. This kinetic bottleneck helps to keep the rod-to-core energy transfer process in the intact phycobilisome irreversible. This is a very useful step because in the Förster mechanism excitation energy can be transferred from a localized bilins to a nearby delocalized pair along the pathway of bilins in either direction, upwards or downwards, in the CPC-containing rod segments and it does not matter whether it is upwards or downwards. Upon impulsive optical excitation, the damping time for macroscopic coherence is very low in the phycobilisome. Similar situation has been observed for the Fenna-Mattews-Olson complex.[43] The microscopic coherence is involved in the progress of excitation energy over long distances down the rods in less than 1 ps and from the rods to the core in about 10 ps. There is a possibility that excitation energy could move sideways between isoenergetic bilins across the CPC disks in >40 ps time scale via the Förster mechanism.[9] The hopping of excitation from α84 to β84 in a given pair takes about 1 ps and ~2-3 ps for pairs longitudinally in a CPC hexamer.[8,9] The reorganizational dynamics of the core discourages excitation energy to escape from the core and that provides a dynamic stabilization.

The overall rate of excitation transfer to the chlorophyll in PS II from phycobilisome is limited by the energy transfer rate from APC_{660} to the terminal emitter. Therefore, any photoregulatory or photoprotective process in the core can compete with this step by introducing a faster quenching mechanism. Bilins has a natural tendency to undergo ring-flip photoisomerization on the picosecond timescale and that could create a trap especially in the β84 sites of APC in the core. This isomerization process could possibly be a mechanism for intrinsic quenching. Few single-molecule fluorescence studies of phycobilisomes have reported the presence of redshifted bilin sites under continuous illumination.[36,37] These traps could act as a faster intrinsic quenching response to fluctuations of the ambient light intensity. There is another slower regulatory response, non-photochemical quenching, present in the cyanobacterial cell involving activation of the orange carotenoid protein (OCP).[71] In this process activated OCP binds to the core of the phycobilisome and introduces a ketocarotenoid to quench the excitation along the pathway from APC_{660} to APC_{680}. These findings strongly suggest that multidimensional electronic spectroscopy will be employed in future study of the details of these quenching mechanisms.

2.5 Conclusion

Multidimensional electronic spectroscopy was employed in intact phycobilisomes to determine the excitation energy transfer mechanisms. The 2DES spectra, global model and oscillation maps strongly suggest that delocalized excitons are present in the rods of the phycobilisome. That could be a compelling functional explanation for the paired bilin chromophores in the hexameric and trimeric phycobiliprotein disks. The coherence analysis suggests that the vibronic wavepackets prominently involving HOOP mode mediate

the excitation energy transfer processes. The kinetic model predicts that the excitation travels fast in <1 ps time scale in the rods and then slows down more than 50 times in the core. The diminished character of ESA in the EADS from the core and slowness of excitation transfer makes it clear that delocalized excitons ultimately collapse onto single bilins in the core. The further analysis of the coherences and a closer look in the X-ray crystal structure of APC indicate that upon photoexcitation the lowest-energy bilins in the core can create the ICT character by undergoing out-of-plane conformational distortions. This ICT character localizes the excitation in the core and excitation energy-transfer occurs via the Förster mechanism. The slowness of the energy transfer process helps the quenching mechanisms to operate smoothly.

REFERENCES

(1) Gantt, E. Phycobilisomes: Light-Harvesting Pigment Complexes. *Bioscience* **1975**, *25*, 781–788, DOI: 10.2307/1297221.

(2) Glazer, A. N. Light Harvesting by Phycobilisomes. *Annu. Rev. Biophys. Biophys. Chem.* **1985**, *14*, 47–77, DOI: 10.1146/annurev.bb.14.060185.000403.

(3) Adir, N. Elucidation of the Molecular Structures of Components of the Phycobilisome: Reconstructing a Giant. *Photosynth. Res.* **2005**, *85*, 15–32, DOI: 10.1007/s11120-004-2143-y.

(4) David, L.; Marx, A.; Adir, N. High-Resolution Crystal Structures of Trimeric and Rod Phycocyanin. *J. Mol. Biol.* **2011**, *405*, 201–213, DOI: 10.1016/j.jmb.2010.10.036.

(5) Liu, H.; Zhang, H.; Niedzwiedzki, D. M.; Prado, M.; He, G.; Gross, M. L.; Blankenship, R. E. Phycobilisomes Supply Excitations to Both Photosystems in a Megacomplex in Cyanobacteria. *Science* **2013**, *342*, 1104–1107, DOI: 10.1126/science.1242321.

(6) van Stokkum, I. H. M.; Gwizdala, M.; Tian, L.; Snellenburg, J. J.; van Grondelle, R.; van Amerongen, H.; Berera, R. A Functional Compartmental Model of the Synechocystis PCC 6803 Phycobilisome. *Photosynth. Res.* **2018**, *135*, 87–102, DOI: 10.1007/s11120-017-0424-5.

(7) Tian, L.; Gwizdala, M.; van Stokkum, I. H. M.; Koehorst, R. B. M.; Kirilovsky, D.; van Amerongen, H. Picosecond Kinetics of Light Harvesting and Photoprotective Quenching in Wild-Type and Mutant Phycobilisomes Isolated from the Cyanobacterium *Synechocystis* PCC 6803. *Biophys. J.* **2012**, *102*, 1692–1700, DOI: 10.1016/j.bpj.2012.03.008.

(8) Sauer, K.; Scheer, H. Excitation Transfer in C-Phycocyanin. Förster Transfer Rate and Exciton Calculations Based on New Crystal Structure Data for C-Phycocyanins from Agmenellum Quadruplicatum and Mastigocladus Laminosus. *Biochimica et Biophysica Acta (BBA) - Bioenergetics* **1988**, *936*, 157–170, DOI: 10.1016/0005-2728(88)90232-0.

(9) Debreczeny, M. P.; Sauer, K.; Zhou, J.; Bryant, D. A. Comparison of Calculated and Experimentally Resolved Rate Constants for Excitation Energy Transfer in C-Phycocyanin. 2. Trimers. *J. Phys. Chem.* **1995**, *99*, 8420–8431, DOI: 10.1021/j100020a081.

(10) Beljonne, D.; Curutchet, C.; Scholes, G. D.; Silbey, R. J. Beyond Förster Resonance Energy Transfer in Biological and Nanoscale Systems. *J. Phys. Chem. B* **2009**, *113*, 6583–6599, DOI: 10.1021/jp900708f.

(11) Rosinski, J.; Hainfeld, J. F.; Rigbi, M.; Siegelman, H. W. Phycobilisome Ultrastructure and Chromatic Adaptation in Fremyella Diplosiphon. *Ann. Bot.* **1981**, *47*, 1–12, DOI: 10.1093/oxfordjournals.aob.a085984.

(12) Duerring, M.; Schmidt, G. B.; Huber, R. Isolation, Crystallization, Crystal Structure Analysis and Refinement of Constitutive C-Phycocyanin from the Chromatically Adapting Cyanobacterium Fremyella Diplosiphon at 1.66 A Resolution. *J. Mol. Biol.* **1991**, *217*, 577–592, DOI: 10.1016/0022-2836(91)90759-y.

(13) Riter, R. E.; Edington, M. D.; Beck, W. F. Isolated-Chromophore and Exciton-State Photophysics in C-Phycocyanin Trimers. *J. Phys. Chem. B* **1997**, *101*, 2366–2371, DOI: 10.1021/jp962609l.

(14) Homoelle, B. J.; Edington, M. D.; Diffey, W. M.; Beck, W. F. Stimulated Photon-Echo and Transient-Grating Studies of Protein-Matrix Solvation Dynamics and Interexciton-State Radiationless Decay in α Phycocyanin and Allophycocyanin. *The Journal of Physical Chemistry B*. **1998**, pp 3044–3052.

(15) Womick, J. M.; Moran, A. M. Exciton Coherence and Energy Transport in the Light-Harvesting Dimers of Allophycocyanin. *J. Phys. Chem. B* **2009**, *113*, 15747–15759, DOI: 10.1021/jp907644h.

(16) Womick, J. M.; Moran, A. M. Nature of Excited States and Relaxation Mechanisms in C-Phycocyanin. *J. Phys. Chem. B* **2009**, *113*, 15771–15782, DOI: 10.1021/jp908093x.

(17) Womick, J. M.; Liu, H.; Moran, A. M. Exciton Delocalization and Energy Transport Mechanisms in R-Phycoerythrin. *J. Phys. Chem. A* **2011**, *115*, 2471–2482, DOI: 10.1021/jp111720a.

(18) Theiss, C.; Schmitt, F.-J.; Pieper, J.; Nganou, C.; Grehn, M.; Vitali, M.; Olliges, R.; Eichler, H. J.; Eckert, H.-J. Excitation Energy Transfer in Intact Cells and in the Phycobiliprotein Antennae of the Chlorophyll d Containing Cyanobacterium Acaryochloris Marina. *J. Plant Physiol.* **2011**, *168*, 1473–1487, DOI: 10.1016/j.jplph.2011.02.002.

(19) Nganou, C.; David, L.; Adir, N.; Mkandawire, M. Linker Proteins Enable Ultrafast Excitation Energy Transfer in the Phycobilisome Antenna System of Thermosynechococcus Vulcanus. *Photochem. Photobiol. Sci.* **2016**, *15*, 31–44, DOI: 10.1039/c5pp00285k.

(20) Fălămaș, A.; Porav, S. A.; Tosa, V. Investigations of the Energy Transfer in the Phycobilisome Antenna of Arthrospira Platensis Using Femtosecond Spectroscopy. *NATO Adv. Sci. Inst. Ser. E Appl. Sci.* **2020**, *10*, 4045, DOI: 10.3390/app10114045.

(21) Domínguez-Martín, M. A.; Sauer, P. V.; Kirst, H.; Sutter, M.; Bína, D.; Greber, B. J.; Nogales, E.; Polívka, T.; Kerfeld, C. A. Structures of a Phycobilisome in Light-Harvesting and

Photoprotected States. *Nature* **2022**, *609*, 835–845, DOI: 10.1038/s41586-022-05156-4.

(22) Zheng, L.; Zheng, Z.; Li, X.; Wang, G.; Zhang, K.; Wei, P.; Zhao, J.; Gao, N. Structural Insight into the Mechanism of Energy Transfer in Cyanobacterial Phycobilisomes. *Nat. Commun.* **2021**, *12*, 5497, DOI: 10.1038/s41467-021-25813-y.

(23) Zhang, J.; Ma, J.; Liu, D.; Qin, S.; Sun, S.; Zhao, J.; Sui, S.-F. Structure of Phycobilisome from the Red Alga Griffithsia Pacifica. *Nature* **2017**, *551*, 57–63, DOI: 10.1038/nature24278.

(24) Ma, J.; You, X.; Sun, S.; Wang, X.; Qin, S.; Sui, S.-F. Structural Basis of Energy Transfer in Porphyridium Purpureum Phycobilisome. *Nature* **2020**, *579*, 146–151, DOI: 10.1038/s41586-020-2020-7.

(25) Jonas, D. M. Two-Dimensional Femtosecond Spectroscopy. *Annu. Rev. Phys. Chem.* **2003**, *54*, 425–463, DOI: 10.1146/annurev.physchem.54.011002.103907.

(26) Li, H.; Bristow, A. D.; Siemens, M. E.; Moody, G.; Cundiff, S. T. Unraveling Quantum Pathways Using Optical 3D Fourier-Transform Spectroscopy. *Nat. Commun.* **2013**, *4*, 1–9, DOI: 10.1038/ncomms2405.

(27) Gantt, E.; Lipschultz, C. A.; Grabowski, J.; Zimmerman, B. K. Phycobilisomes from Blue-Green and Red Algae: Isolation Criteria and Dissociation Characteristics. *Plant Physiol.* **1979**, *63*, 615–620, DOI: 10.1104/pp.63.4.615.

(28) Aráoz, R.; Häder, D.-P. Ultraviolet Radiation Induces Both Degradation and Synthesis of Phycobilisomes in Nostoc Sp.: A Spectroscopic and Biochemical Approach. *FEMS Microbiol. Ecol.* **1997**, *23*, 301–313, DOI: 10.1111/j.1574-6941.1997.tb00411.x.

(29) Gurchiek, J. K.; Rose, J. B.; Guberman-Pfeffer, M. J.; Tilluck, R. W.; Ghosh, S.; Gascón, J. A.; Beck, W. F. Fluorescence Anisotropy Detection of Barrier Crossing and Ultrafast Conformational Dynamics in the S2 State of β-Carotene. *J. Phys. Chem. B* **2020**, *124*, 9029–9046, DOI: 10.1021/acs.jpcb.0c06961.

(30) Rose, J. B.; Beck, W. F. Fluorescence of Carotenoids: Probing Binding Site Interactions and Conformational Motion in Carotenoproteins. *Methods Enzymol.* **2022**, *674*, 85–111, DOI: 10.1016/bs.mie.2022.04.007.

(31) Shim, S.-H.; Zanni, M. T. How to Turn Your Pump-Probe Instrument into a Multidimensional Spectrometer: 2D IR and Vis Spectroscopies via Pulse Shaping. *Phys. Chem. Chem. Phys.* **2009**, *11*, 748–761, DOI: 10.1039/b813817f.

(32) Lozovoy, V. V.; Pastirk, I.; Dantus, M. Multiphoton Intrapulse Interference. IV. Ultrashort Laser Pulse Spectral Phase Characterization and Compensation. *Opt. Lett.* **2004**, *29*, 775–777, DOI: 10.1364/ol.29.000775.

(33) Augulis, R.; Zigmantas, D. Two-Dimensional Electronic Spectroscopy with Double Modulation Lock-in Detection: Enhancement of Sensitivity and Noise Resistance. *Opt. Express* **2011**, *19*, 13126–13133, DOI: 10.1364/OE.19.013126.

(34) van Stokkum, I. H. M.; Larsen, D. S.; van Grondelle, R. Global and Target Analysis of Time-Resolved Spectra. *Biochim. Biophys. Acta* **2004**, *1657*, 82–104, DOI: 10.1016/j.bbabio.2004.04.011.

(35) Tian, L.; van Stokkum, I. H. M.; Koehorst, R. B. M.; Jongerius, A.; Kirilovsky, D.; van Amerongen, H. Site, Rate, and Mechanism of Photoprotective Quenching in Cyanobacteria. *J. Am. Chem. Soc.* **2011**, *133*, 18304–18311, DOI: 10.1021/ja206414m.

(36) Krüger, T. P. J.; van Grondelle, R.; Gwizdala, M. The Role of Far-Red Spectral States in the Energy Regulation of Phycobilisomes. *Biochim. Biophys. Acta Bioenerg.* **2019**, *1860*, 341–349, DOI: 10.1016/j.bbabio.2019.01.007.

(37) Wahadoszamen, M.; Krüger, T. P. J.; Ara, A. M.; van Grondelle, R.; Gwizdala, M. Charge Transfer States in Phycobilisomes. *Biochim. Biophys. Acta Bioenerg.* **2020**, *1861*, 148187, DOI: 10.1016/j.bbabio.2020.148187.

(38) Edington, M. D.; Riter, R. E.; Beck, W. F. Interexciton-State Relaxation and Exciton Localization in Allophycocyanin Trimers. *J. Phys. Chem.* **1996**, *100*, 14206–14217, DOI: 10.1021/jp960454b.

(39) Cheng, Y.-C.; Fleming, G. R. Coherence Quantum Beats in Two-Dimensional Electronic Spectroscopy. *J. Phys. Chem. A* **2008**, *112*, 4254–4260, DOI: 10.1021/jp7107889.

(40) Ginsberg, N. S.; Cheng, Y.-C.; Fleming, G. R. Two-Dimensional Electronic Spectroscopy of Molecular Aggregates. *Acc. Chem. Res.* **2009**, *42*, 1352–1363, DOI: 10.1021/ar9001075.

(41) Collini, E.; Wong, C. Y.; Wilk, K. E.; Curmi, P. M. G.; Brumer, P.; Scholes, G. D. Coherently Wired Light-Harvesting in Photosynthetic Marine Algae at Ambient Temperature. *Nature* **2010**, *463*, 644–647, DOI: 10.1038/nature08811.

(42) Butkus, V.; Zigmantas, D.; Valkunas, L.; Abramavicius, D. Vibrational vs. Electronic Coherences in 2D Spectrum of Molecular Systems. *Chem. Phys. Lett.* **2012**, *545*, 40–43, DOI: 10.1016/j.cplett.2012.07.014.

(43) Duan, H.-G.; Prokhorenko, V. I.; Cogdell, R. J.; Ashraf, K.; Stevens, A. L.; Thorwart, M.; Miller, R. J. D. Nature Does Not Rely on Long-Lived Electronic Quantum Coherence for

Photosynthetic Energy Transfer. *Proc. Natl. Acad. Sci. U. S. A.* **2017**, *114*, 8493–8498, DOI: 10.1073/pnas.1702261114.

(44) Tiwari, V.; Peters, W. K.; Jonas, D. M. Electronic Resonance with Anticorrelated Pigment Vibrations Drives Photosynthetic Energy Transfer Outside the Adiabatic Framework. *Proc. Natl. Acad. Sci. U. S. A.* **2013**, *110*, 1203–1208, DOI: 10.1073/pnas.1211157110.

(45) Kneip, C.; Hildebrandt, P.; Németh, K.; Mark, F.; Schaffner, K. Interpretation of the Resonance Raman Spectra of Linear Tetrapyrroles Based on DFT Calculations. *Chem. Phys. Lett.* **1999**, *311*, 479–484, DOI: 10.1016/S0009-2614(99)00868-4.

(46) Kneip, C.; Hildebrandt, P.; Schlamann, W.; Braslavsky, S. E.; Mark, F.; Schaffner, K. Protonation State and Structural Changes of the Tetrapyrrole Chromophore during the Pr --> Pfr Phototransformation of Phytochrome: A Resonance Raman Spectroscopic Study. *Biochemistry* **1999**, *38*, 15185–15192, DOI: 10.1021/bi990688w.

(47) Andel, F., 3rd; Murphy, J. T.; Haas, J. A.; McDowell, M. T.; van der Hoef, I.; Lugtenburg, J.; Lagarias, J. C.; Mathies, R. A. Probing the Photoreaction Mechanism of Phytochrome through Analysis of Resonance Raman Vibrational Spectra of Recombinant Analogues. *Biochemistry* **2000**, *39*, 2667–2676, DOI: 10.1021/bi991688z.

(48) Dasgupta, J.; Frontiera, R. R.; Taylor, K. C.; Lagarias, J. C.; Mathies, R. A. Ultrafast Excited-State Isomerization in Phytochrome Revealed by Femtosecond Stimulated Raman Spectroscopy. *Proc. Natl. Acad. Sci. U. S. A.* **2009**, *106*, 1784–1789, DOI: 10.1073/pnas.0812056106.

(49) Osoegawa, S.; Miyoshi, R.; Watanabe, K.; Hirose, Y.; Fujisawa, T.; Ikeuchi, M.; Unno, M. Identification of the Deprotonated Pyrrole Nitrogen of the Bilin-Based Photoreceptor by Raman Spectroscopy with an Advanced Computational Analysis. *J. Phys. Chem. B* **2019**, *123*, 3242–3247, DOI: 10.1021/acs.jpcb.9b00965.

(50) Butkus, V.; Alster, J.; Bašinskaitė, E.; Augulis, R. N.; Neuhaus, P.; Valkunas, L.; Anderson, H. L.; Abramavicius, D.; Zigmantas, D. Discrimination of Diverse Coherences Allows Identification of Electronic Transitions of a Molecular Nanoring. *J. Phys. Chem. Lett.* **2017**, *8*, 2344–2349, DOI: 10.1021/acs.jpclett.7b00612.

(51) Pollard, W. T.; Mathies, R. A. Analysis of Femtosecond Dynamic Absorption Spectra of Nonstationary States. *Annu. Rev. Phys. Chem.* **1992**, *43*, 497–523, DOI: 10.1146/annurev.pc.43.100192.002433.

(52) Tully, J. C. Perspective: Nonadiabatic Dynamics Theory. *J. Chem. Phys.* **2012**, *137*, 22A301, DOI: 10.1063/1.4757762.

(53) Womick, J. M.; Moran, A. M. Vibronic Enhancement of Exciton Sizes and Energy Transport in Photosynthetic Complexes. *J. Phys. Chem. B* **2011**, *115*, 1347–1356, DOI: 10.1021/jp106713q.

(54) Tiwari, V.; Peters, W. K.; Jonas, D. M. Electronic Energy Transfer through Non-Adiabatic Vibrational-Electronic Resonance. I. Theory for a Dimer. *J. Chem. Phys.* **2017**, *147*, 154308, DOI: 10.1063/1.5005835.

(55) Tiwari, V.; Jonas, D. M. Electronic Energy Transfer through Non-Adiabatic Vibrational-Electronic Resonance. II. 1D Spectra for a Dimer. *J. Chem. Phys.* **2018**, *148*, 084308, DOI: 10.1063/1.5003193.

(56) Brejc, K.; Ficner, R.; Huber, R.; Steinbacher, S. Isolation, Crystallization, Crystal Structure Analysis and Refinement of Allophycocyanin from the Cyanobacterium Spirulina Platensis at 2.3 A Resolution. *J. Mol. Biol.* **1995**, *249*, 424–440, DOI: 10.1006/jmbi.1995.0307.

(57) Kim, P. W.; Freer, L. H.; Rockwell, N. C.; Martin, S. S.; Lagarias, J. C.; Larsen, D. S. Femtosecond Photodynamics of the Red/Green Cyanobacteriochrome NpR6012g4 from Nostoc Punctiforme. 1. Forward Dynamics. *Biochemistry* **2012**, *51*, 608–618, DOI: 10.1021/bi201507k.

(58) Sanchez-Galvez, A.; Hunt, P.; Robb, M. A.; Olivucci, M.; Vreven, T.; Schlegel, H. B. Ultrafast Radiationless Deactivation of Organic Dyes: Evidence for a Two-State Two-Mode Pathway in Polymethine Cyanines. *J. Am. Chem. Soc.* **2000**, *122*, 2911–2924, DOI: 10.1021/ja993985x.

(59) Bonačić-Koutecký, V.; Koutecký, J.; Michl, J. Neutral and Charged Biradicals, Zwitterions, Funnels in S_1, and Proton Translocation: Their Role in Photochemistry, Photophysics, and Vision. *Angew. Chem. Int. Ed Engl.* **1987**, *26*, 170–189, DOI: 10.1002/anie.198701701.

(60) Michl, J.; Bonačić-Kouteck\`y, V. Electronic Aspects of Organic Photochemistry. *(No Title)* **1990**.

(61) Klessinger, M.; Michl, J. Excited States and Photochemistry of Organic Molecules. *(No Title)* **1995**.

(62) Levine, B. G.; Martínez, T. J. Isomerization through Conical Intersections. *Annu. Rev. Phys. Chem.* **2007**, *58*, 613–634, DOI: 10.1146/annurev.physchem.57.032905.104612.

(63) Guo, H.; Yarkony, D. R. Accurate Nonadiabatic Dynamics. *Phys. Chem. Chem. Phys.* **2016**, *18*, 26335–26352, DOI: 10.1039/c6cp05553b.

(64) Atchity, G. J.; Xantheas, S. S.; Ruedenberg, K. Potential Energy Surfaces near Intersections. *J. Chem. Phys.* **1991**, *95*, 1862–1876.

(65) Jumper, C. C.; Anna, J. M.; Stradomska, A.; Schins, J.; Myahkostupov, M.; Prusakova, V.; Oblinsky, D. G.; Castellano, F. N.; Knoester, J.; Scholes, G. D. Intramolecular Radiationless Transitions Dominate Exciton Relaxation Dynamics. *Chem. Phys. Lett.* **2014**, *599*, 23–33, DOI: 10.1016/j.cplett.2014.03.007.

(66) Jumper, C. C.; van Stokkum, I. H. M.; Mirkovic, T.; Scholes, G. D. Vibronic Wavepackets and Energy Transfer in Cryptophyte Light-Harvesting Complexes. *J. Phys. Chem. B* **2018**, *122*, 6328–6340, DOI: 10.1021/acs.jpcb.8b02629.

(67) Ishizaki, A.; Calhoun, T. R.; Schlau-Cohen, G. S.; Fleming, G. R. Quantum Coherence and Its Interplay with Protein Environments in Photosynthetic Electronic Energy Transfer. *Phys. Chem. Chem. Phys.* **2010**, *12*, 7319–7337, DOI: 10.1039/c003389h.

(68) Ghosh, S.; Bishop, M. M.; Roscioli, J. D.; LaFountain, A. M.; Frank, H. A.; Beck, W. F. Excitation Energy Transfer by Coherent and Incoherent Mechanisms in the Peridinin–Chlorophyll a Protein. *J. Phys. Chem. Lett.* **2017**, *8*, 463–469, DOI: 10.1021/acs.jpclett.6b02881.

(69) Fleming, G. R.; Cho, M. CHROMOPHORE-SOLVENT DYNAMICS. *Annu. Rev. Phys. Chem.* **1996**, *47*, 109–134, DOI: 10.1146/annurev.physchem.47.1.109.

(70) Tilluck, R. W.; Ghosh, S.; Guberman-Pfeffer, M. J.; Roscioli, J. D.; Gurchiek, J. K.; LaFountain, A. M.; Frank, H. A.; Gascón, J. A.; Beck, W. F. Interexciton Nonradiative Relaxation Pathways in the Peridinin-Chlorophyll Protein. *CR-PHYS-SC* **2021**, *2*, DOI: 10.1016/j.xcrp.2021.100380.

(71) Kerfeld, C. A.; Melnicki, M. R.; Sutter, M.; Dominguez-Martin, M. A. Structure, Function and Evolution of the Cyanobacterial Orange Carotenoid Protein and Its Homologs. *New Phytol.* **2017**, *215*, 937–951, DOI: 10.1111/nph.14670.

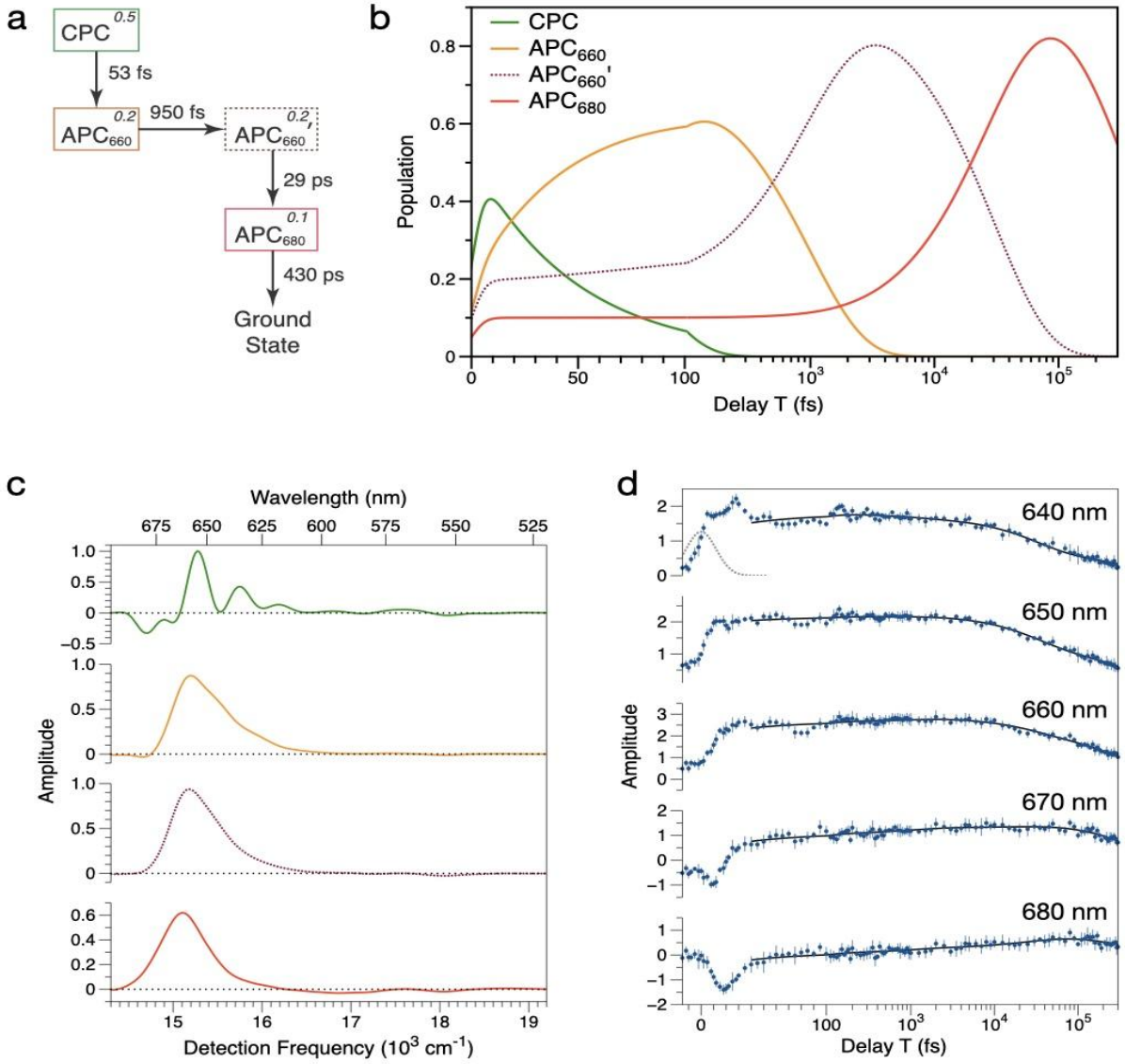

Figure A2.1. Global and target model for the 645-660 nm strip of the excitation axis of the 2DES spectrum. a, Four-compartment kinetic scheme and time constants for the excitation energy transfer process with the initial fractional excitation for each box. b, Time evolution of the populations of each box. c, Evolution-associated difference spectra (EADS). d, Amplitude transients at five detected wavelengths. The corresponding global model data is shown in black line. At each point 95% confidence interval is shown by bars. The instrument response function with a Gaussian 12-fs full width at half max is shown in a gray dotted plot centered at T = 0 fs for the 640-nm transient. A semilogarithmic T axis with the linear-log split at 100 fs is used for b and d.

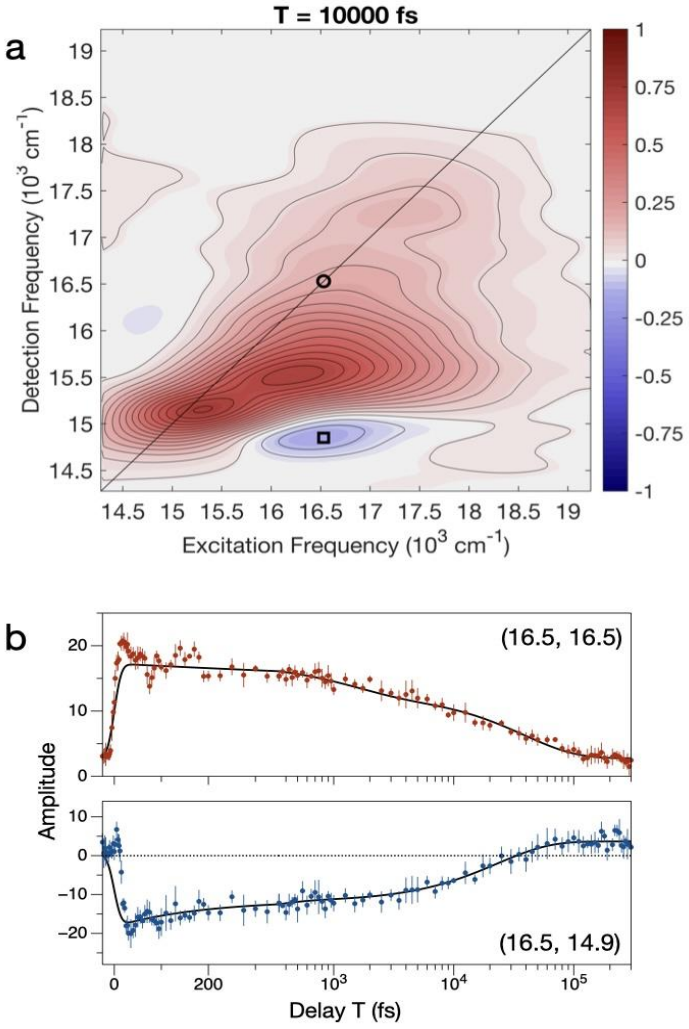

Figure A2.2. Decay of excited-state absorption (ESA) and diagonal ground-state bleaching (GSB) in the 2DES spectra. a, 2DES spectrum at T = 10 fs recorded at room temperature (23 ^{0}C) in intact phycobilisomes isolated from *Fremyella diplosiphon*. b, Amplitude transients sampled at marked coordinates (in 10^3 cm^{-1}) in the 2DES spectrum with 95% confidence interval at each point indicated with a bar. The fitted plot is shown in black solid line. The fit function was composed with two exponential components convoluted with a 12-fs Gaussian instrument-response function. Fit function, $A(T) = IRF * \sum_i a_i e^{(-T/\tau_i)} + a_0$. For the diagonal (16.5,16.5) transient: a_0 = -0.24, a_1 = 4.9, τ_1 = 1.4 ps, a_2 = 9.8, τ_2 = 38 ps. For the ESA (16.5,14.9) transient: a_0 = 3.2, a_1 = -6.6, τ_1 = 180 fs, a_2 = -16, τ_2 = 23 ps. (T<40 fs data was not included for modeling).

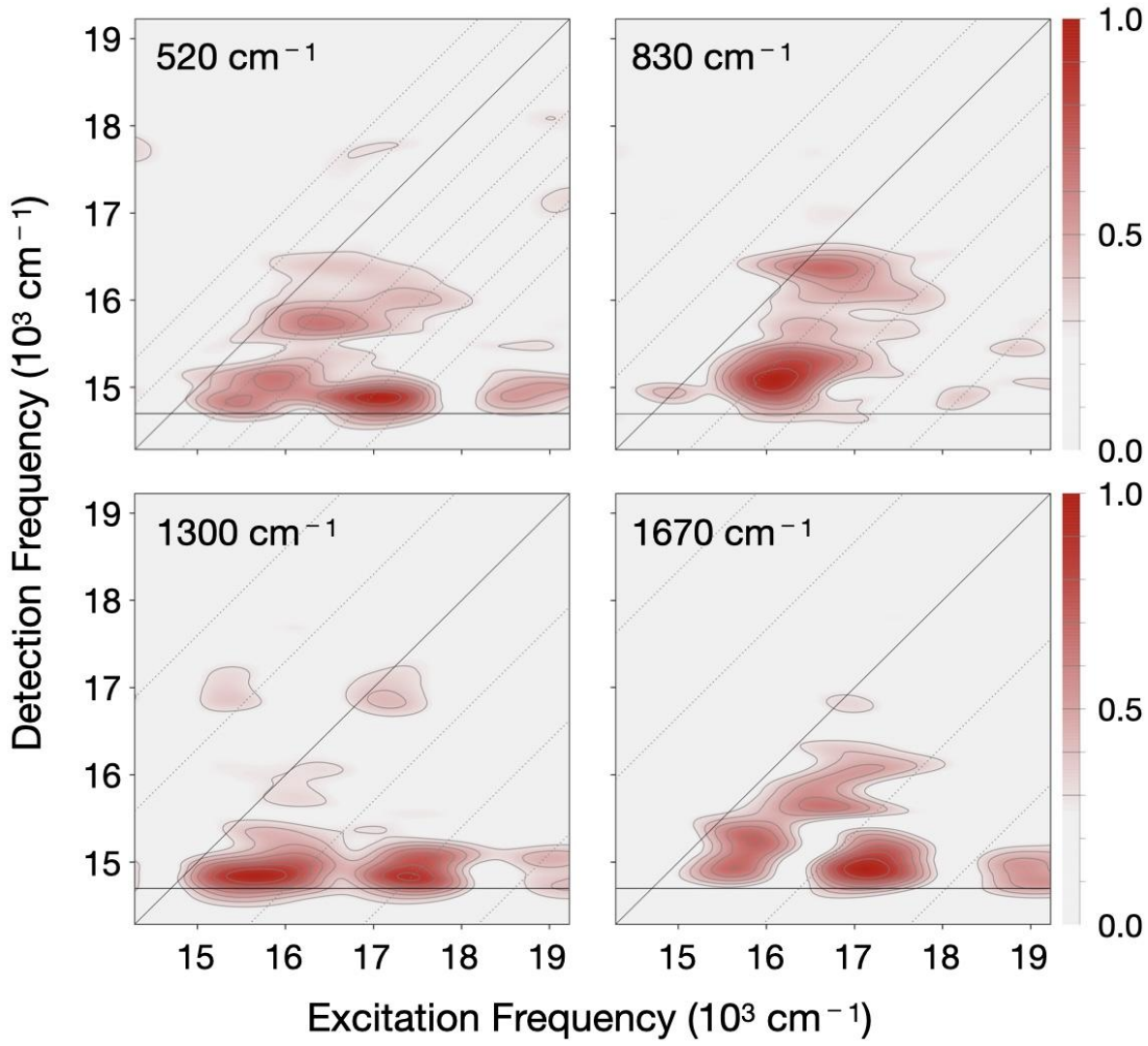

Figure A2.3. Oscillation maps for the Hann-windowed T = 50-500 fs range for the principal modulation components at 520, 830, 1300 and 1670 cm^{-1}. The non-oscillatory contributions were removed by subtracting an overdetermined 2D global model. The dashed diagonal lines in the oscillation maps are spaced by the selected modulation frequency. The black horizontal line along the detection axis shows the emission maximum of the intact phycobilisomes.

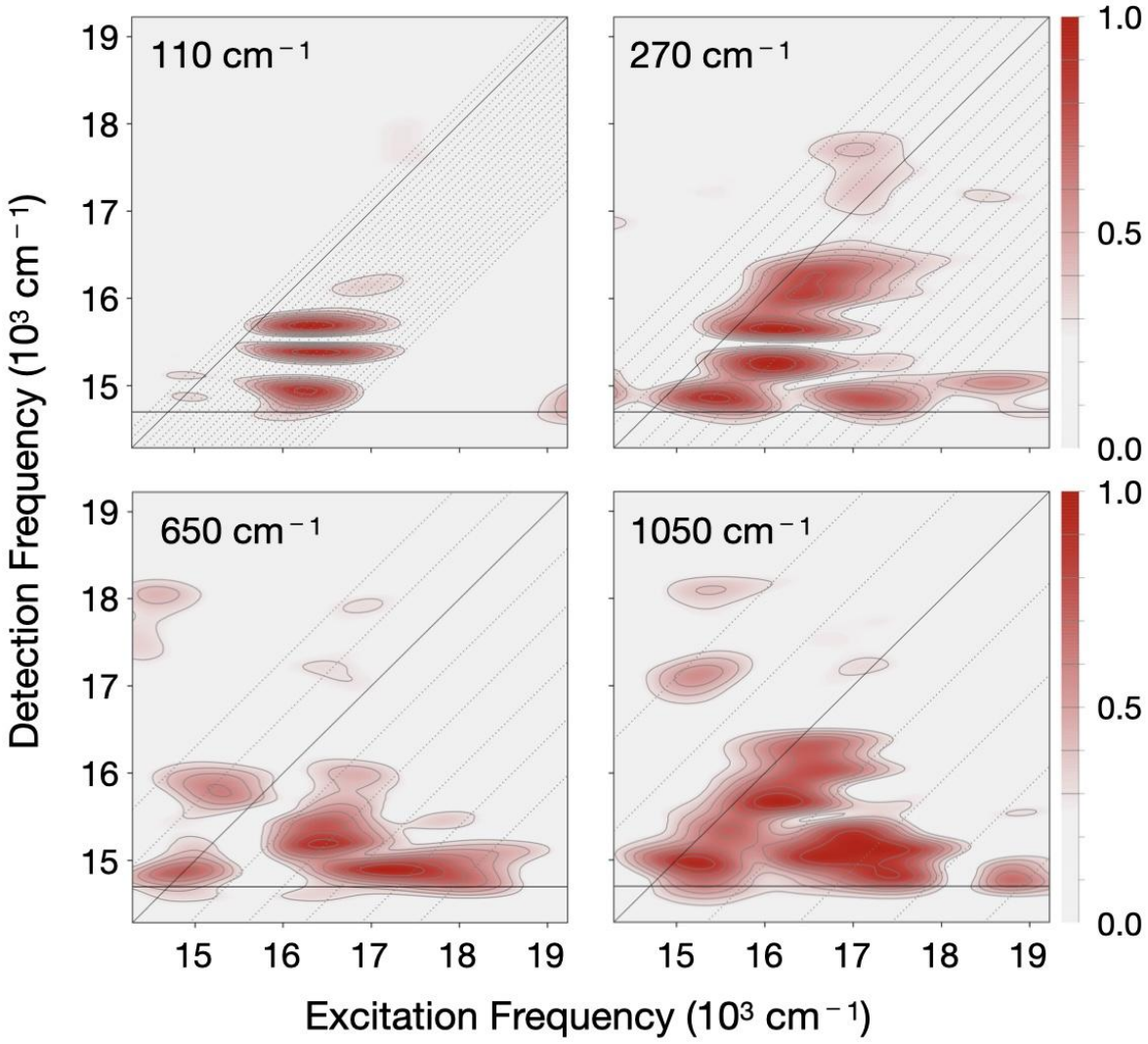

Figure A2.4. Oscillation maps for the Hann-windowed T = 50-500 fs range for the principal modulation components at 110, 270, 650 and 1050 cm^{-1}. The non-oscillatory signals were removed by subtracting an overdetermined 2D global model. The dashed diagonal lines in the oscillation maps are spaced by the selected modulation frequency. The black horizontal line along the detection axis represents the emission maximum of the intact phycobilisomes.

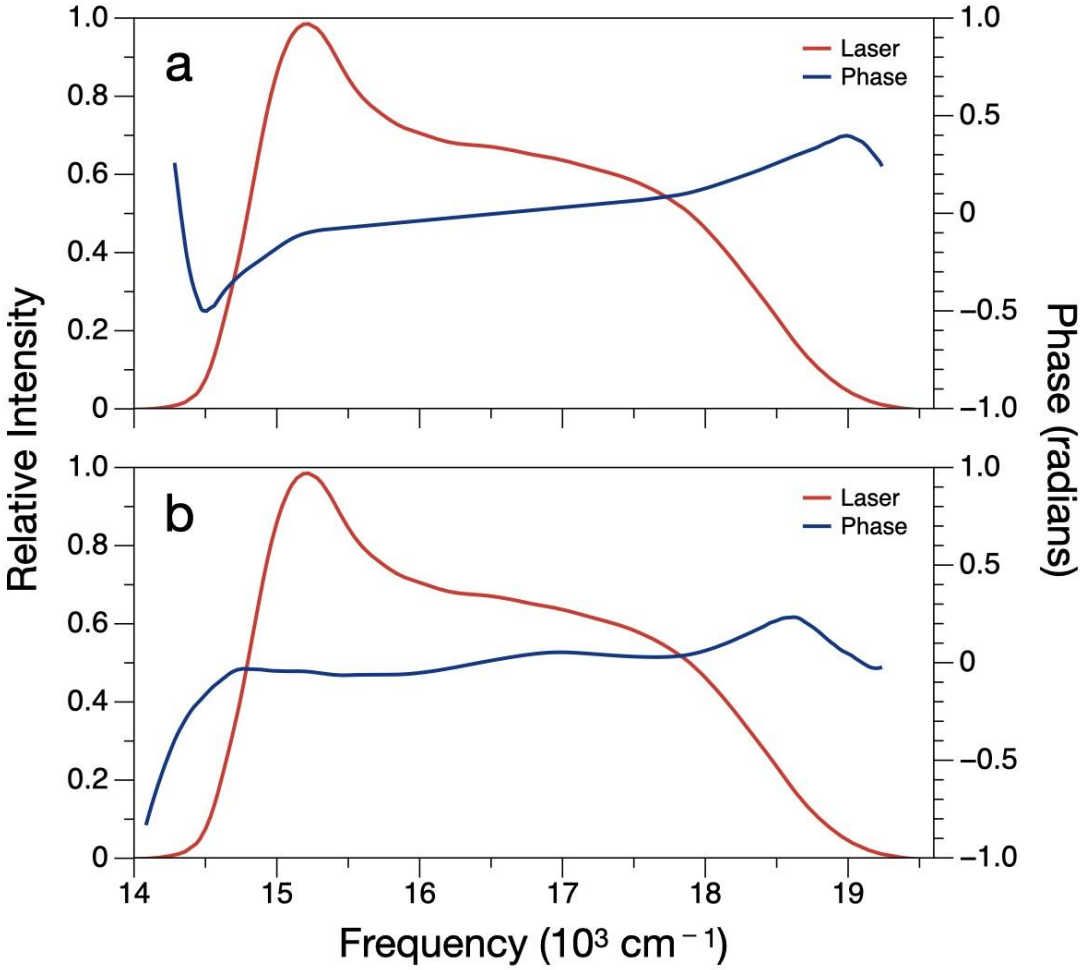

Figure A2.5. Laser intensity and residual phase spectrum after compression of the laser pulses used in the 2DES experiment: a, for the pump beam, and b, for the probe beam of the 2DES spectrometer.

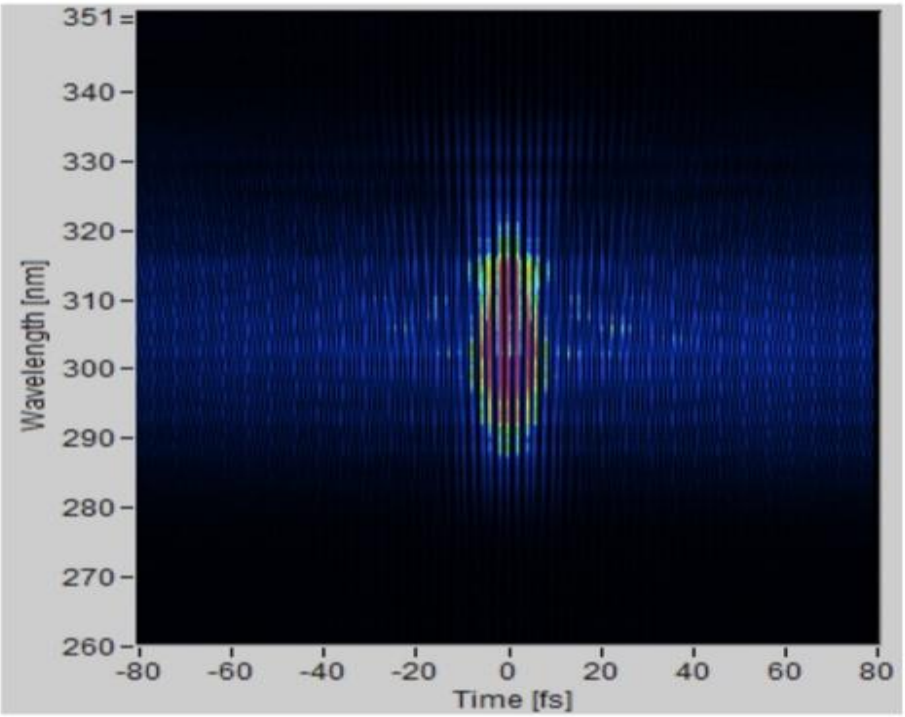

Figure A2.6. SHG-FROG spectrogram for the pump pulses, as measured with scanned pulse pairs prepared by the pump beam's pulse shaper in the 2DES spectrometer.

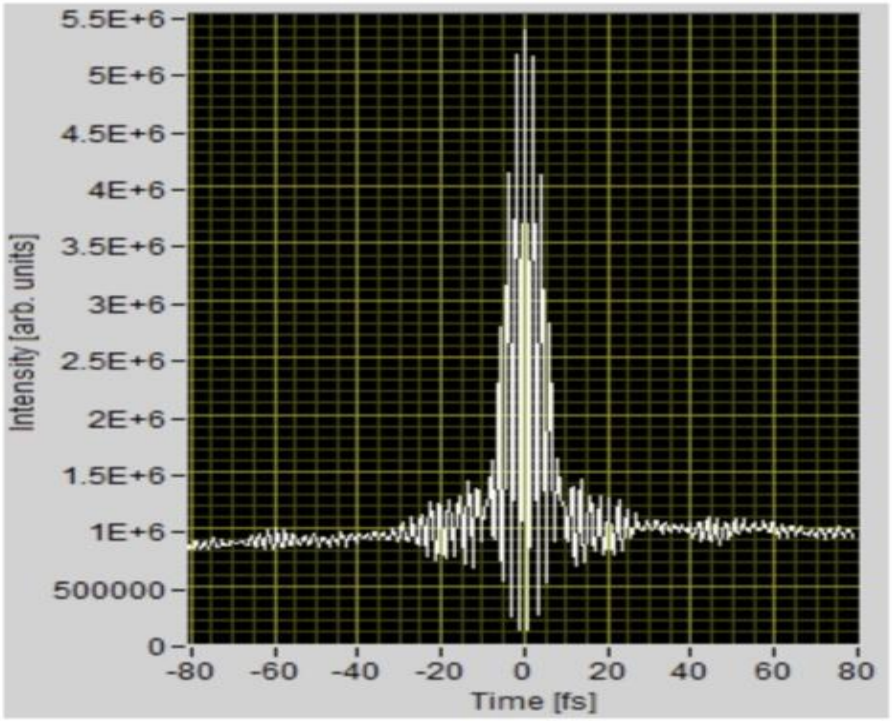

Figure A2.7. Interferometric autocorrelation of the pump pulses, determined as the integral of the SHG-FROG spectrogram (Figure A2.6).

A

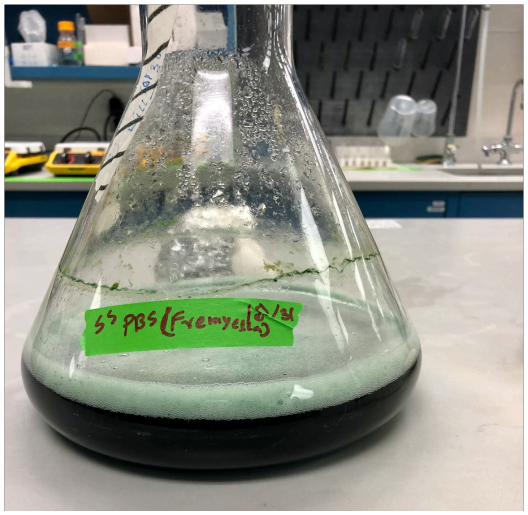

B

Figure A2.8. Cyanobacteria culture and isolated phycobilisomes. a, Full grown cyanobacteria *Fremyella diplosiphon* culture illuminated under white light. b, Blue color isolated phycobilisomes in sucrose gradient (small tubes) after overnight ultracentrifugation step.

Table 2.1. Preparation of BG11 (for 1L volume)

Chemicals	Volume (ml)	Chemicals	Volume (ml)
$NaNO_3$	1	Na_2CO_3	1
$CaCl_2$	1	Trace metals	1
$FeNH_4$	1	1M HEPES	10
EDTA	1	Water	973
K_2HPO_4	1		

Table 2.2. Sucrose gradient used in big tubes for purification of intact phycobilisomes

Sucrose Conc (M)	Volume (mL)
1.5	5
1	7
0.75	7
0.5	7
0.25	5

Table 2.3. Sucrose gradient used in small tubes for purification of intact phycobilisomes

Sucrose Conc (M)	Volume (mL)
1.5	3.5
1	5
0.75	3.5
0.5	3.5

Chapter 3: Excitation Energy Transfer in Intact Phycobilisomes from Red-Light Grown *Fremyella diplosiphon*

Phycobilisomes, a major light-harvesting protein in cyanobacteria, harvest solar energy and transfer that energy to the reaction center. Intact phycobilisomes contain different disk-shaped hexameric $(\alpha\beta)_6$ phycobiliproteins (PBP) that absorb different colors of light. The cylindrical rod structures have phycocyanin (CPC, λ_{max} = 620 nm) and phycoerythrin (PE, λ_{max} = 570 nm) whereas the core structure consists of allophycocyanin (APC, λ_{max} = 650 nm). Cyanobacteria produce phycobilisomes containing different ratios of PBPs depending upon the ambient light condition as a part of complementary chromatic adaptation (CCA) process to acquire optimum number of photons. Here we harvested *Fremyella diplosiphon* cells under illumination of high intensity red light that produce shorter rod lengths by not including PE at the end of the rods and similar core structure. Two-dimensional electronic spectroscopy (2DES) was employed in the red light grown intact phycobilisomes to study the energy transfer mechanisms. The global model for 560-580 nm excitation strip shows that excitation moves faster down the rods for red light grown samples compared to white light grown samples. But the time constants are similar for the transfer of the excitation in the core. The evolution associated difference spectra (EADS) show similar characteristics as that of the white light sample. This result supports the idea of delocalized exciton character in the rods of phycobilisomes proposed in the study of excitation energy transfer process in white light grown phycobilisomes.

3.1 Introduction

The cyanobacteria and red algae can grow in different ecological conditions (solar light intensity and color, temperature, nutrients, CO_2 concentration, etc.). These organisms modify their different cellular processes to accommodate changes in the environment. One of the most interesting processes is called complementary chromatic adaptation (CCA), a response to the change in incident light quality and quantity. The most common consequence of CCA is the change in the structure of the photosynthetic light-harvesting protein such as phycobilisomes.

The phycobilisomes, the primary light-harvesting complex in cyanobacteria and red algae, absorb solar photons and channel that solar energy to the nearest chlorophyll a in PS I or PS II.[1,2] The basic structure of a phycobilisome made of disk-shaped phycobiliproteins has two main parts; a triangular core and rod-like structures around it. The core contains allophycocyanin (APC) and the rods contain phycocyanin (PC). APC and PC absorb mostly the red part of the solar spectrum. Some cyanobacteria incorporate phycoerythrin (PE) at the end of the rod that can absorb green light. During CCA phycobiliprotein levels in phycobilisomes can change according to the situation.

Engelmann and Gaidukov first reported in 1902 that the cyanobacterium *Oscillatoria sancta* appeared in blue-green color when grown in orange light and in red color when grown in green light.[3,4] For the first time they used the term “Complementary Chromatic Adaptation” (CCA). They suggested that the distribution of the chromophores in the cyanobacteria correlated with the color of light in the growth condition. However, subsequent studies by other researchers could not repeat this observation with other strains of Cyanobacteria. In 1921 Boresch reproduced the result of Engelmann and

Gaidukov and showed that the color of the cyanobacterial culture depends on the phycoerythrin (PE) - phycocyanin (PC) ratio.[5] This ratio was related to the color of illuminating light (Figure 3.2). Later on this change in pigmentation became the defining feature of CCA.[6] The rich history of the CCA can be found in the review paper from N. Tandeau de Marsac (2003).[7]

From the current understanding of CCA and the present genetic perspective, the phrase "complementary chromatic adaptation" is an inaccurate term. The word 'adaptation' means the permanent change in the genetic composition of an organism that helps it to utilize a specific ecological situation.[6] So far the information available regarding the CCA suggest that immediate changes for this cellular response are not permanent and reversible. The changes for CCA occur at the level of gene expression rather than genome structure. Therefore 'acclimation' might be a more suitable word than 'adaptation'. But the word 'adaptation' has been used so much from the past that the researchers are reluctant to rename this process.

In the 1950s and 1960s Fujita and Hattori carried forward the progress of CCA.[8-11] They generated action spectra for the phycobiliproteins. Action spectra are the part of the light spectrum that are the most effective for conducting a given cellular response.[6] They demonstrated that photoreversible pigments responded to the green (~540 nm) and red light (~640 nm) to control CCA in *Tolypothrix tenuis* (PCC 7101). They also showed that even exposures of only a few minutes of red or green light can dictate which phycobiliprotein to produce. This response was not sensitive to the photosynthesis inhibitor which indicated that the CCA was not controlled via photosynthesis. Additional studies conducted in the 1970s and 1980s on action spectra using *Fremyella diplosiphon*

UTEX 481 (*Calothris* or *Tolypothrix* sp. PCC 7601), *Tolypothrix tenuis* (PCC 7101), *Synechocystis* sp. PCC 6701 supported the result of Hattori and Fujita by showing that CCA was maximally effective to green and red light in these cyanobacteria species as well.[12-16]

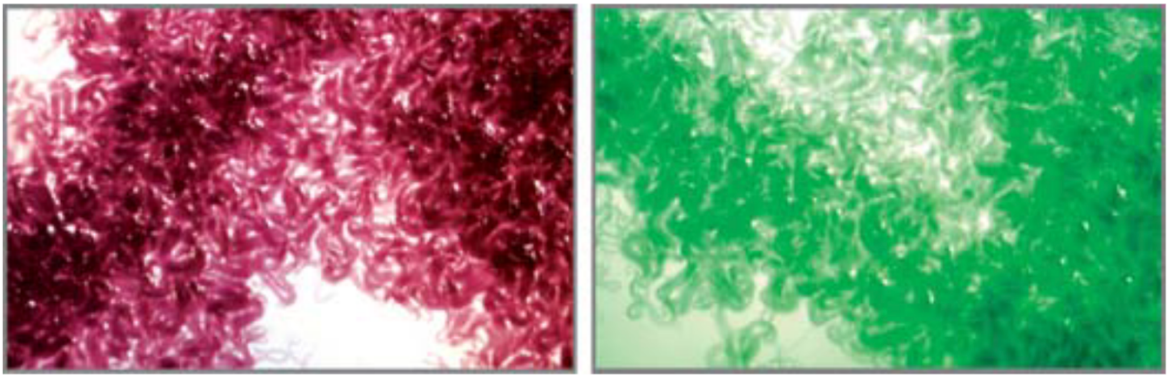

Figure 3.1. *Fremyella diplosiphon* culture is grown on agar plates in green light (left) and red light (right). The accumulation of different chromophores into phycobilisomes makes the cells brick red or blue green. Taken from Kehoe and Gutu, reference 6, used with permission.

All the cyanobacteria that can produce both PE and PC can be divided into three categories based on their CCA responses.[17,18] Group I strains did not show any CCA response because they did not change the population of PE or PC in response to the change of light color. Group II strains increased PE levels in presence of green light whereas they didn't change the PC levels during the light change green to red. Group III strains were capable of changing both PE and PC levels in response to the change in light quality: in particular, increased PE in green light and PC in red light. It is worthwhile to report that a range of species-dependent structural changes in PBS morphology has been observed even in the same group.[19–23] But the discussion will focus on the effect of CCA in *Fremyella diplosiphon* since our study involves this cyanobacterium species.

The *Fremyella diplosiphon* belongs to Group III since they change the amount of PE and PC to optimize the capture of the most abundant wavelengths in the spectra. This is because

PE absorbs green light and PC absorbs red light. Figure 3.1.2 shows the structure of phycobilisomes from *F. diplosiphon* grown under red and green light. This figure represents the extreme of the CCA response. In case of white light (both green and red light are present) some intermediate structure can be expected. N. Tandeau De Marsac showed that the phycobiliprotein composition of the cells of strain 7409 grown under white light was approximately intermediate between the red and green light grown cells phycobiliprotein composition.[17]

In the core of phycobilisomes from *F. diplosiphon* there are APC, core linker protein (apcC) and core-membrane linker protein (apcE). They do not have any significant difference between red-light grown and green-light grown phycobilisomes.[6,17,18,24] The core-proximal disk of each rod contains a type of PC called "constitutive PC" (PC_C). The α and β subunits of constitutive PC have the same structure for red-light and green-light grown phycobilisomes. These subunits are numbered as α_2 and β_1 (following the numbering system from Bryant, D. 1981[18,24] where the number of α and β subunits were assigned according to their position in the polyacrylamide gel). The core-distal phycobiliprotein disks are different during CCA. In the green light condition PE disks (up to three) may be present (Figure 3.1.2). All the α and β subunits of PE are the same for all three disks. During red-light growth, instead of PE there are two PC disks after the constitutive PC. These two PC disks are called "inducible PC" (PC_i). The inducible PC contains α_1 and β_2. The α_1 (λ_{max} = 623 nm) and α_2 (λ_{max} = 622 nm) have similar absorption spectra. However, the absorption spectrum of β_1 (λ_{max} = 610 nm) is red-shifted than that of β_2 (λ_{max} = 603 nm).[24]

So far, I have talked about the structural change of phycobilisomes due to change in light quality (color). Light quantity (intensity) also can induce changes in the structure of phycobilisomes. In general, phycobiliprotein levels per cell increase in low light intensity growth culture as compared to a high light intensity growth culture.[25,26] Phycobiliprotein levels can increase in a cell by increasing the size and/ or number of phycobilisomes per cell.[27] Cyanobacterium Synechocystis sp. 6301 increases the length of the rod when it is shifted from high to low intensity illumination.[28] Shifting illumination from 3000 foot-candles to 50 foot-candles increases the number of phycobilisomes almost to double in a cell for the red alga *Griffithsia pacifica* with no alteration in the length of the rods.[29] Light intensity can also alter the pigment content in phycobiliproteins. Yu et al. reported that in red algae *Callithamnion roseum* PE covalently binds more phycourobilin than phycoerythrobilin under low light intensity. This is because phycourobilin has a higher extinction coefficient than phycoerythrin.[30]

Recently the Montgomery group studied the effect of light (red and green) intensity in phycobiliprotein level in *F. diplosiphon*.[31,32] They found that the phycobiliprotein level decreases in cells with increase in light intensity for both red and green light cases. The results showed the extent of decrease in the amount of each phycobiliprotein (PE, PC and APC) was very similar. That result indicates that the number of phycobilisomes in *F. diplosiphon* per cell was decreased with increase in light intensity rather than the shorter size of the rods. Also, the absorption spectra of phycobilisomes isolated from *F. diplosiphon* grown under high-intensity red light and low-intensity red light are the same (Figure A3.2).

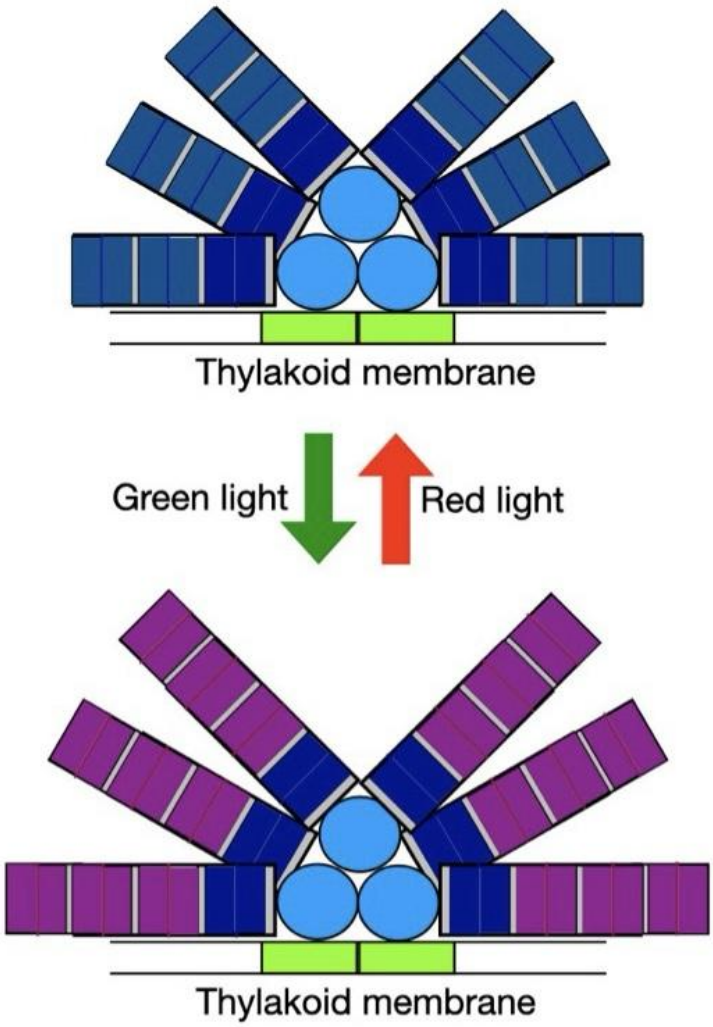

Figure 3.2. The structure of phycobilisomes and phycobiliprotein extract from *Fremyella diplosiphon* grown under red and green light. The green rectangles associated with the thylakoid membrane are photosystem II. Both phycobilisome structures contain a light blue color tricylindrical core and 6 rods are attached with the core. Each disk-type structural unit is a hexameric phycobiliprotein. The core of the phycobilisomes contain APC (light blue) and the rods contain constitutive PC (dark blue), inducible PC (medium blue), and/or PE (pink). The figure is redrawn from Kehoe and Gutu, reference 6.

During CCA the morphology of the *F. diplosiphon* cell changes drastically. The cells grown under green light have almost 10 times higher filament length than that of the red-light grown cells. Also, the red light grown cells are more rounded structure. The chlorophyll a content in the cyanobacteria cells does not differ significantly when the

illuminating light condition changes from red to green.[17] Intensity variation study in *F. diplosiphon* from the Montgomery group showed that with higher light intensity carotenoid population in cells also increases.[31,32]

For this study intact phycobilisomes were isolated from WT *Fremyella diplosiphon* cells that were grown under the illumination of high intensity red light. The red-light grown phycobilisomes do not contain phycoerythrin (PE) at the end of the rods. Two-dimensional electronic spectroscopy (2DES) was employed to study the excitation energy transfer processes in intact phycobilisomes. Global and target model for the 560-580 nm excitation strip shows that 4 compartments with 2 kinetically distinct phycocyanin (PC) compartments is sufficient to fit the data. The kinetic model indicates the excitation moves faster down the rods of the phycobilisome compared to that of the white-light grown phycobilisomes. But in the core of the phycobilisome the energy transfer takes similar time as compared to white-light grown samples to reach the terminal emitter, APC_{680}.

The kinetic model shows a shorter excited-state lifetime for the terminal emitter from the red-light grown phycobilisomes than that of the white-light ones. Time-correlated single photon counting (TCSPC) experiments were performed with the red- and white-light grown phycobilisomes to have a better understanding of the excited-state lifetime of the terminal emitter. Surprisingly, the kinetic models from the TCSPC data do not have a significant difference in excitation transfer rate between red- and white-light grown samples. A new kinetic component at ~600 ps has been observed which can be an energy transfer step in the core or an intrinsic quenching mechanism. More detailed analysis is required to explain the faster ground-state recovery for the red-light grown sample.

3.2 Experimental Methods

3.2.1 Sample Preparation

For the red light grown phycobilisome samples the subcultures of WT *Fremyella diplosiphon* were grown in an incubator under the constant illumination of low intensity red light. Inside the chamber no extra CO_2 was provided, and the shaker was running at 160 rpm. Since the light intensity and CO_2 concentration were low, the cyanobacteria culture grows slowly. After inoculation to a 1L BG11 medium the culture was placed inside a Percival (Growth chamber for cyanobacteria from Geneva Scientific) where 3% CO_2 concentration was maintained. The Percival does not have a shaker. So, the culture was placed on a magnetic stirrer and a magnetic stirring bar was used to stir the culture. At the beginning the culture was a faint green color since there were not many cells present yet. For the first 2 days the illuminating red light intensity was medium (~50 μE $m^{-2}s^{-1}$). Here red-light LEDs were used. The spectrum of the illuminating light has been shown in Figure 3.3. Once we observe the culture has grown moderately (light green color) then light intensity is increased to the highest level (~150 μE $m^{-2}s^{-1}$). If we use the high intensity from the beginning, then all the cells will die instead of growing. After 2-3 days the cells were harvested to isolate the intact phycobilisomes. The isolation protocol has been described in detail in the previous chapter (see section 2.2.1).

The ambient light spectra (Figure 3.3) shows that the white light spectrum is a fluorescent white light that has a higher contribution from the red light (600-670 nm) compared to green light (500-570 nm). So, we can say that the white light is a 'red-rich white light'.

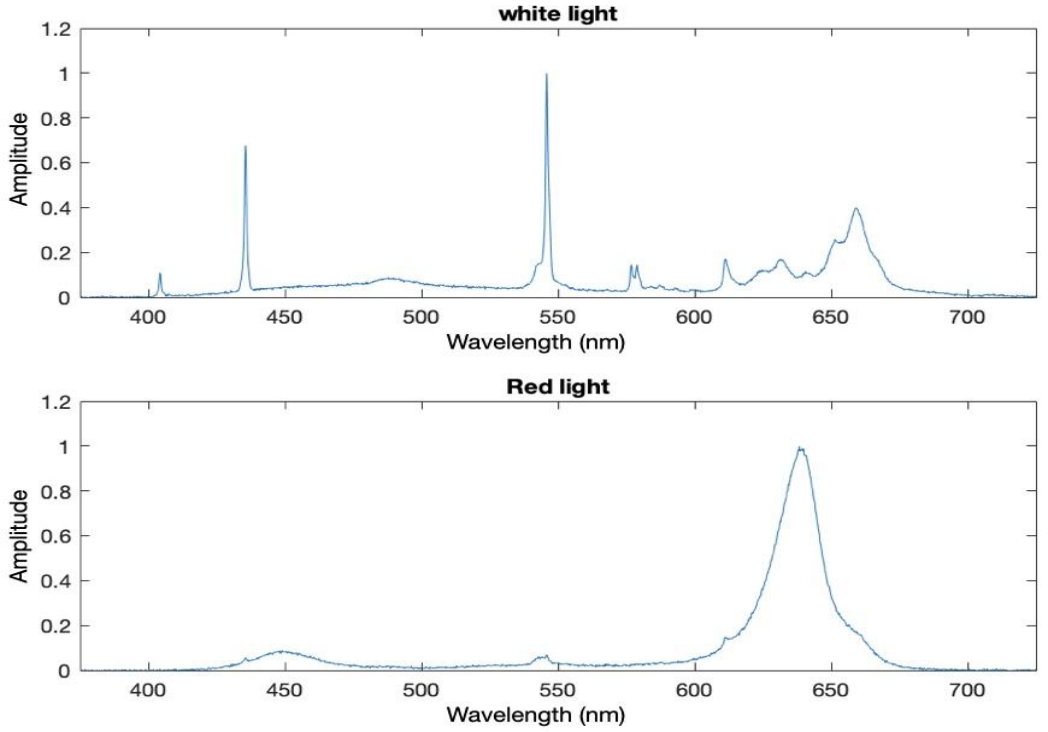

Figure 3.3. Illuminating light spectra for the white light and red-light sources. The spectra were normalized to their maximum.

3.2.2 Linear Spectroscopy

Linear absorption spectra of intact phycobilisomes samples were recorded using a Shimadzu UV-2600 spectrophotometer at room temperature (23°C). For the 2DES study the concentration of the phycobilisome sample was adjusted to obtain 0.3 OD (in 1 mm cuvette) by adding 0.8 M potassium phosphate buffer solution (pH 7). For the fluorescence experiments the OD value of the sample was adjusted to obtain 0.1 for a 1 cm path length at the excitation wavelength. The fluorescence spectra were recorded with a home-built fluorescence spectrometer which has been discussed in length in section 2.2.2. For low temperature absorption and fluorescence 60% and 40% glycerol with 1.25 M phosphate buffer were used as a solvent respectively.

3.2.3. Two-Dimensional Electronic Spectroscopy (2DES)

The two-dimensional electronic spectroscopy experiments were performed with 7.2 fs laser pulses in intact phycobilisomes at room temperature (23 ^{0}C). The details of the 2DES instrument and experimental procedure have been described in the previous chapter (section 2.2.3). For these experiments 3 nJ/pulses were used.

3.2.4 Time-Correlated Single Photon Counting (TCSPC)

The fluorescence lifetime decays were measured using the time-correlated single photon counting (TCSPC) instrument[33,34] at room temperature (23°C). The light source for this instrument is a synchronously pumped cavity-dumped dye laser (Coherent 702) that was excited by a continuous-wave (CW) passively mode-locked Nd:YVO_4 laser (Spectra Physics Vanguard). The Nd:YVO_4 laser produces 2.5 W of average power at 532 nm at a 40 MHz repetition rate with 13 ps pulses. Rhodamine dyes were used in the dye laser that produced 5 ps laser pulses at the excitation wavelengths (Rhodamine 6G for 580 nm 600 nm, and Rhodamine 640 for 645 nm). The repetition rate of the dye laser was controlled by the cavity-dumper (Coherent 7210). The output of the dye laser was divided into two; one portion was directed to a reference photodiode (Becker and HicklPHD-400-N) and the other portion was directed to the sample. The excitation energy at the sample position was controlled by using constant neutral-density (ND) filters. A polarizer was used before the sample position to selectively pass the vertically polarized light. A static cuvette with 1 cm optical path length was used at the sample position. The emitting photons were collected using a 40x reflecting microscope objective at 90^0 with respect to the excitation laser beam. The collected photons were separated into polarization components parallel (0^0) and perpendicular (90^0) to the vertically polarized excitation pulse using a polarizing cube

beam splitter. Microchannel plate photomultiplier tubes (MCP-PMT, ID Quantique) each equipped with a subtractive double monochromator (Spectral Products CM-112) for wavelength selection were used to detect the parallel and perpendicular polarized signal components simultaneously. The detection electronics (Becker & Hickl SPC-132) resolved the parallel and perpendicular transients separately, yielding ~100 ps response functions for each detection channel. The detection electronics include a time-to-amplitude converter (TAC) and a constant fraction discriminator (CFD) that temporally resolves the fluorescence signal for each polarization component. The data was collected using multichannel analyzers (MCAs). The in-house written LabVIEW (National Instruments) program on a PC controls the entire process including detection wavelength and time, data acquisition. Steady state fluorescence spectra from intact phycobilisome samples were collected before and after the TCSPC experiments to check the permanent photodamage.

3.3 Results and Discussion

3.3.1 Linear Spectroscopy

Figure 3.4 presents the linear absorption spectra of intact phycobilisomes isolated from *Fremyella* grown under white light and red light in 0.8 M phosphate buffer solution at room temperature (23^{o}C). The spectra were plotted as the oscillator strength, $\varepsilon(\nu)$, and the wavenumber ν (cm^{-1}). The wavelength axis was also added at the top of the plot. Both spectra were normalized with respect to the maximum absorption. The absorption spectra of the red light grown sample (red plot) does not have the peak ~570 nm due to absence of phycoerythrin (PE) at the end of the rod. Also, the red plot has a lower intensity 640-690 nm region with respect to the absorption spectra of the white light grown sample.

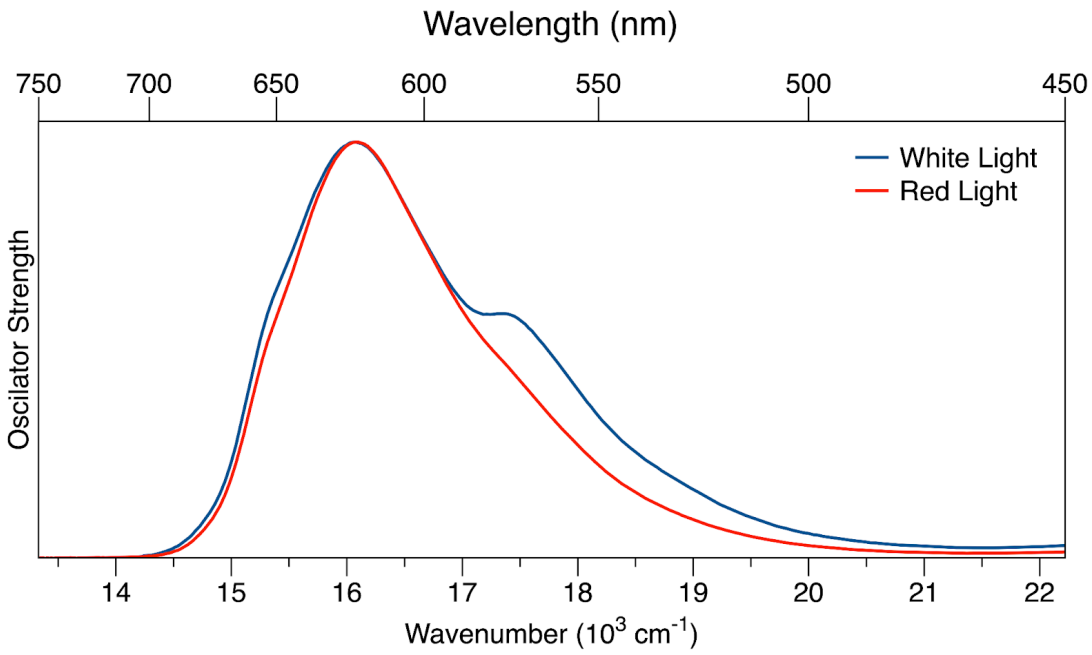

Figure 3.4. Linear absorption spectra of intact phycobilisomes isolated from *Fremyella* grown under medium intensity white light (blue line) and high intensity red light (red line) in phosphate buffer solution at room temperature (23°C). Both spectra were normalized to their maximum.

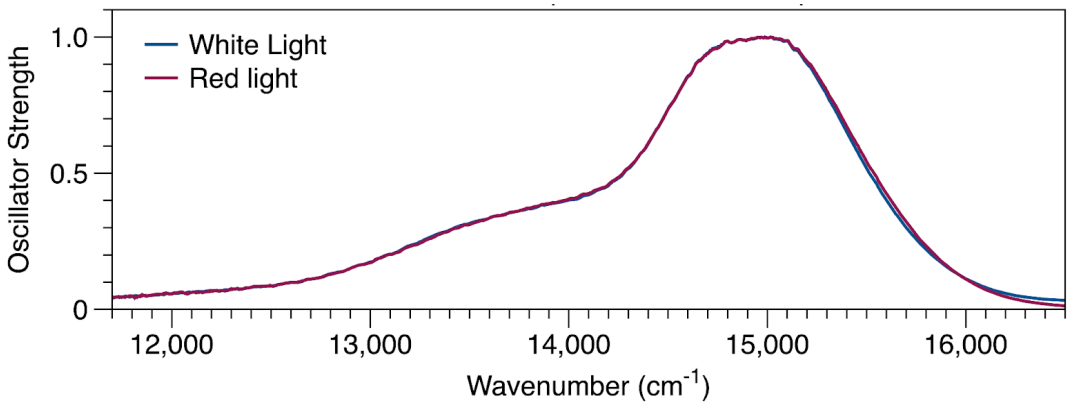

Figure 3.5. Fluorescence spectra of intact phycobilisomes isolated from *Fremyella diplosiphon* grown under white light (blue line) and red light (red line) in phosphate buffer solution excited at 550 nm at room temperature (23 ^{0}C). Blue and red plot was normalized to their respective maximum.

Figure 3.5 shows the fluorescence spectra of intact phycobilisomes isolated from *Fremyella* grown under white light (blue line) and red light (red line) in 0.8 M phosphate buffer at room temperature (23 ^{0}C). The spectra were plotted as the oscillator strength,

$\lambda^2 F(\nu)\nu^3$ (λ - wavelength, $F(\nu)$ - fluorescence intensity), and the wavenumber ν (cm^{-1}). The blue and the red plot was normalized with respect to their maximum. The samples were excited at 550 nm. Both plots don't have any noticeable difference. Their maximum at 672 nm indicates that the phycobilisomes were intact.

All the phycobiliprotein peaks in the absorption spectra of the intact phycobilisomes at 77 K (Figure 3.6) are well resolved and relatively narrower with respect to that of the room temperature one (Figure 3.4). The peak for PE is observed at 572 nm for the white-light grown phycobilisomes. This peak is missing in the red-light grown sample. There are two partially resolved peaks ~600 nm. This is probably originating from β-subunits of CPC. The peak position is blue shifted in intact phycobilisomes than the isolated proteins.[24,35] This is probably due to have better overlap with the PE spectra in white-light grown samples and to absorb more photons below 600 nm regions in the red-light grown samples. The absorption maxima are at 630 nm. This is originating from the α-subunit of CPC.[24,35] Interestingly the absorption peak appears for phycobilisomes in cyanobacteria cells at ~630 nm (Figure A3.1). The absorption peak of the α-subunit of CPC is red-shifted in intact phycobilisomes than that of the isolated phycobiliprotein at room temperature (23 ^{0}C). This would probably provide better spectral overlap with the absorption spectra of APC. The peak of APC is at 654 nm which is ~2 nm red-shifted than that of the isolated APC peak at room temperature.

Apart from missing the PE peak, there is no significant difference in lineshape between the absorption spectrum from red and white light grown phycobilisomes (Figure 3.6). Several CCA studies[17,22,24] showed that phycobilisomes isolated from *F. diplosiphon* grown under red light have higher CPC:APC ratio than that of the white light grown sample. The

absorption spectra normalized to APC maximum show that there are more CPC disks in the red light grown sample than that of the white light grown sample. Also, it is indicating that with higher intensity illuminating light the length of the rods does not alter in these cyanobacteria (see the Figure A3.2). Probably the number of phycobilisomes per cell are lower with respect to lower intensity illumination. There is no such difference between the absorption spectrum from red-light and white light beyond 650 nm. This indicates that there is no significant change in the core of phycobilisomes under different illuminating light conditions. This result is also in-line with the previous CCA studies.[6,17,24] The lineshape of the two absorption spectra in the ~590-605 nm region are similar. That indicates both phycobilisomes (red-light and white light grown) contain constitutive PC and inducible PC disks in the rods.

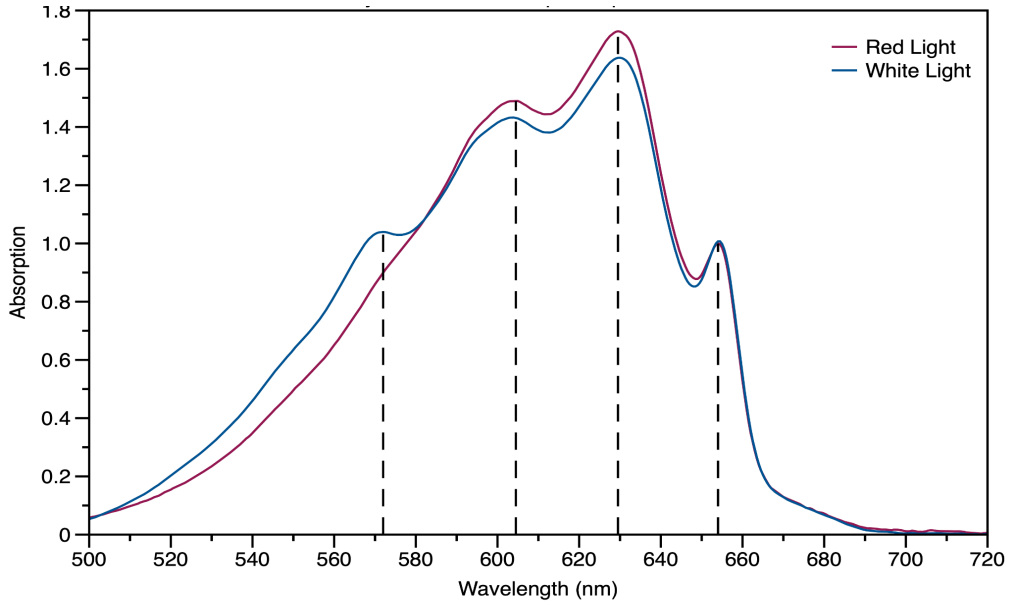

Figure 3.6. Absorption spectra of the intact phycobilisomes isolated from *Fremyella diplosiphon* grown in high intensity red light (red plot) and medium intensity white light (blue plot) at 77 K. The spectra were normalized with respect to the absorption maxima for the peak at 654 nm. The dotted lines represent the peak positions.

Figure 3.7 shows the fluorescence oscillator strength spectra with the wavenumber in the x-axis. The low temperature spectra have narrower lineshape than the room temperature emission spectra (Figure 3.5). The maximum of the low temperature spectra is redshifted to 685 nm. This is because most of the emission is coming out the terminal emitter (APC_{680}).[36] The white light grown sample has slightly higher intensity around 667 nm. Mostly APC_{660} emits in this region. There are some vibrational peaks at the lower wavenumber region ~740-775 nm. Other than higher intensity at 667 nm there is no difference in fluorescence spectra between red-light and white light grown samples. In figure A3.3 fluorescence spectrum from the broken phycobilisomes confirms that phycobilisomes in Figure 3.7 were intact, otherwise there would not be a peak at 685 nm from the terminal emitter after exciting the sample at 550 nm.

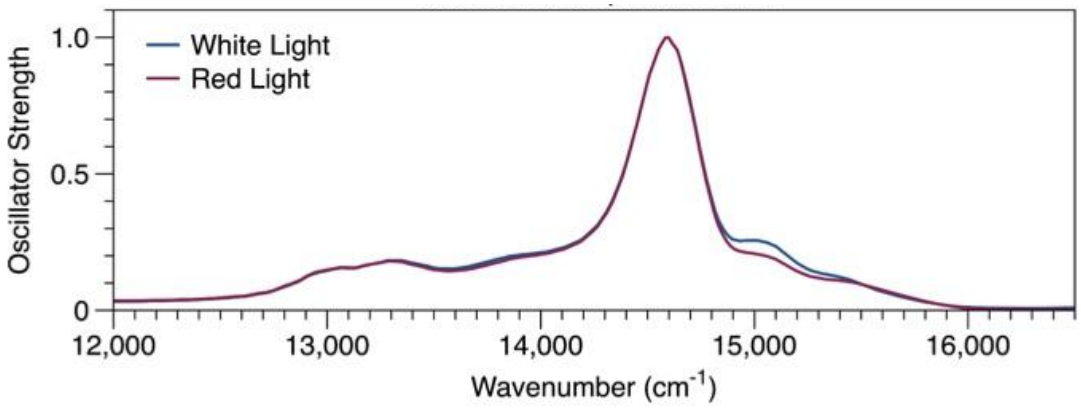

Figure 3.7. Fluorescence oscillator strength spectra of intact phycobilisome isolated from *F. diplosiphon* grown under red (red plot) and white (blue plot) light, at 77 K. The spectra were normalized to their maximum. The excitation wavelength was 550 nm.

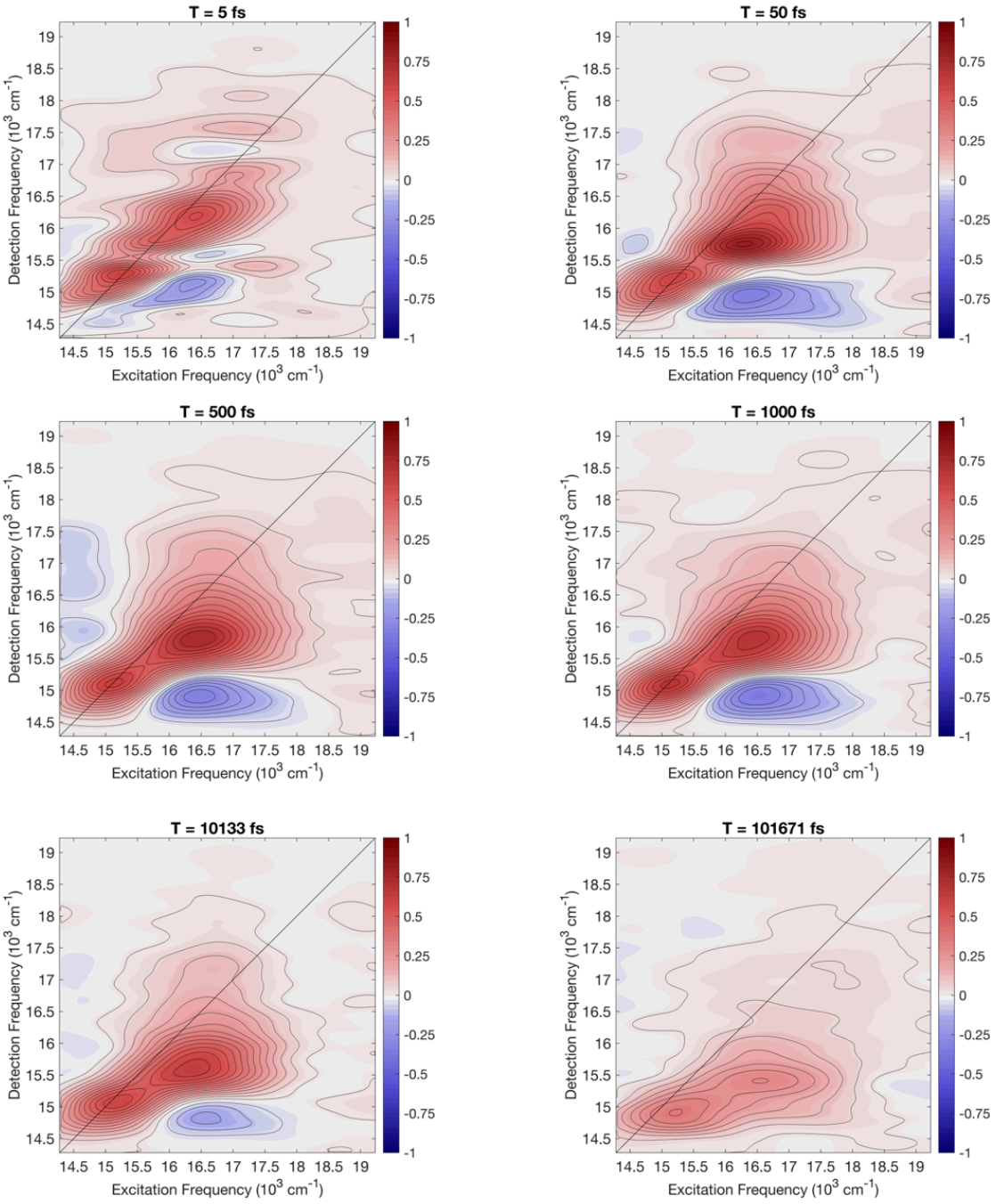

Figure 3.8. A series of 2DES spectra at different population time (T) from intact phycobilisomes isolated from *Fremyella diplosiphon* grown under high intensity red light at room temperature (23 ^{0}C). The signal amplitude is normalized with respect to the maximum intensity in the entire data set.

3.3.2 2DES Spectra

A series of 2DES spectra from intact phycobilisomes isolated from *Fremyella diplosiphon* grown under high intensity red-light at room temperature (23 ^{0}C) are shown in Figure 3.8. In the 2DES spectra x and y-axis represent the excitation and detection axis respectively. Both axes are in the wavenumber unit. The positive amplitude from ground-state bleaching (GSB) and stimulated emission (SE) signals are shown in red color and the negative amplitude from excited-state absorption (ESA) signals are shown in blue color. The signal amplitude is normalized with respect to the maximum intensity in the entire data set. This is an average data from three successive scans. The 2DES spectra have similar features compared to those obtained from white-light grown samples (Figure 2.5). For example, at early population time mostly the diagonal peaks are observed at ~620 nm and ~650 nm from CPC in the rods and APC_{660} in the core, along with the off-diagonal short lived amplitude modulation. At later time 2DES spectra exhibit a prominent below the diagonal red peak due to the energy transfer from rods to the core of the phycobilisome. Finally, they align along the fluorescence maximum of the sample at 672 nm. This indicates that we can observe the energy transfer in intact phycobilisomes in the 2DES spectra. The only noticeable difference here with the white light grown sample (Figure 2.5) is that there is not much signal after ~17500 cm^{-1} (570 nm) in both axes. This is because the red-light grown phycobilisomes do not contain PE at the end of the rods.

3.3.3 Global and Target Model

Figure 3.9 represents the global and target model[37] that can describe the approximate energy transfer process in intact phycobilisomes isolated from *Fremyella diplosiphon* grown under high intensity red light. Here the 560-580-nm region of the excitation axis was taken

for the modeling whereas in the previous chapter it was 550-580 nm for the white-light grown sample (Figure 2.6). This is because the red-light grown samples do not have a strong signal 550-560 nm due to absence of PE at the end of the rod. Here also our goal is to determine the excitation energy transfer rate from rods to the core of the phycobilisomes. The initial excitation values for each compartment in the global model is an estimated value. The exact values can be calculated by generating a deconvolution plot like white light sample case (Figure 2.3). However, a small change in this value does not have significant effect in the time constants in the kinetic scheme.

The kinetic model (Figure 3.9) from the red-light grown phycobilisomes shows excitation energy moves down the rod faster (170 fs) than that of the white light grown sample (560 fs). For the white-light sample that contains 4 disks in the rods,[22] the major portion of excitation is starting from PE which is at the end of the rods (4th disk). For the red-light sample three CPC disks in the rods are equally possible to accept the photon. Therefore, the excitation is traveling a smaller average distance in the rods for red-light phycobilisomes which takes lesser time to travel. The kinetic model (Figure A3.4) from the intact phycobilisomes grown under low intensity red light shows slightly higher time constant 430 fs for this step. That is still faster with respect to that of the white-light grown sample. In apparent conflict with this picture, Kolodny et al.[38,39] reported that in case of marine cyanobacteria *Synechococcus* WH8102 species excitation energy reaches faster to the core for the phycobilisome that has longer rods than that of the shorter rod length. They performed time-correlated single photon counting (TCSPC) experiments to measure the excitation energy transfer processes. They suggested that in the phycobilisomes with longer

rods the coupling between chromophores increased from the formation of additional coupled pathways by rearranging the rod packing.

Similarly, for the next step excitation energy reaches to the core (APC_{660}) faster for the red light grown sample in 6-7 ps than that of the white light grown sample in 13 ps. This can be again attributed from the fact that the red-light sample has smaller average rod lengths. Engel and coworkers[40] have measured 8 ps time constant with their 2DES polarization scheme for the energy transfer from rods to the core for intact phycobilisomes from *synechocystis* sp. PCC 6803 that has a similar rod structure with 3 CPC disks. But, in the core of phycobilisome energy transfers to the terminal emitters (APC_{680}) at the similar time constant (~40-45 ps) as compared to that of the white-light grown sample. Surprisingly, the excited state lifetime of the terminal emitter for the high intensity red-light grown sample (~200 ps) is about two times faster than that of the white light grown samples (~400 ps). The low intensity red-light grown sample shows a 600 ps time constant for this ground state recovery. It is hard to explain this phenomena from given the fact that previous CCA studies reported that core of the phycobilisomes from both red and white light grown cyanobacteria have similar structure.[17,18,24]

The evolution associated difference spectra (EADS) for the CPC_1 box shows a series of positive going ground-state bleaching (GSB) and stimulated emission (SE) peaks in the 600-640 nm region. Then there are two negative going excited-state emission (ESA) peaks at 650 nm and 670 nm which are the absorption maxima for the APC_{660} and the terminal emitter. This indicates that bilin chromophores are in a shared ground state condition. The intensity of the ESA peaks for the next compartments are becoming lower which indicates that the delocalized states are increasingly localized in the core. This is similar to that of the

white-light sample. The population plot shows the evolution of the excited-state population for each compartment.

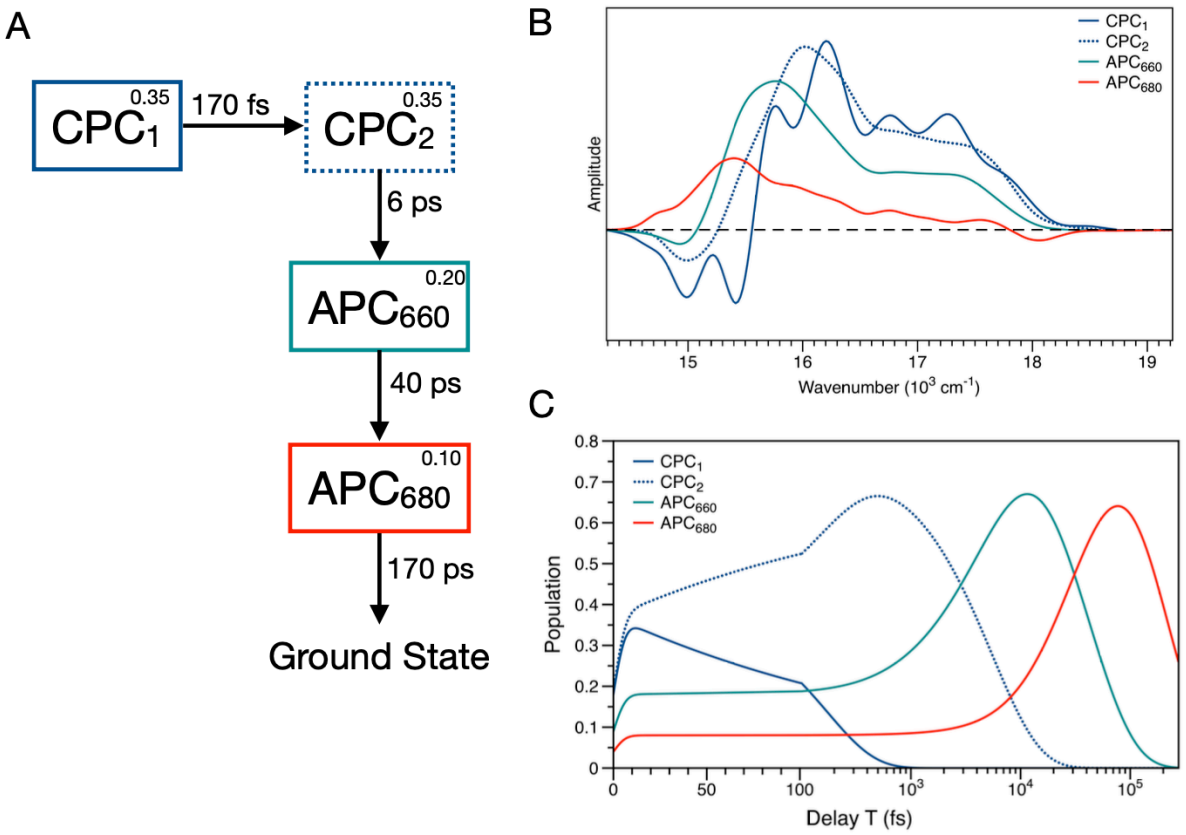

Figure 3.9. Global and target model for the 560-580 nm region of the excitation axis of the 2DES spectra obtained from phycobilisomes grown under high intensity red-light. a, Kinetic scheme and time constants for energy transfer process from rod to the core with initial excitation for each compartment. b, Evolution associated difference spectra (EADS). c, Time evolution of the population in each compartment. The x-axis of the population plot is in semilogarithmic scale where 100 fs is the breaking point.

Figure 3.10 shows the global and target model for the directly excited core region of the intact phycobilisomes. In this model 4 compartments are needed with two kinetically distinct APC compartments. Compared to the directly excited core model from white light grown sample (Figure A2.1), the red light grown sample shows similar time constants. Excitation population moves slightly slowly in 40 ps from APC_{660} to the terminal emitter.

Another interesting result is that the ground state recovery is also similar to white light grown sample in ~400 ps and it is different from the model from excitation of the rods.

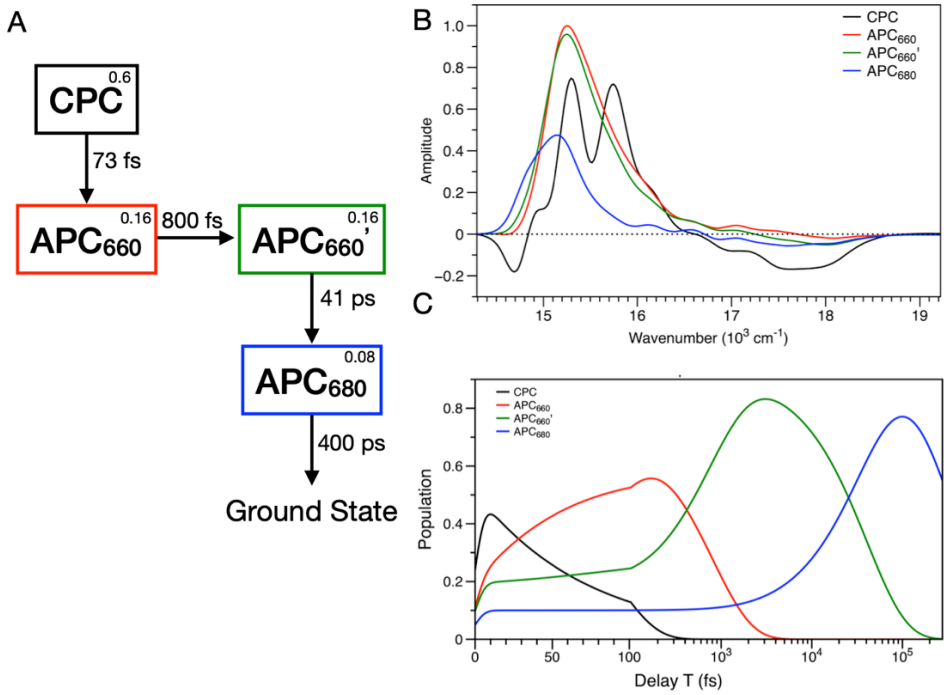

Figure 3.10. Global and target model for the 645-660 nm region of the excitation axis of the 2DES spectra obtained from intact phycobilisomes grown under high intensity red light. a, Kinetic scheme and time constants for energy transfer process along with the initial excitation for each compartment. b, Evolution associated difference spectra (EADS). c, Time evolution of the population in each compartment. The x-axis of the population plot is in semilogarithmic scale where 100 fs is the breaking point.

The EADS of the first box has an ESA peak ~670 nm which is the absorption maximum of the terminal emitter. The next compartments don't contain significant ESA character. The population plot shows the movement of excitation across all the compartments along the population time *T*.

These global models show that the excited-state lifetime for the bilins in the terminal emitter is below 500 ps. But the fluorescence lifetime of a bilin chromophore is 2-4 ns.[41,42] so, there is a clear difference between these two time constants. We need to examine that

time constant closely. It is very hard to determine the actual time constant for the ground-state recovery using the 2DES set up that can only measure data till 300 ps and the laser spectrum that does not have significant intensity after 670 nm. To understand deeply what is actually happening to the terminal emitter, longer time data (more than 1 ns) is required. Therefore, time-correlated single photon counting (TCSPC) experiments were performed where data was collected till 10 ns.

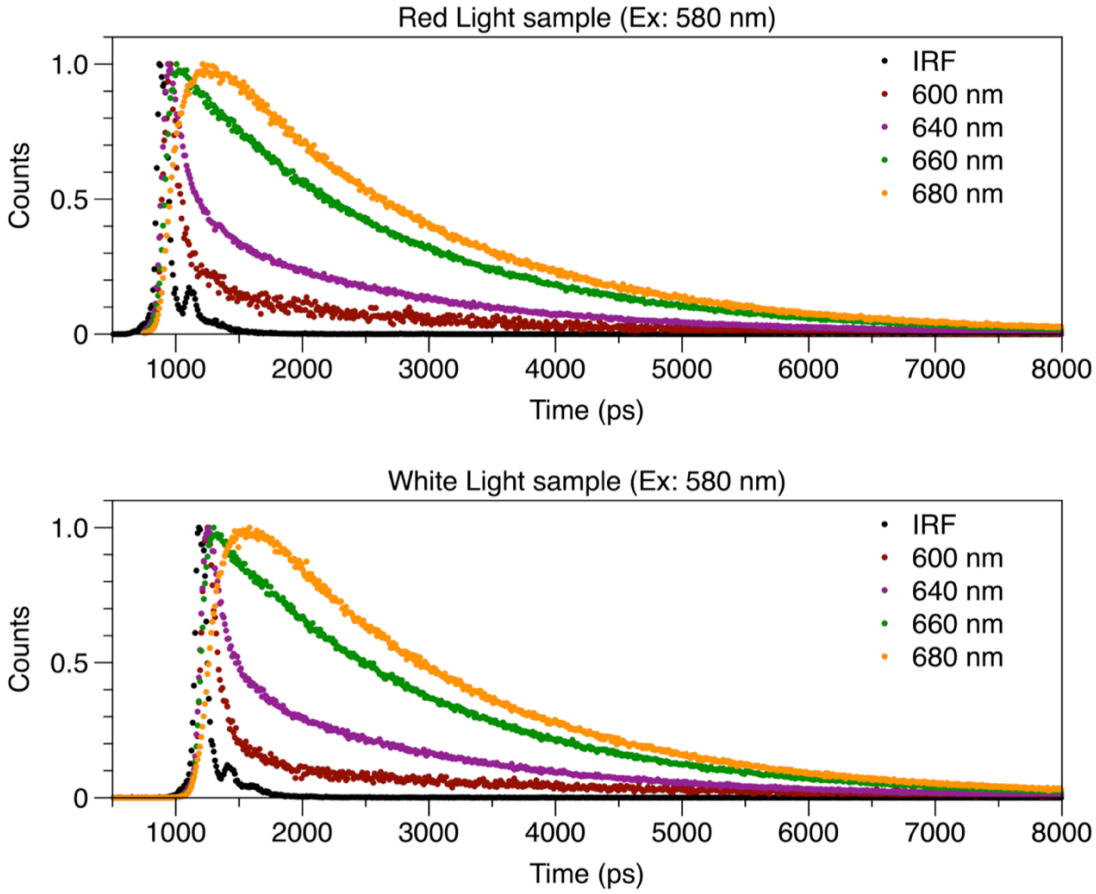

Figure 3.11. Time-correlated single photon counting (TCSPC) experimental results at different detection wavelengths after excitation at 580 nm from intact phycobilisome samples isolated from *F. diplosiphon* grown under red and white light. The black trace is the instrument response function (IRF) that has a FWHM ~100 ps. Photon counts at each detection wavelength are normalized at their maximum.

3.3.4 TCSPC Experiments

For these time-correlated single photon counting (TCSPC) experiments (Figure 3.11) the excitation wavelength was 580 nm that excited mostly phycocyanobilin (PCB) chromophores in the CPC disks in the rods. Detection at 600 and 640 nm are mostly the emission of photons from CPC. The longer detection wavelength has slower decay. Similar to this trend, the decay of the 660 nm kinetic trace is slower than that of the 640-nm trace. The 660-nm emission generated from APC_{660} in the core of phycobilisome. The 680-nm trace has a delayed rise and longer decay time. The delayed rise indicates the excitation population transferred from CPC to APC_{660} to terminal emitter (APC_{680}). The slower decay refers to the transfer of excitation getting slower with each step. Therefore, these kinetic traces show the energy transfer is occurring in the intact phycobilisomes. We performed global and target models of TCSPC experimental data to get the time constants.

The global and target model (Figure 3.12 and 3.13) shows that 4 compartments with two kinetically distinct APC_{680} boxes are required to sufficiently fit the data. Figure 3.12 represents the global model from the red-light grown phycobilisomes and figure 3.13 shows the global model for white-light grown samples. The compartments in the kinetic scheme were identified by looking at the peak in the evolution associated spectra (EAS) for each compartment. The EAS spectra resemble the fluorescence spectra of the phycobiliproteins. The black plot has a maximum ~650 nm which is the fluorescence maxima of CPC. Here the black plot is very noisy since the data quality below 100 ps is not good. Similarly, the red curve corresponds to APC_{660} that has emission maxima at 660 nm. The last two boxes have the identical lineshape, only the intensities are different. Those two boxes were characterized as APC_{680} or terminal emitters.

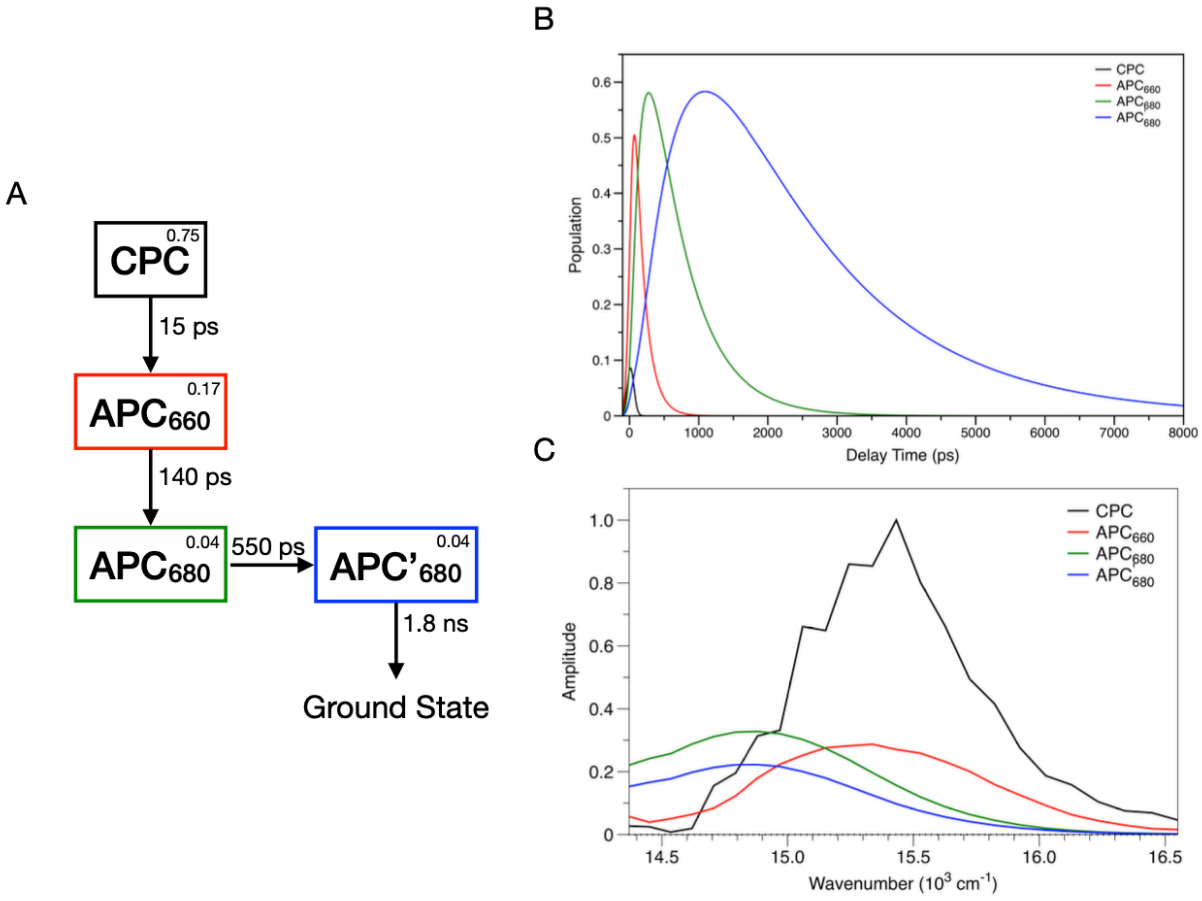

Figure 3.12. Global and target model for the TCSPC data (excitation wavelength: 580 nm; detection wavelengths: 600 to 700 nm with 4 nm steps) obtained from intact phycobilisomes isolated from *F. diplosiphon* grown under red light with 300 µW average excitation power and 4 MHz repetition rate (0.08 nJ/pulse). a, 4-compartment kinetic scheme with time constants for each step. b, Population plot for each compartment. The x-axis is in linear scale. c, Evolution associated spectra (EAS).

For the red-light grown sample energy moves from the rods to the core in 15 ps whereas it is 25 ps for white light grown sample. But it is not possible to know the exact value of that energy transfer rate since the IRF is ~100 ps. Then the excitation flows to APC_{680} from APC_{660} in ~140 ps for both samples. The excited state population moves to another terminal emitter in ~600 ps for the samples. The red-light grown sample is slightly faster than the white-light grown sample in this step. Then the population decays to the ground state for both samples in ~1.8 ns that matches with the ground state recovery time

for any bilin chromophore.[41,42] The population plot shows the evolution of excited state population from rods to core and finally to the TEs. These two kinetic models and their time constants are similar to the work presented by Akhtar et al.[43] where they employed TCSPC experiments in intact phycobilisomes isolated from *Anabaena variabilis* (PCC 7120). They suggested that the ~600 ps component is originating from an intrinsic quenching mechanism or energy transfer in the core between two APC_{680} units. Similar kinetic model was obtained with a faster energy transfer rate by using higher excitation energy per pulse (Figure A3.5). van Stokkum et al.[44] also reported a similar time constant in intact phycobilisomes from *Synechocystis* sp. PCC 6803 where they assumed that step as an additional quenching state.

The global and target models from TCSPC experiments show longer time constants for each step. The last time constant 1.8 ns confirms that the samples are behaving properly. Our initial thinking was that higher excitation pulse energy is creating shorter time constants for the kinetic model of the 2DES spectra. These TCSPC experiments were performed with lower pulse energy (0.08 nJ) than those used in the 2DES experiments (3nJ/pulse). Several TCSPC experiments were performed with different excitation energy per pulse in intact phycobilisomes from *F. diplosiphon* grown under red- and white-light. Additionally, using a cavity dumper a lower repetition rate to 154 kHz (lowest limit in that instrument) was used to match the 100 kHz repetition rate of the 2DES experiments. The figure 3.14 shows that with higher pulse energy the excitation population decays faster. The decay trace was fitted (Figure 3.14) with a linear combination of 3 Gaussian functions convoluted with an instrument response function (IRF) that was constructed with a linear

combination of 3 Gaussian functions. The figure 3.13 shows only two fitted traces for simplicity. The decay parameters can be found from table 3.1.

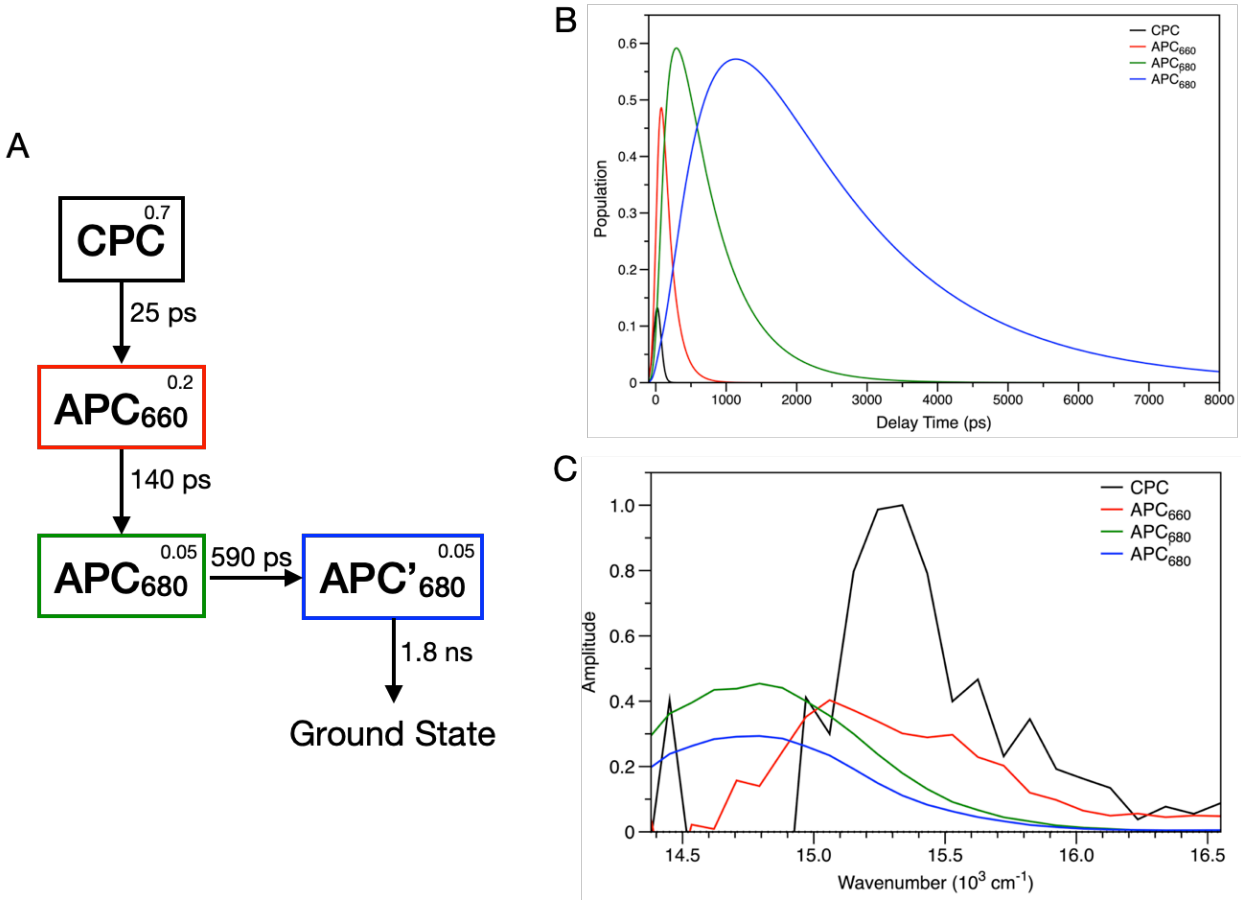

Figure 3.13. Global and target model for the TCSPC data (excitation wavelength: 580 nm; detection wavelengths: 600 to 700 nm with 4 nm steps) obtained from intact phycobilisomes isolated from *F. diplosiphon* grown under white light with 300 µW average excitation power and 4 MHz repetition rate (0.08 nJ/pulse). a, 4-compartment kinetic scheme with time constants for each step. b, Population plot for each compartment. The x-axis is in linear scale. c, Evolution associated spectra (EAS).

The figure 3.16 shows that the longest decay parameter (τ_3) decreases with increase in the average excitation power used in the experiments. The points can be fitted with a straight line. This plot indicates that with ~3 nJ/pulse energy the ground state recovery for the terminal emitter would > 1 ps. Therefore, the 200 or 400 ps time constant that we

observe in the global and kinetic model from 2DES data is not the ground state recovery. That could be an energy transfer process in the core or a quenching mechanism. More experiments need to be done to identify which process that time constant represents. The global model from the TCSPC data shows that the 500-700 ps time constant is an energy transfer step in the core between two APC_{680} units. Since the EAS of the last two compartments has the same features, it can be said that both 500-700 ps and the 1.5 ps time constants are originating from the same type of bilin chromophores. It might be worth noting here that the amplitude of the ~600 ps component (τ_2) in the fit parameter (Table 3.1) increases with the excitation energy.

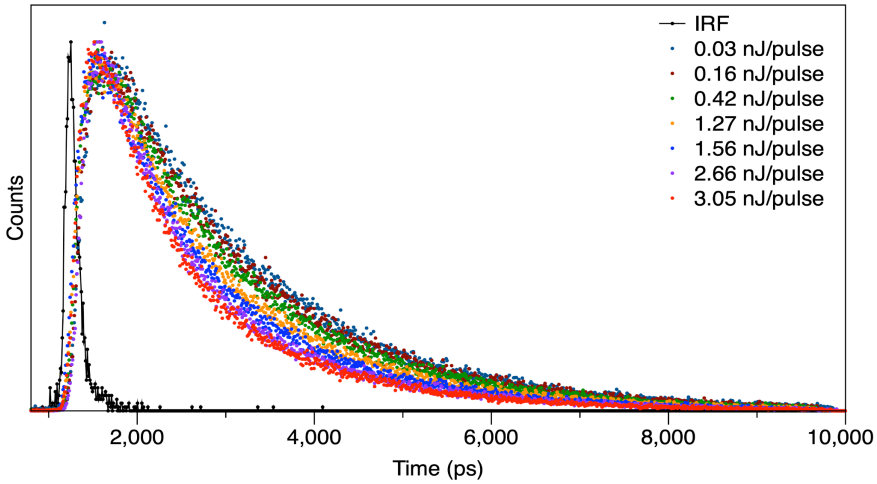

Figure 3.14. Kinetic traces from TCSPC experiments with different excitation energy per pulse for intact phycobilisomes samples grown under red light. The excitation wavelength was 600 nm, and the detection wavelength was 680 nm. All the traces were normalized with respect to their maxima. The black trace shows the IRF (~100 ps FWHM).

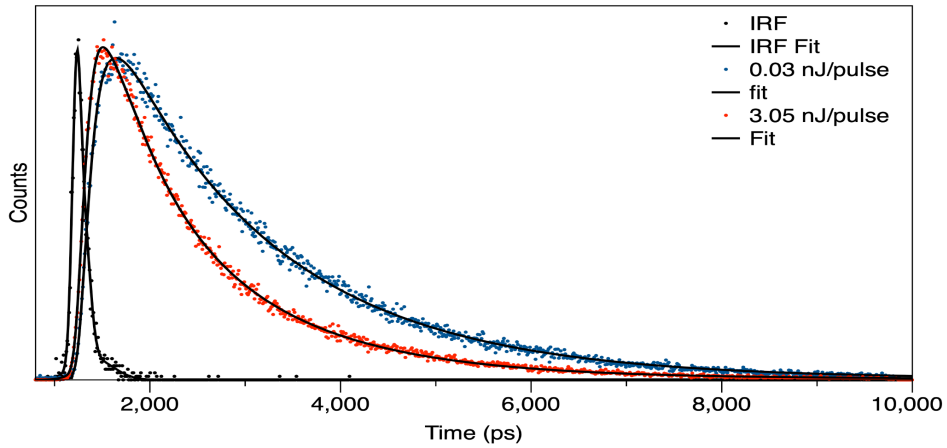

Figure 3.15. Kinetic traces and fits from TCSPC experiments with two different excitation energy per pulse for intact phycobilisomes samples grown under red light. The excitation wavelength was 600 nm, and the detection wavelength was 680 nm. All the traces were normalized with respect to their maxima. The black trace shows the instrument response function (IRF) with ~100 ps FWHM.

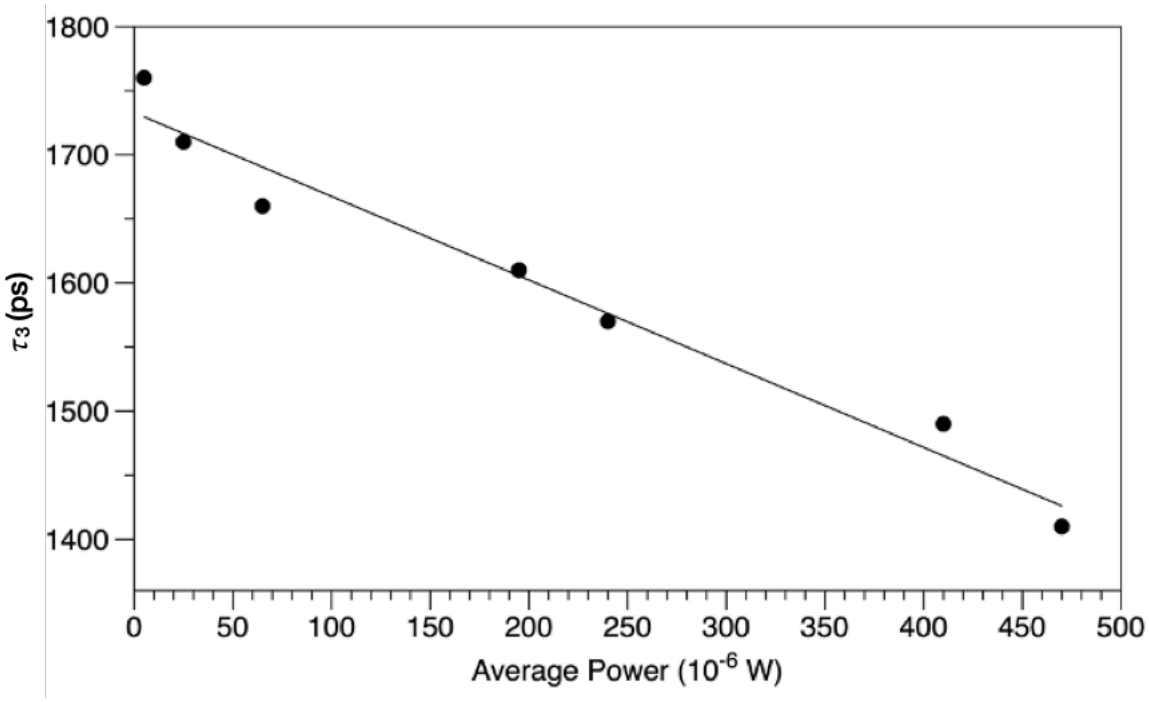

Figure 3.16. The longest decay parameter was plotted against the average power of excitation pulses used in TCSPC experiments for red-light grown intact phycobilisomes. The straight line shows the approximate fit for the points.

3.4 Conclusions

The main goal of this project was to study excitation energy transfer processes in intact phycobilisomes that have different structure than the white-light grown phycobilisomes. Therefore, *Fremyella diplosiphon* were grown under the illumination of red-light as they do not produce PE in this condition as CCA response and rod lengths become shorter. The 2DES was employed in intact phycobilisomes to study the excitation transfer mechanisms. The global and target model for the 560-580 nm excitation strip shows that the transfer of excitation takes a shorter time to reach the core of the phycobilisome. Additionally, the kinetic model predicted a twice shorter excited-state lifetime for the bilins in the APC_{680} than that of the white-light grown phycobilisomes. Due to limitations in our 2DES instrument (delay time and laser spectra) it is not possible to detect the exact excited-state lifetime for those bilins. That motivated us to perform TCSPC experiments. The fluorescence lifetime for the bilins at APC_{680} was measured ~1.5 ns from TCSPC experiments. Additionally, a 600-ps decay was detected which could be similar to the ground-state recovery time constant of the kinetic model from the 2DES data. This additional decay pathway could be a non-radiative pathway to the ground-state or just be another energy transfer step in the core. We cannot confirm the origin of this time constant at this point of time. New experiments and the analysis need to be done.

REFERENCES

(1) Glazer, A. N. Phycobilisomes: Structure and Dynamics. *Annu. Rev. Microbiol.* **1982**, *36*, 173–198, DOI: 10.1146/annurev.mi.36.100182.001133.

(2) Glazer, A. N. Phycobilisome a Macromolecular Complex Optimized for Light Energy Transfer. *Biochimica et Biophysica Acta (BBA) - Reviews on Bioenergetics* **1984**, *768*, 29–51, DOI: 10.1016/0304-4173(84)90006-5.

(3) Engelmann, T. W. Ueber Experimentelle Erzeugung Zweckmassiger Aenderrungen Der Farbung Pflanzlicher Chromophylle Durch Farbiges Licht. *Arch. Anat. Physiol. Lpz. ; Physiol. Abt* **1902**, 333–335.

(4) Gaidukov, N. 66. N. Gaidukov: Weitere Untersuchungen Über Den Einfluss Farbigen Lichtes Auf Die Färbung Der Oscillarien. *Ber. Dtsch. Bot. Ges.* **1903**, *21*, 484–492, DOI: 10.1111/j.1438-8677.1903.tb05185.x.

(5) Boresch, K. *Die Komplementäre Chromatische Adaptation*; Fischer, **1921**.

(6) Kehoe, D. M.; Gutu, A. Responding to Color: The Regulation of Complementary Chromatic Adaptation. *Annu. Rev. Plant Biol.* **2006**, *57*, 127–150, DOI: 10.1146/annurev.arplant.57.032905.105215.

(7) Tandeau de Marsac, N. Phycobiliproteins and Phycobilisomes: The Early Observations. *Photosynth. Res.* **2003**, *76*, 193–205, DOI: 10.1023/A:1024954911473.

(8) Hattori, A.; Fujita, Y. FORMATION OF PHYCOBILIN PIGMENTS IN A BLUE-GREEN ALGA, TOLYPOTHRIX TENUIS, AS INDUCED BY ILLUMINATION WITH COLORED LIGHTS. *J. Biochem.* **1959**, *46*, 521–524.

(9) Hattori, A.; Fujita, Y. EFFECT OF PRE-ILLUMINATION ON THE FORMATION OF PHYCOBILIN PIGMENTS IN A BLUE-GREEN ALGA, TOLYPOTHRIX TENUIS. *J. Biochem.* **1959**, *46*, 1259–1261, DOI: 10.1093/oxfordjournals.jbchem.a127028.

(10) FUJITA; YOSHIHIKO; HATTORI; AKIHIKO. Formation of Phycoerythrin in Pre-Illuminated Cells of Tolypothrix Tenuis with Special Reference to Nitrogen Metabolism. *Plant Cell Physiol.* **1960,** *1*, 281–292.

(11) Fujita, Y.; Hattori, A. PHOTOCHEMICAL INTERCONVERSION BETWEEN PRECURSORS OF PHYCOBILIN CHROMOPROTEIDS IN TOLYPOTHRIX TENUIS. *Plant Cell Physiol.* **1962**, *3*, 209–220, DOI: 10.1093/oxfordjournals.pcp.a078958.

(12) Diakoff, S.; Scheibe, J. Action Spectra for Chromatic Adaptation in Tolypothrix Tenuis. *Plant Physiol.* **1973**, *51*, 382–385, DOI: 10.1104/pp.51.2.382.

(13) Haury, J. F.; Bogorad, L. Action Spectra for Phycobiliprotein Synthesis in a Chromatically Adapting Cyanophyte, Fremyella Diplosiphon. *Plant Physiol.* **1977**, *60*, 835–839, DOI: 10.1104/pp.60.6.835.

(14) Ohki, K.; Watanabe, M.; Fujita, Y. Action of Near UV and Blue Light on the Photocontrol of Phycobiliprotein Formation; A Complementary Chromatic Adaptation. *Plant Cell Physiol.* **1982**, *23*, 651–656, DOI: 10.1093/oxfordjournals.pcp.a076392.

(15) de Marsac, N. T.; Castets, A. M.; Cohen-Bazire, G. Wavelength Modulation of Phycoerythrin Synthesis in Synechocystis Sp. 6701. *J. Bacteriol.* **1980**, *142*, 310–314, DOI: 10.1128/jb.142.1.310-314.1980.

(16) Vogelmann, T. C.; Scheibe, J. Action Spectra for Chromatic Adaptation in the Blue-Green Alga Fremyella Diplosiphon. *Planta* **1978**, *143*, 233–239, DOI: 10.1007/BF00391993.

(17) Tandeau de Marsac, N. Occurrence and Nature of Chromatic Adaptation in Cyanobacteria. *J. Bacteriol.* **1977**, *130*, 82–91, DOI: 10.1128/jb.130.1.82-91.1977.

(18) Bryant, D. A. The Photoregulated Expression of Multiple Phycocyanin Species. A General Mechanism for the Control of Phycocyanin Synthesis in Chromatically Adapting Cyanobacteria. *Eur. J. Biochem.* **1981**, *119*, 425–429, DOI: 10.1111/j.1432-1033.1981.tb05625.x.

(19) Bryant, D. A.; Guglielmi, G.; de Marsac, N. T.; Castets, A.-M.; Cohen-Bazire, G. The Structure of Cyanobacterial Phycobilisomes: A Model. *Arch. Microbiol.* **1979**, *123*, 113–127, DOI: 10.1007/BF00446810.

(20) Ohki, K.; Fujita, Y. Photoregulation of Phycobilisome Structure during Complementary Chromatic Adaptation in the Marine Cyanophyte Phormidium Sp. C861. *J. Phycol.* **1992**, *28*, 803–808, DOI: 10.1111/j.0022-3646.1992.00803.x.

(21) Ohki, K.; Gantt, E.; Lipschultz, C. A.; Ernst, M. C. Constant Phycobilisome Size in Chromatically Adapted Cells of the Cyanobacterium Tolypothrix Tenuis, and Variation in Nostoc Sp. *Plant Physiol.* **1985**, *79*, 943–948, DOI: 10.1104/pp.79.4.943.

(22) Rosinski, J.; Hainfeld, J. F.; Rigbi, M.; Siegelman, H. W. Phycobilisome Ultrastructure and Chromatic Adaptation in Fremyella Diplosiphon. *Ann. Bot.* **1981**, *47*, 1–12, DOI: 10.1093/oxfordjournals.aob.a085984.

(23) Westermann, M.; Wehrmeyer, W. A New Type of Complementary Chromatic Adaptation Exemplified ByPhormidium Sp. C86: Changes in the Number of Peripheral Rods and in the Stoichiometry of Core Complexes in Phycobilisomes. *Arch. Microbiol.* **1995**, *164*, 132–141, DOI: 10.1007/BF02525319.

(24) Bryant, D. A.; Cohen-Bazire, G. Effects of Chromatic Illumination on Cyanobacterial Phycobilisomes. Evidence for the Specific Induction of a Second Pair of Phycocyanin

Subunits in Pseudanabaena 7409 Grown in Red Light. *Eur. J. Biochem.* **1981**, *119*, 415–424, DOI: 10.1111/j.1432-1033.1981.tb05624.x.

(25) Öquist, G. Light-induced Changes in Pigment Composition of Photosynthetic Lamellae and Cell-free Extracts from the Blue-green Alga *Anacystis Nidulans*. *Physiol. Plant.* **1974**, *30*, 45–48, DOI: 10.1111/j.1399-3054.1974.tb04989.x.

(26) Lönneborg, A.; Lind, L. K.; Kalla, S. R.; Gustafsson, P.; Oquist, G. Acclimation Processes in the Light-Harvesting System of the Cyanobacterium Anacystis Nidulans Following a Light Shift from White to Red Light. *Plant Physiol.* **1985**, *78*, 110–114, DOI: 10.1104/pp.78.1.110.

(27) Grossman, A. R. Chromatic Adaptation and the Events Involved in Phycobilisome Biosynthesis. *Plant Cell Environ.* **1990**, *13*, 651–666, DOI: 10.1111/j.1365-3040.1990.tb01081.x.

(28) Glazer, A. N. 2 - Photosynthetic Accessory Proteins with Bilin Prosthetic Groups. In *Photosynthesis*; Hatch, Boardman, N. K., Eds.; Academic Press, **1981**; pp 51–96.

(29) Waaland, J. R.; Waaland, S. D.; Bates, G. CHLOROPLAST STRUCTURE AND PIGMENT COMPOSITION IN THE RED ALGA GRIFFITHSIA PACIFICA: REGULATION BY LIGHT INTENSITY1. *J. Phycol.* **1974**, *10*, 193–199, DOI: 10.1111/j.1529-8817.1974.tb02697.x.

(30) Yu, M. H.; Glazer, A. N.; Spencer, K. G.; West, J. A. Phycoerythrins of the Red Alga Callithamnion: VARIATION IN PHYCOERYTHROBILIN AND PHYCOUROBILIN CONTENT. *Plant Physiol.* **1981**, *68*, 482–488, DOI: 10.1104/pp.68.2.482.

(31) Pattanaik, B.; Whitaker, M. J.; Montgomery, B. L. Light Quantity Affects the Regulation of Cell Shape in Fremyella Diplosiphon. *Front. Microbiol.* **2012**, *3*, 170, DOI: 10.3389/fmicb.2012.00170.

(32) Walters, K. J.; Whitaker, M. J.; Singh, S. P.; Montgomery, B. L. Light Intensity and Reactive Oxygen Species Are Centrally Involved in Photoregulatory Responses during Complementary Chromatic Adaptation in Fremyella Diplosiphon. *Commun. Integr. Biol.* **2013**, *6*, e25005, DOI: 10.4161/cib.25005.

(33) Pillman, H. A.; Blanchard, G. J. Effects of Ethanol on the Organization of Phosphocholine Lipid Bilayers. *J. Phys. Chem. B* **2010**, *114*, 3840–3846, DOI: 10.1021/jp910897t.

(34) Hossain, M. I.; Blanchard, G. J. The Effect of Dilution on Induced Free Charge Density Gradients in Room Temperature Ionic Liquids. *Phys. Chem. Chem. Phys.* **2022**, *24*, 3844–3853, DOI: 10.1039/d1cp05027c.

(35) Bryant, D. A.; Cohen-Bazire, G.; Glazer, A. N. Characterization of the Biliproteins of Gloeobacter Violaceus Chromophore Content of a Cyanobacterial Phycoerythrin

Carrying Phycourobilin Chromophore. *Arch. Microbiol.* **1981**, *129*, 190–198, DOI: 10.1007/BF00425249.

(36) Stadnichuk, V. I.; Lukashev, E. P.; Yanyushin, M. F.; Zlenko, D. V.; Muronez, E. M.; Stadnichuk, I. N.; Krasilnikov, P. M. Energy Transfer Pathways among Phycobilin Chromophores and Fluorescence Emission Spectra of the Phycobilisome Core at 293 and 77 K. *Dokl. Biochem. Biophys.* **2015**, *465*, 401–405, DOI: 10.1134/S1607672915060149.

(37) van Stokkum, I. H. M.; Larsen, D. S.; van Grondelle, R. Global and Target Analysis of Time-Resolved Spectra. *Biochim. Biophys. Acta* **2004**, *1657*, 82–104, DOI: 10.1016/j.bbabio.2004.04.011.

(38) Kolodny, Y.; Zer, H.; Propper, M.; Yochelis, S.; Paltiel, Y.; Keren, N. Marine Cyanobacteria Tune Energy Transfer Efficiency in Their Light-Harvesting Antennae by Modifying Pigment Coupling. *FEBS J.* **2021**, *288*, 980–994, DOI: 10.1111/febs.15371.

(39) Kolodny, Y.; Avrahami, Y.; Zer, H.; Frada, M. J.; Paltiel, Y.; Keren, N. Phycobilisome Light-Harvesting Efficiency in Natural Populations of the Marine Cyanobacteria Synechococcus Increases with Depth. *Commun Biol* **2022**, *5*, 727, DOI: 10.1038/s42003-022-03677-2.

(40) Sohoni, S.; Lloyd, L. T.; Hitchcock, A.; MacGregor-Chatwin, C.; Iwanicki, A.; Ghosh, I.; Shen, Q.; Hunter, C. N.; Engel, G. S. Phycobilisome's Exciton Transfer Efficiency Relies on an Energetic Funnel Driven by Chromophore-Linker Protein Interactions. *J. Am. Chem. Soc.* **2023**, *145*, 11659–11668, DOI: 10.1021/jacs.3c01799.

(41) Grabowski, J.; Gantt, E. PHOTOPHYSICAL PROPERTIES OF PHYCOBILIPROTEINS FROM PHYCOBILISOMES: FLUORESCENCE LIFETIMES, QUANTUM YIELDS, AND POLARIZATION SPECTRA. *Photochem. Photobiol.* **1978**, *28*, 39–45, DOI: 10.1111/j.1751-1097.1978.tb06927.x.

(42) Wong, D.; Pellegrino, F.; Alfano, R. R.; Zilinskas, B. A. FLUORESCENCE RELAXATION KINETICS AND QUANTUM YIELD FROM THE ISOLATED PHYCOBILIPROTEINS OF THE BLUE-GREEN ALGA *NOSTOC* SP. MEASURED AS A FUNCTION OF SINGLE PICOSECOND PULSE INTENSITY, *I*. *Photochem. Photobiol.* **1981**, *33*, 651–662, DOI: 10.1111/j.1751-1097.1981.tb05471.x.

(43) Akhtar, P.; Biswas, A.; Petrova, N.; Zakar, T.; van Stokkum, I. H. M.; Lambrev, P. H. Time-Resolved Fluorescence Study of Excitation Energy Transfer in the Cyanobacterium Anabaena PCC 7120. *Photosynth. Res.* **2020**, *144*, 247–259, DOI: 10.1007/s11120-020-00719-w.

(44) van Stokkum, I. H. M.; Gwizdala, M.; Tian, L.; Snellenburg, J. J.; van Grondelle, R.; van Amerongen, H.; Berera, R. A Functional Compartmental Model of the Synechocystis PCC 6803 Phycobilisome. *Photosynth. Res.* **2018**, *135*, 87–102, DOI: 10.1007/s11120-017-0424-5.

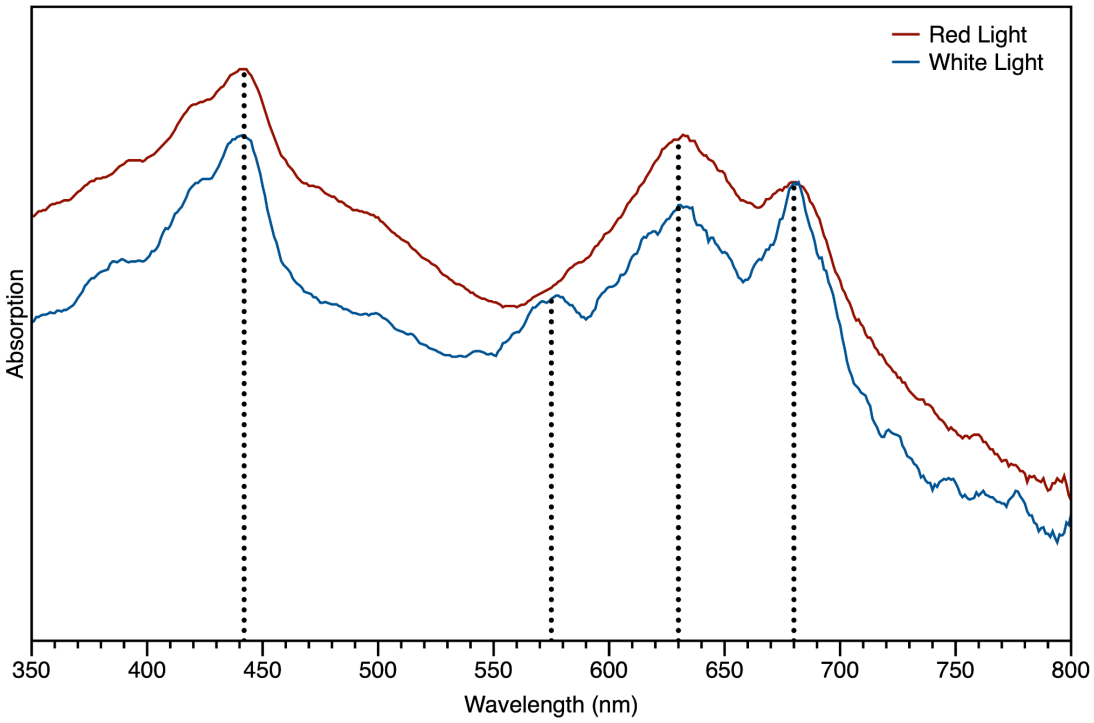

Figure A3.1. Whole cell absorption spectra from the *Fremyella diplosiphon* grown under white and red light. The dotted line represents the absorption peaks. The spectra were normalized with respect to the chlorophyll Q_Y peak at 682 nm. The bluest peak is at 440 nm from Chlorophyll. The red-light cells have relatively higher absorption in the 470-500 nm region due to a higher population of orange carotenoid protein (OCP). This is due to high intensity illumination in the growth chamber. The peak for PE is at 575 nm that is missing in the red-light grown sample. The red-light grown sample has higher absorption in the phycocyanin peak region at 630 nm.

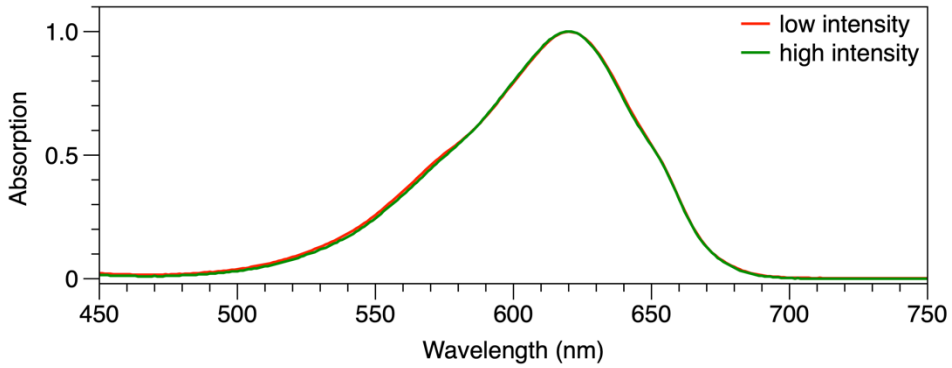

Figure A3.2. Absorption spectra of intact phycobilisomes isolated from *Fremyella diplosiphon* grown under high and low intensity red-light. No significant difference is observed between two spectra.

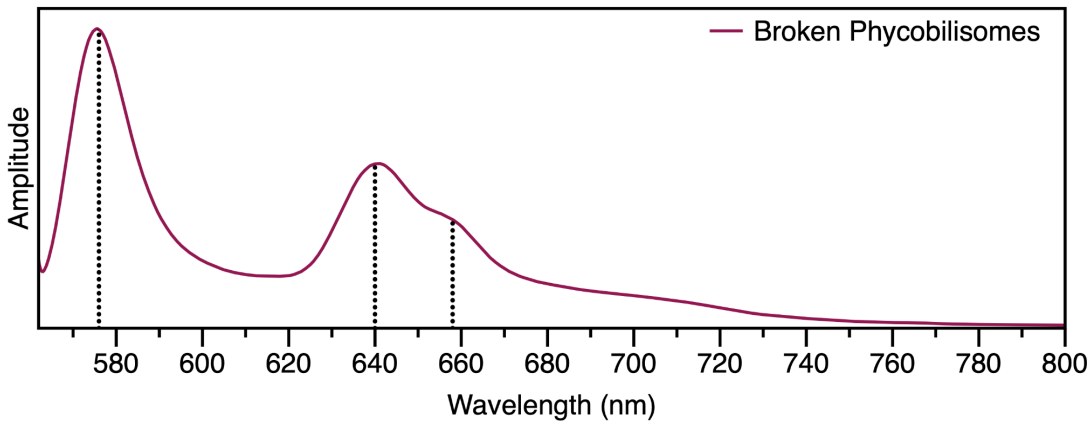

Figure A3.3. Fluorescence spectrum at 77 K of broken phycobilisomes from *Fremyella diplosiphon* grown under white light excited at 550 nm. The dotted vertical lines show the emission peaks for PE (578 nm), CPC (640 nm) and APC_{660} (658 nm). The emission peak for the terminal emitter at 685 nm is absent. A 10 times lower concentrated (0.08 M) phosphate buffer solution was used to break the intact phycobilisomes.

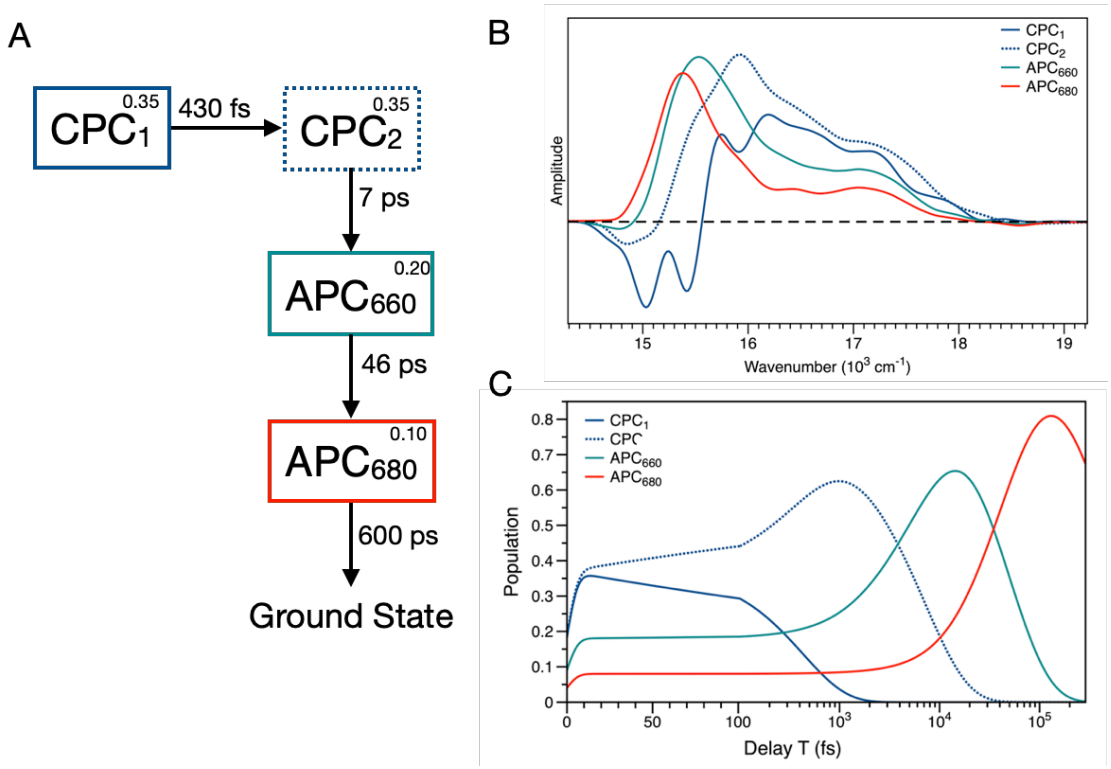

Figure A3.4. Global and target model for the 550-580 nm region of the excitation axis of the 2DES spectra obtained from phycobilisomes grown under low intensity red-light. a, Kinetic scheme and time constants for energy transfer process from rod to the core with initial excitation for each compartment. b, Evolution associated difference spectra (EADS). c, Time evolution of the population in each compartment. The x-axis of the population plot is in semilogarithmic scale where 100 fs is the breaking point.

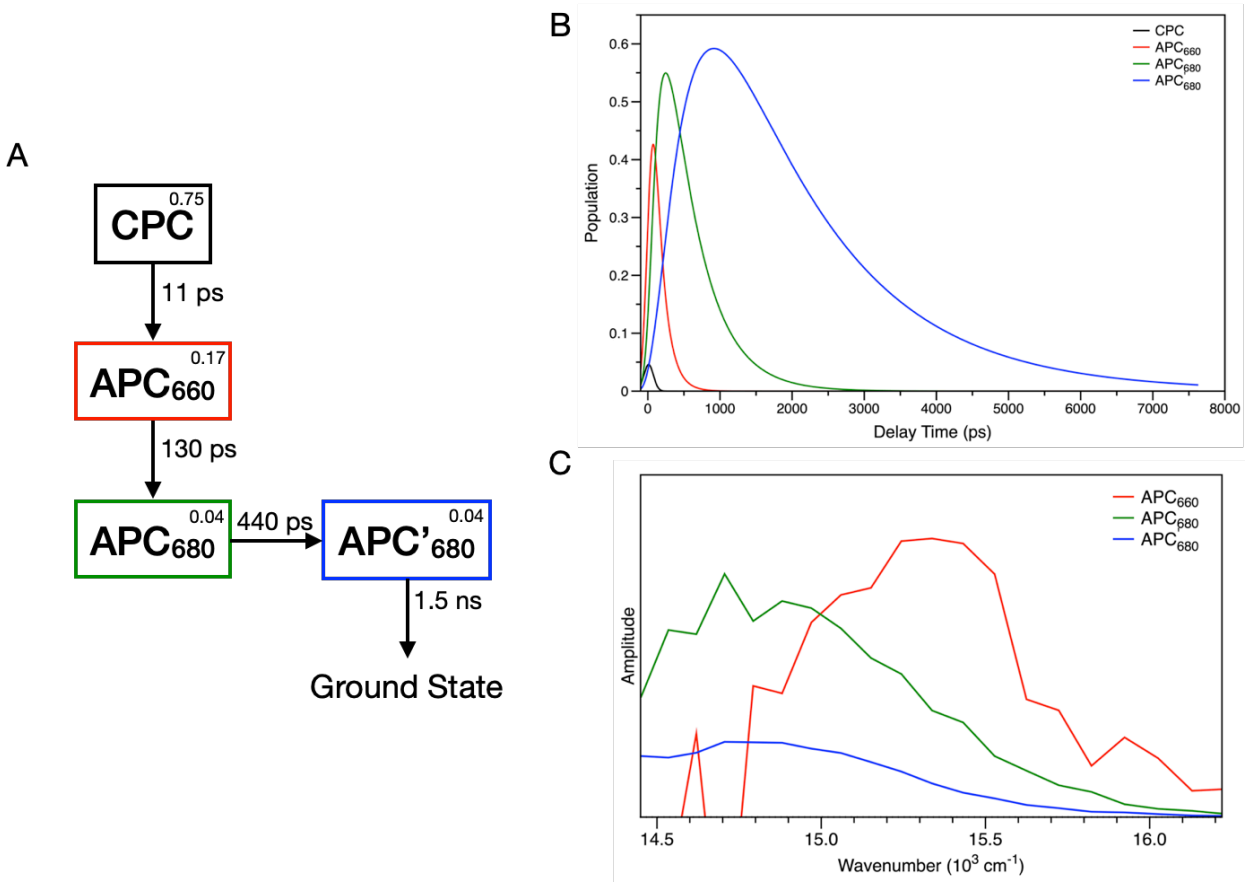

Figure A3.5. Global and target model for the TCSPC data (excitation wavelength: 600 nm; detection wavelengths: 616 to 700 nm with 4 nm steps) obtained from intact phycobilisomes isolated from *F. diplosiphon* grown under high intensity red light with 500 µW average excitation power and 154 kHz repetition rate (3.2 nJ/pulse). a, 4-compartment kinetic scheme with time constants for each step. b, Population plot for each compartment. The x-axis is in linear scale. c, Evolution associated spectra (EAS). The data is very noisy. EAS plot for CPC compartment is not included here.

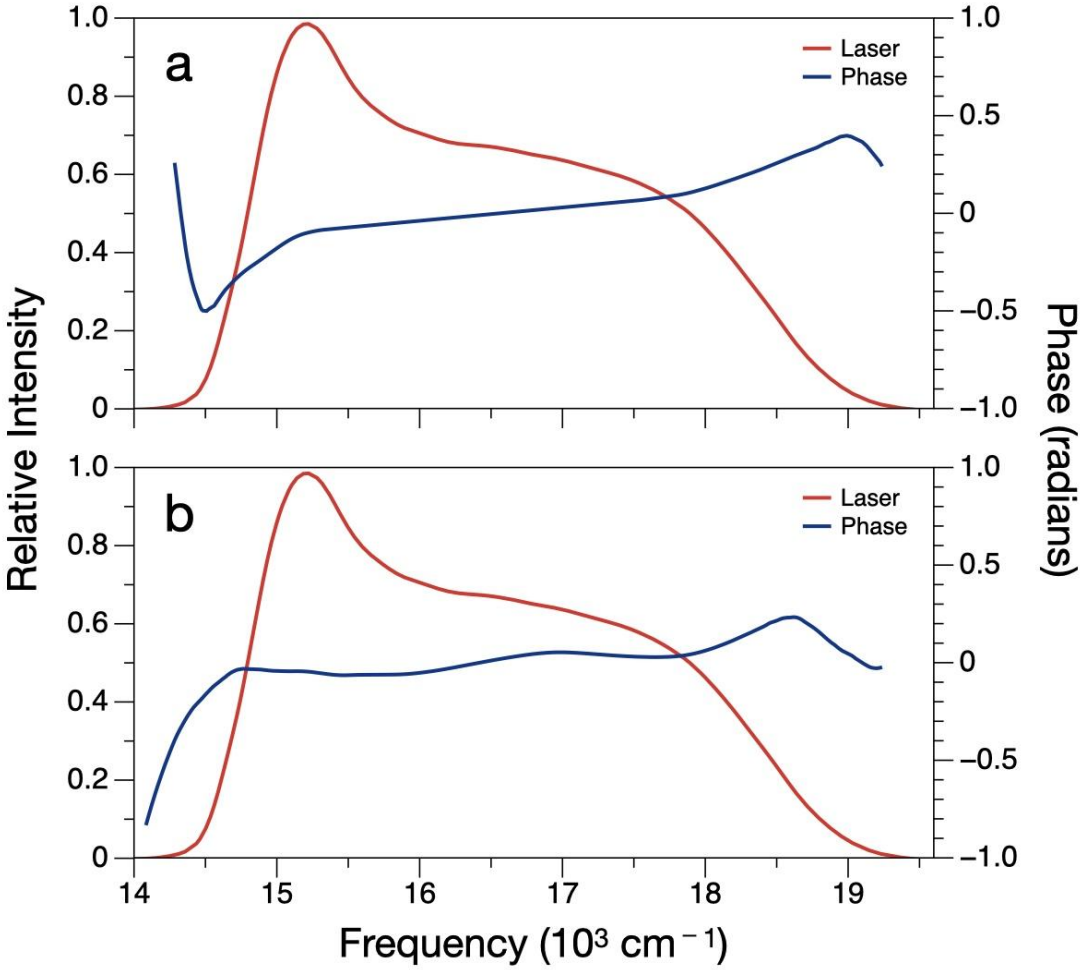

Figure A3.6. Laser intensity and residual phase spectrum after compression of the laser pulses used in the 2DES experiment: (a) for the pump beam, and (b) for the probe beam of the 2DES spectrometer.

Table 3.1. Fit parameters for the kinetic traces obtained from TCSPC experiments of red-light grown intact phycobilisomes (Excitation wavelength: 600 nm, Detection wavelength: 680 nm) $model = IRF * \sum_{i=1}^{3} a_i e^{(-T/\tau_i)} + a_0$

Energy per pulse (nJ)	a_1	τ_1 **(ps)**	a_2	τ_2 **(ps)**	a_3	τ_3 **(ps)**
0.03	-0.17	85	0.01	578	0.12	1760
0.16	-0.16	77	0.01	500	0.12	1707
0.42	-0.13	60	0.01	502	0.12	1660
1.27	-0.12	66	0.04	550	0.1	1609
1.56	-0.08	89	0.05	608	0.09	1572
2.66	-0.21	84	0.07	536	0.09	1490
3.05	-0.15	61	0.06	526	0.08	1413

Chapter 4: Future Work: Non-Photochemical Quenching in Intact Phycobilisomes by Orange Carotenoid Protein

This chapter contains discussion about some of the projects that are ongoing in the Beck Laboratory with intact phycobilisomes using the broadband two-dimensional electronic spectroscopy (2DES) instrument. We discuss mainly a specific research project about the photoprotection mechanisms in the core of the intact phycobilisomes by orange carotenoid protein (OCP). An overview of the structure of OCP and photoprotection mechanism is provided here. Then we talk about the problem with this current thinking about this mechanism followed by a suggested new pathway and proposed experimental process to test this new hypothesis. Lastly there are few other suggested projects related to the excitation energy transfer processes in the intact phycobilisomes that has different structures from complementary chromatic adaptation (CCA) process and mutation.

4.1 Photoprotection in Phycobilisomes

Phycobilisomes harvest mid-visible solar energy and channel that energy to the nearest chlorophyll in the thylakoid membrane bound photosystem (PS) I and II in cyanobacteria and red algae.[1,2] The $(\alpha\beta)_6$ hexameric phycobiliproteins phycoerythrin (PE) and phycocyanin (CPC) form cylindrical rods which are attached to the core segment made of another phycobiliprotein allophycocyanin (APC).[3,4] The core is linked with the PS II with linker protein which are a second kind of non-chromophorylated protein[5] found in phycobilisomes. Phycobilisomes construct a funnel-shaped energy structure by including blue-shifted bilin chromophores in the rods and red-shifted chromophores in the core.[6]

In optimum conditions energy absorbed in the rods of the phycobilisomes transfers to the core and moves to chlorophyll in PS II and PS I very efficiently. From there excitation

energy reaches to the reaction center (RC) where the photosynthesis occurs by creating a charge separation from the electron transfer process.[7] The primary charge separation takes place in ~3 ps. In high intensity light condition phycobilisomes would transfer more and faster excitation energy to the reaction center. If the reaction center cannot process that amount of energy so fast, then there would remain some excess energy. That excess amount of energy can create triplet chlorophyl which makes singlet oxygen. This singlet is a highly reactive agent that is capable destroying the whole reaction center apparatus.[8–10]

To avoid that catastrophic situation photosynthetic organisms have developed several photoprotective mechanisms involving carotenoid molecule, most widely occurring pigments in nature. The carotenoid molecules serve as photoprotector[11,12] by three ways: (1) reduce the amount of energy funneled to reaction center, (2) quench triplet chlorophyll to prevent singlet oxygen formation, (3) scavenge singlet oxygen directly. An example of the first kind of photoprotection act is the nonphotochemical quenching process in the intact phycobilisomes by orange carotenoid protein (OCP) that contain a single carotenoid molecule (more about OCP is discussed in the following section). In this process excess energy transfer to OCP from the core of the phycobilisomes. Few single molecular fluorescence studies[13,14] have reported a second type of photoprotection mechanism called intrinsic photoprotection mechanism where excess energy in the core of phycobilisome dissipate as thermal energy.

4.2 Orange Carotenoid Protein (OCP)

The orange carotenoid protein (OCP)[15–17] is the most characterized carotenoid containing protein. OCP, a water soluble 35-kD protein contains a single noncovalently bound carotenoid molecule. In 1981 Holt and Krogmann first described the carotenoid

binding proteins. Kerfeld et al. in 2003 reported the X-ray crystal structure of OCP from *Arthospira maxima* with 2.1 Å resolution.[11] The crystal structure shows that OCP contain two domains: all α-helical N-terminal domain (NTD) and a mixed α/β C-terminal domain (CTD). The carotenoid chromophore inside the OCP is 3'-hydroxyequinenone or canthaxanthin (CAN) molecule that spans both protein domains. Upon photoexcitation with strong mid-visible light OCP transforms to an activated state called OCP^R that has a red-shifted absorption maximum about 50 nm from its resting orange form (OCP^O).[18,19] In the activated OCP^R form the carotenoid molecule translocated into the NTD from CTD.[18] This activated form is responsible for the nonphotochemical quenching in phycobilisomes.

4.3 Photophysics of Carotenoids

Carotenoid molecules contain a long-conjugated isoprenoid backbone with various functional groups at the end of the chain. They fall under C_{2h} symmetry group due to their planner structure. Therefore, the ground state S_0 has $1A_g^-$ symmetry whereas the first excited state S_1, and second excited state S_2 have $2A_g^-$ and $1Bu^+$ symmetries respectively.[20] The first excited state S_1 is a dark state because the transition from S_0 to S_1 is symmetrically forbidden. The S_1 state can be populated with two-photon excitation from the ground state. In contrary, the second excited state S_2 which is a bright state that absorb a blue-green light.[21,22] These transitions are the π to π^* transitions. The optically prepared S_2 state shows a very short lifetime (<100 fs) and relaxes to S_1 state in a nonradiative pathway.[23,24] Several studies have reported that the decay of S_2 to S_1 undergoes through an intermediate state S_x that has a lifetime less than 20 fs.[25–27,45] The lifetime for S_1 state is 3-4 ps. The energy difference between S_0 and S_1 corresponds to about 660 nm which is similar to the emission maximum of APC in the core of the phycobilisomes.[28] Like S_1 state there is another dark

excited state called S*. The origin of the S* state is controversial.[25] Some studies[29–31] suggested S* state as a singlet excited state that has a distinct conformation of the carotenoid populated via a distortion of the conjugated chain. Other studies assigned it to a hot ground state.[32] The S* state has a different spectrum and a longer lifetime (~15 ps) than S_1 state.

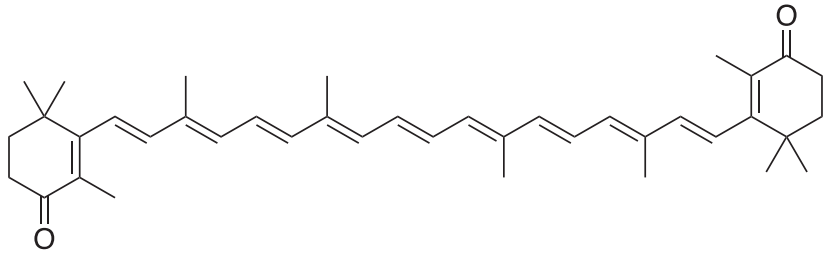

Figure 4.1. Structure of canthaxanthin.[45]

4.4 Mechanism of Nonphotochemical Quenching by OCP in the Phycobilisome

In high intensity light condition OCP absorb blue-green light and transform to its active form OCP^R. In the that activated state carotenoid molecule moves 12 Å inside the NTD.[18] The NTD binds to the core of the phycobilisome specifically with the allophycocyanin.[33] The recent cryo-EM structure[34] of the phycobilisome in quenched state shows that two dimer of OCP^R can bind to the core simultaneously. Several studies showed that only the NTD part of OCP is required for the photoprotection mechanism. Also, separate studies show OCP does not bind with the rods of the phycobilisome and resting state OCP^O state is unable to attach with the phycobilisome. In this bound state the carotenoid molecule is very close to the phycocyanobilin chromophore in APC.[34] The carotenoid accepts the excess energy from the bilins in APC and dissipate that energy as heat.[18,35] In dark another protein fluorescence recovery protein (FRP)[33,36] attaches with the CTD of the OCP^R and assists to unbound from phycobilisome and return to its resting structure OCP^O. In vivo OCP^R can return to OCP^O

state in few hours in presence of FRP, but the phycobilisome-OCP complex is very stable over 1 day in vitro without. FRP.

4.5 Main Questions and Proposed Experiments

Even though the overall process of non-photochemical quenching by OCP appears to be fairly well understood, the detailed photophysical mechanism for the quenching of the excitons in the phycobilisome has not yet been worked out. The main questions are as follows: (1) which energy state of OCP is accepting the energy from APC? (2) What is the nature of this excitation energy transfer step? (3) How long does it take to transfer energy from APC to OCP? (4) How is the unbound OCP^R different from bound OCP^R?

The conventional thinking would be that bilins in APC transfer excess energy to the carotenoid via Förster mechanism.[37,38] A key part in Förster mechanism is that there should be some overlap between the emission spectrum of the donor and the absorption spectrum of the acceptor. The emission spectrum for APC is in 620 - 720 nm region. The absorption spectrum for S_0 to S_2 is in 450-520 nm region. Therefore, no overlap is possible. The only option would be to transfer energy to the lower energy S_1 state which was suggested to overlap with APC emission spectra.[28] But the transition from the S_0 to S_1 is forbidden by selection rule. Then in which state carotenoid accepts energy from APC.

Several studies[39–42] on light-harvesting complex II showed that chlorophyll transfer energy to the S_1 state of the carotenoid. They suggested that a partial mixing of the excited states of the carotenoid and chlorophyll and a complex picture is required. There might be partial mixing of the excited states in carotenoid and bilins in APC from the originating from the close positioning of the carotenoid from the bilins in APC. That would indicate that energy transfer occurs via a quantum coherent mechanism. Another possible way might be

that upon binding with the core of phycobilisome carotenoid molecule becomes distorted structure and no longer falls into C_{2h} symmetry group. In that condition optical transfer is possible from S_0 to S_1. A similar picture have suggested by Liguori et al.[43] Although they suggested that the acceptor state is S* state created from the distorted structure of carotenoid prepared after binding to the core of phycobilisome. The other possibility would be that carotenoid influences bilin chromophore to change its structure or photophysical property to behave as an energy trap. The broadband two-dimensional electronic spectroscopy (2DES) will be used to study the excitation energy transfer mechanisms in phycobilisome – OCP complex for testing these hypotheses.

If OCP behaves as a quencher in the phycobilisome - OCP complex, then we can expect a different kinetic model than that of the only phycobilisomes (Figure 2.6). Specifically, there would be an additional compartment that accepts major portion of the excitation energy from the APC_{660} compartment. If the evolution associated difference spectrum (EADS) for that addition box shows a negative going ESA character similar to S_1 state of a carotenoid, then the acceptor state of the carotenoid would be the S_1 state. Also, the lifetime of that state needs to be similar (3-5 ps) to S_1 state lifetime of a carotenoid. If the carotenoid is strongly coupled with the bilin chromophore in the phycobilisome - OCP complex, then we can expect a redshift in the EADS of the OCP compartment. It would be hard to observe any actual ESA peaks in the 2DES spectra near 660 nm originating from the S_1 state of the OCP. This is because bilins in the phycobilisomes exhibit strong positive going GSB and SE signals in that region.

4.6 Effect of CCA in the Excitation Energy Transfer

When cyanobacteria *Fremyella diplosiphon* grow in green light they make phycobilisomes with higher number of phycoerythrin (PE) disks in the rod than that of CPC disks.[44] It would be interesting to see the difference in excitation energy transfer rate in the rods of phycobilisomes between the green-light grown sample and the red-light grown sample that has higher CPC disks. The energy transfer mechanisms in the core from direct excitation can be investigated using two-dimensional electronic spectroscopy on a mutant phycobilisomes that do not produce rods. Then we can compare the results with the model where core is excited from the excitation energy transfer from the rods.

The global and target models from the 2DES data on green light grown *Fremyella diplosiphon* samples are expected to be different than that of the white light (Figure 2.6)[46] and red light (Figure 3.9) grown samples. The model from green light grown sample may contain more than one PE compartments and one CPC compartment.

REFERENCES

(1) Glazer, A. N. Phycobilisomes: Structure and Dynamics. *Annu. Rev. Microbiol.* **1982**, *36*, 173–198, DOI: 10.1146/annurev.mi.36.100182.001133.

(2) Gantt, E. Phycobilisomes: Light-Harvesting Pigment Complexes. *Bioscience* **1975**, *25*, 781–788, DOI: 10.2307/1297221.

(3) Bryant, D. A.; Guglielmi, G.; de Marsac, N. T.; Castets, A.-M.; Cohen-Bazire, G. The Structure of Cyanobacterial Phycobilisomes: A Model. *Arch. Microbiol.* **1979**, *123*, 113–127, DOI: 10.1007/BF00446810.

(4) Rosinski, J.; Hainfeld, J. F.; Rigbi, M.; Siegelman, H. W. Phycobilisome Ultrastructure and Chromatic Adaptation in Fremyella Diplosiphon. *Ann. Bot.* **1981**, *47*, 1–12, DOI: 10.1093/oxfordjournals.aob.a085984.

(5) Liu, L.-N.; Chen, X.-L.; Zhang, Y.-Z.; Zhou, B.-C. Characterization, Structure and Function of Linker Polypeptides in Phycobilisomes of Cyanobacteria and Red Algae: An Overview. *Biochim. Biophys. Acta* **2005**, *1708*, 133–142, DOI: 10.1016/j.bbabio.2005.04.001.

(6) Glazer, A. N. Phycobilisome a Macromolecular Complex Optimized for Light Energy Transfer. *Biochimica et Biophysica Acta (BBA) - Reviews on Bioenergetics* **1984**, *768*, 29–51, DOI: 10.1016/0304-4173(84)90006-5.

(7) Blankenship, R. E. *Molecular Mechanisms of Photosynthesis*; John Wiley & Sons, 2021.

(8) Aro, E. M.; Virgin, I.; Andersson, B. Photoinhibition of Photosystem II. Inactivation, Protein Damage and Turnover. *Biochim. Biophys. Acta* **1993**, *1143*, 113–134, DOI: 10.1016/0005-2728(93)90134-2.

(9) Tyystjärvi, E. Photoinhibition of Photosystem II and Photodamage of the Oxygen Evolving Manganese Cluster. *Coord. Chem. Rev.* **2008**, *252*, 361–376, DOI: 10.1016/j.ccr.2007.08.021.

(10) Vass, I. Role of Charge Recombination Processes in Photodamage and Photoprotection of the Photosystem II Complex. *Physiol. Plant.* **2011**, *142*, 6–16, DOI: 10.1111/j.1399-3054.2011.01454.x.

(11) Kerfeld, C. A.; Sawaya, M. R.; Brahmandam, V.; Cascio, D.; Ho, K. K.; Trevithick-Sutton, C. C.; Krogmann, D. W.; Yeates, T. O. The Crystal Structure of a Cyanobacterial Water-Soluble Carotenoid Binding Protein. *Structure* **2003**, *11*, 55–65, DOI: 10.1016/S0969-2126(02)00936-X.

(12) Wilson, A.; Ajlani, G.; Verbavatz, J.-M.; Vass, I.; Kerfeld, C. A.; Kirilovsky, D. A Soluble Carotenoid Protein Involved in Phycobilisome-Related Energy Dissipation in Cyanobacteria. *Plant Cell* **2006**, *18*, 992–1007, DOI: 10.1105/tpc.105.040121.

(13) Krüger, T. P. J.; van Grondelle, R.; Gwizdala, M. The Role of Far-Red Spectral States in the Energy Regulation of Phycobilisomes. *Biochim. Biophys. Acta Bioenerg.* **2019**, *1860*, 341–349, DOI: 10.1016/j.bbabio.2019.01.007.

(14) Wahadoszamen, M.; Krüger, T. P. J.; Ara, A. M.; van Grondelle, R.; Gwizdala, M. Charge Transfer States in Phycobilisomes. *Biochim. Biophys. Acta Bioenerg.* **2020**, *1861*, 148187, DOI: 10.1016/j.bbabio.2020.148187.

(15) Kay Holt, T.; Krogmann, D. W. A Carotenoid-Protein from Cyanobacteria. *Biochimica et Biophysica Acta (BBA) - Bioenergetics* **1981**, *637*, 408–414, DOI: 10.1016/0005-2728(81)90045-1.

(16) Wu, Y. P.; Krogmann, D. W. The Orange Carotenoid Protein of Synechocystis PCC 6803. *Biochim. Biophys. Acta* **1997**, *1322*, 1–7, DOI: 10.1016/s0005-2728(97)00067-4.

(17) Kerfeld, C. A. Structure and Function of the Water-Soluble Carotenoid-Binding Proteins of Cyanobacteria. *Photosynth. Res.* **2004**, *81*, 215–225, DOI: 10.1023/B:PRES.0000036886.60187.c8.

(18) Leverenz, R. L.; Sutter, M.; Wilson, A.; Gupta, S.; Thurotte, A.; de Carbon, C. B.; Petzold, C. J.; Ralston, C.; Perreau, F.; Kirilovsky, D.; et al. A 12 Å Carotenoid Translocation in a Photoswitch Associated with Cyanobacterial Photoprotection. *Science* **2015**, *348*, 1463–1466, DOI: 10.1126/science.aaa7234.

(19) Gupta, S.; Guttman, M.; Leverenz, R. L.; Zhumadilova, K.; Pawlowski, E. G.; Petzold, C. J.; Lee, K. K.; Ralston, C. Y.; Kerfeld, C. A. Local and Global Structural Drivers for the Photoactivation of the Orange Carotenoid Protein. *Proc. Natl. Acad. Sci. U. S. A.* **2015**, *112*, E5567-74, DOI: 10.1073/pnas.1512240112.

(20) Polívka, T.; Sundström, V. Ultrafast Dynamics of Carotenoid Excited States-from Solution to Natural and Artificial Systems. *Chem. Rev.* **2004**, *104*, 2021–2071, DOI: 10.1021/cr020674n.

(21) Fiedor, L.; Dudkowiak, A.; Pilch, M. The Origin of the Dark S1 State in Carotenoids: A Comprehensive Model. *J. R. Soc. Interface* **2019**, *16*, 20190191, DOI: 10.1098/rsif.2019.0191.

(22) Gurchiek, J. K.; Rose, J. B.; Guberman-Pfeffer, M. J.; Tilluck, R. W.; Ghosh, S.; Gascón, J. A.; Beck, W. F. Fluorescence Anisotropy Detection of Barrier Crossing and Ultrafast Conformational Dynamics in the S2 State of β-Carotene. *J. Phys. Chem. B* **2020**, *124*, 9029–9046, DOI: 10.1021/acs.jpcb.0c06961.

(23) Ghosh, S.; Bishop, M. M.; Roscioli, J. D.; LaFountain, A. M.; Frank, H. A.; Beck, W. F. Excitation Energy Transfer by Coherent and Incoherent Mechanisms in the Peridinin–Chlorophyll a Protein. *J. Phys. Chem. Lett.* **2017**, *8*, 463–469, DOI: 10.1021/acs.jpclett.6b02881.

(24) Ghosh, S.; Bishop, M. M.; Roscioli, J. D.; Mueller, J. J.; Shepherd, N. C.; LaFountain, A. M.; Frank, H. A.; Beck, W. F. Femtosecond Heterodyne Transient-Grating Studies of Nonradiative Decay of the S2 (1(1)Bu(+)) State of β-Carotene: Contributions from Dark Intermediates and Double-Quantum Coherences. *J. Phys. Chem. B* **2015**, *119*, 14905–14924, DOI: 10.1021/acs.jpcb.5b09405.

(25) Polívka, T.; Sundström, V. Dark Excited States of Carotenoids: Consensus and Controversy. *Chem. Phys. Lett.* **2009**, *477*, 1–11, DOI: 10.1016/j.cplett.2009.06.011.

(26) Cerullo, G.; Polli, D.; Lanzani, G.; De Silvestri, S.; Hashimoto, H.; Cogdell, R. J. Photosynthetic Light Harvesting by Carotenoids: Detection of an Intermediate Excited State. *Science* **2002**, *298*, 2395–2398, DOI: 10.1126/science.1074685.

(27) Sugisaki, M.; Fujiwara, M.; Nair, S. V.; Ruda, H. E.; Cogdell, R. J.; Hashimoto, H. Excitation-Energy Dependence of Transient Grating Spectroscopy in \beta-Carotene. *Phys. Rev. B Condens. Matter* **2009**, *80*, 035118, DOI: 10.1103/PhysRevB.80.035118.

(28) Polívka, T.; Zigmantas, D.; Sundström, V.; Formaggio, E.; Cinque, G.; Bassi, R. Carotenoid S1 State in a Recombinant Light-Harvesting Complex of Photosystem II. *Biochemistry* **2002**, *41*, 439–450, DOI: 10.1021/bi011589x.

(29) Konold, P. E.; van Stokkum, I. H. M.; Muzzopappa, F.; Wilson, A.; Groot, M.-L.; Kirilovsky, D.; Kennis, J. T. M. Photoactivation Mechanism, Timing of Protein Secondary Structure Dynamics and Carotenoid Translocation in the Orange Carotenoid Protein. *J. Am. Chem. Soc.* **2019**, *141*, 520–530, DOI: 10.1021/jacs.8b11373.

(30) Khan, T.; Kuznetsova, V.; Dominguez-Martin, M. A.; Kerfeld, C. A.; Polívka, T. UV Excitation of Carotenoid Binding Proteins OCP and HCP: Excited-state Dynamics and Product Formation. *ChemPhotoChem* **2022**, *6*, DOI: 10.1002/cptc.202100194.

(31) Liguori, N.; Xu, P.; van Stokkum, I. H. M.; van Oort, B.; Lu, Y.; Karcher, D.; Bock, R.; Croce, R. Different Carotenoid Conformations Have Distinct Functions in Light-Harvesting Regulation in Plants. *Nat. Commun.* **2017**, *8*, 1994, DOI: 10.1038/s41467-017-02239-z.

(32) Balevičius, V., Jr; Abramavicius, D.; Polívka, T.; Galestian Pour, A.; Hauer, J. A Unified Picture of S* in Carotenoids. *J. Phys. Chem. Lett.* **2016**, *7*, 3347–3352, DOI: 10.1021/acs.jpclett.6b01455.

(33) Gwizdala, M.; Wilson, A.; Kirilovsky, D. In Vitro Reconstitution of the Cyanobacterial Photoprotective Mechanism Mediated by the Orange Carotenoid Protein in Synechocystis PCC 6803. *Plant Cell* **2011**, *23*, 2631–2643, DOI: 10.1105/tpc.111.086884.

(34) Domínguez-Martín, M. A.; Sauer, P. V.; Kirst, H.; Sutter, M.; Bína, D.; Greber, B. J.; Nogales, E.; Polívka, T.; Kerfeld, C. A. Structures of a Phycobilisome in Light-Harvesting and Photoprotected States. *Nature* **2022**, *609*, 835–845, DOI: 10.1038/s41586-022-05156-4.

(35) Bao, H.; Melnicki, M. R.; Kerfeld, C. A. Structure and Functions of Orange Carotenoid Protein Homologs in Cyanobacteria. *Curr. Opin. Plant Biol.* **2017**, *37*, 1–9, DOI: 10.1016/j.pbi.2017.03.010.

(36) Boulay, C.; Wilson, A.; D'Haene, S.; Kirilovsky, D. Identification of a Protein Required for Recovery of Full Antenna Capacity in OCP-Related Photoprotective Mechanism in Cyanobacteria. *Proc. Natl. Acad. Sci. U. S. A.* **2010**, *107*, 11620–11625, DOI: 10.1073/pnas.1002912107.

(37) Tian, L.; van Stokkum, I. H. M.; Koehorst, R. B. M.; Jongerius, A.; Kirilovsky, D.; van Amerongen, H. Site, Rate, and Mechanism of Photoprotective Quenching in Cyanobacteria. *J. Am. Chem. Soc.* **2011**, *133*, 18304–18311, DOI: 10.1021/ja206414m.

(38) Tian, L.; Gwizdala, M.; van Stokkum, I. H. M.; Koehorst, R. B. M.; Kirilovsky, D.; van Amerongen, H. Picosecond Kinetics of Light Harvesting and Photoprotective Quenching in Wild-Type and Mutant Phycobilisomes Isolated from the Cyanobacterium *Synechocystis* PCC 6803. *Biophys. J.* **2012**, *102*, 1692–1700, DOI: 10.1016/j.bpj.2012.03.008.

(39) Son, M.; Pinnola, A.; Gordon, S. C.; Bassi, R.; Schlau-Cohen, G. S. Observation of Dissipative Chlorophyll-to-Carotenoid Energy Transfer in Light-Harvesting Complex II in Membrane Nanodiscs. *Nat. Commun.* **2020**, *11*, 1295, DOI: 10.1038/s41467-020-15074-6.

(40) Holleboom, C.-P.; Walla, P. J. The Back and Forth of Energy Transfer between Carotenoids and Chlorophylls and Its Role in the Regulation of Light Harvesting. *Photosynth. Res.* **2014**, *119*, 215–221, DOI: 10.1007/s11120-013-9815-4.

(41) Liao, P.-N.; Holleboom, C.-P.; Wilk, L.; Kühlbrandt, W.; Walla, P. J. Correlation of Car S1 → Chl with Chl → Car S1 Energy Transfer Supports the Excitonic Model in Quenched Light Harvesting Complex II. *J. Phys. Chem. B* **2010**, *114*, 15650–15655, DOI: 10.1021/jp1034163.

(42) Bode, S.; Quentmeier, C. C.; Liao, P.-N.; Hafi, N.; Barros, T.; Wilk, L.; Bittner, F.; Walla, P. J. On the Regulation of Photosynthesis by Excitonic Interactions between Carotenoids and Chlorophylls. *Proceedings of the National Academy of Sciences* **2009**, *106*, 12311–12316, DOI: 10.1073/pnas.0903536106.

(43) Liguori, N.; Van Stokkum, I. H. M.; Muzzopappa, F.; Kennis, J. T. M.; Kirilovsky, D.; Croce, R. The molecular origin of the OCP-dependent non-photochemical quenching mechanism in cyanobacteria https://chemrxiv.org/engage/api-gateway/chemrxiv/assets/orp/resource/item/631f27625351a33cdbf77ff0/original/the-molecular-origin-of-the-ocp-dependent-non-photochemical-quenching-mechanism-in-cyanobacteria.pdf.

(44) Kehoe, D. M.; Gutu, A. Responding to Color: The Regulation of Complementary Chromatic Adaptation. *Annu. Rev. Plant Biol.* **2006**, *57*, 127–150, DOI: 10.1146/annurev.arplant.57.032905.105215.

(45) Mohan T M, N.; Leslie, C. H.; Sil, S.; Rose, J. B.; Tilluck, R. W.; Beck, W. F. Broadband 2DES Detection of Vibrational Coherence in the Sx State of Canthaxanthin. *J. Chem. Phys.* **2021**, *155*, 035103, DOI: 10.1063/5.0055598.

(46) Sil, S.; Tilluck, R. W.; Mohan T M, N.; Leslie, C. H.; Rose, J. B.; Domínguez-Martín, M. A.; Lou, W.; Kerfeld, C. A.; Beck, W. F. Excitation Energy Transfer and Vibronic Coherence in Intact Phycobilisomes. *Nat. Chem.* **2022**, *14*, 1286-1294, DOI: 10.1038/s41557-022-01026-8.